EFFECTS OF SEDIMENT LOAD ON THE VELOCITY FIELD AND FRICTION FACTOR OF TURBULENT FLOW IN AN OPEN CHANNEL

Thesis by

George N. Nomicos

In Partial Fulfillment of the Requirements

For the Degree of

Doctor of Philosophy

California Institute of Technology

Pasadena, California

1956

ACKNOWLEDGMENTS

The writer wishes to express his deep indebtedness and sincere appreciation to his advisor, Dr. Vito A. Vanoni, Professor of Hydraulics, for his helpful guidance and generous assistance throughout the course of this research.

Sincere thanks are due to Professor Norman H. Brooks for his valuable criticism and discussion during the progress of this investigation.

The experimental work was carried out with the aid of U. S. Army Corps of Engineers, Missouri River Division, Contract DA-25-075-eng-3866.

ABSTRACT

An experimental investigation was made of the friction characteristics of streams with sediment load. Measurements of velocity and sediment profiles, and calculations of friction factor, f, and von Karman's constant, k, were made in a 40-foot tilting flume. Several runs were made with uniform flow and various bed configurations using sands of two sizes (.10 mm and .16 mm). For better understanding of the effect of sediment on von Karman's constant k and the friction factor, uniform clear water flows were established on stabilized natural sand beds. The depth and the mean velocity were kept the same as those of the movable bed stream for which the sand bed was stabilized, and a direct comparison was made. Then, by adding loose sand in steps and establishing uniform flow, the change in von Karman's constant and the friction factor with sediment load was studied. It was found that both the friction coefficient f, and von Karman's k, decreased as the sediment load was increased, although the coefficient f decreased by a much smaller percentage than the constant k. It is hypothesized that the sediment load appreciably reduces the rate of turbulent energy diffusion, thus reducing the turbulence level of the fully established uniform flow and changing the balance of turbulence energy.

In a very small region near the bed the turbulent energy production, diffusion, viscous action and dissipation of energy due to sediment in suspension are all of about equal importance. A theoretical study was made of the distribution of both the production of turbulent energy and the dissipation of energy by the sediment along a vertical profile for hydrodynamically smooth beds, and it was made possible to integrate them to the bottom of the stream.

TABLE OF CONTENTS

TABLE OF CONTENTS (Cont'd)

TABLE OF CONTENTS (Cont'd)

TABLE OF CONTENTS (Cont'd)

CHAPTER I

INTRODUCTION AND GENERAL OUTLINE

A. Introduction

In any boundary layer problem the estimation of the wall shearing stress is of great importance and it can not be evaluated without knowing the flow conditions in a layer very close to the boundary.

For laminar boundary layers the theoretical relationships between velocity profile and shear have been worked out satisfactorily. However, for turbulent boundary layers an exact mathematical relationship has not been derived yet. From the basic hydrodynamic equations one may derive relations similar to those of laminar boundary layers using the time averages of the flow quantities. However, an exact calculation of the flow is not possible, because the turbulent transport of the stream properties by turbulent motions is still unknown.

The transfer process shapes the mean-flow field through momentum transfer and supplies the mechanism by which the turbulence energy is withdrawn from the mean-flow field. For this reason the nature of the transfer mechanism should first be investigated thoroughly and mathematical relationships should be expressed for the essential processes in the turbulent motions.

In the last few years various experimental and theoretical investigations bearing on this problem have been carried out. Laufer[1, 2] presented some significant experimental features of flow in a two-dimensional channel and an understanding of the

turbulent energy balance in a fully developed pipe flow. Rannie[3] presented a new and relatively simple theoretical description for the velocity profile at close proximity to the wall for hydrodynamically smooth boundaries, by making an intelligent assumption on the structure of turbulent fluctuations. His analysis gave a very satisfactory agreement between the heat transfer coefficients calculated from his theory and those measured in experiments.

Sediment laden flows behave differently from clear water flows, because the suspended sediment load dissipates turbulent energy by viscous shear in settling. In order to obtain a complete understanding of the turbulent-energy balance, it is necessary to investigate the flow conditions very close to the wall taking into consideration the energy dissipated by the process of transferring and keeping the sediment load in suspension.

Until some satisfactory expressions are derived for the mechanism of the turbulent motions of clear and sediment-laden fluids, the laws for turbulent wall shear must be determined by experimental investigation.

B. General Outline

In the present work a study was made of the friction characteristics of some laboratory streams transporting sediment. The purpose was to investigate the effect of sediment in suspension on the velocity field and the friction factor of an open channel.

Experimentally this was done by establishing a uniform flow in a sediment laden stream with movable bed. Then the

natural sand bed of the above stream was stabilized using chemical grouts, so that there would not be any change in the grain roughness at the surface of the bed. A uniform flow of clear water was established over the stabilized natural sand bed. Keeping the mean depth and velocity the same in this set of two flows a direct comparison of the friction factor was made. Several sets of such experiments were made varying the sediment load of each set and measuring many flow characteristics, like surface and bed profiles, velocity profiles, concentration profiles and friction factors.

No attempt was made experimentally to reveal the structure of the turbulent motions, the nature of the transfer mechanism of the flows, or the effect of suspended sediment on them. However, assuming that Rannie's[3] assumption holds for sediment laden streams, the distribution of turbulent-energy-production along a vertical profile was obtained, for the region in the immediate proximity of the bed.

A function was assumed for the settling velocity of the sediment in the region very close to the wall, such that the settling velocity becomes zero at the level of the bed itself. Thus the differential equation for concentration derived from "Reynolds' Analogy" could then be integrated in the region very close to the bed, satisfying the boundary condition $C = C_o$ at $y = 0$, where C is the sediment concentration and y is the distance from the bed of the stream.

For the region away from the bed, the differential equation for concentration derived from "Reynolds' Analogy" and

von Karman's logarithmic law for the velocity, was integrated. The boundary condition for this equation was taken at the matching point y_1 of Rannie's and von Karman's velocity profiles. The concentration at this point was given by the formula for the region very close to the bed.

From the above formulas the energy dissipation due to suspended sediment was obtained. From this the ratio of the average rate of sediment-energy dissipation to the average rate of turbulent-energy production was calculated. Both von Karman's constant k, and the percentage of change in the friction factor, between a clear water and sediment laden uniform flow were plotted against this calculated ratio.

A large number of experiments with various sizes of sand and flow characteristics are required for the determination of laws and relationships that can express the dependence of the friction factor on the sediment load and the stream characteristics. The experimental work would be reduced only if the complete structure of the turbulent energy were thoroughly understood over the entire profile. Only then could mathematical relationships be derived for the balance of all kinds and forms of the turbulent energy and for the nature of the transfer mechanism. If this could be done, then the effect of sediment load on the flow characteristics could be expressed in a mathematical form.

CHAPTER II

ANALYTICAL CONSIDERATIONS

A. Energy Equation for Turbulent Flow

Since the turbulent energy and its diffusion have a direct effect on the diffusion of sediment and hence on the flow characteristics of sediment laden streams, it was considered useful to derive the total energy and mechanical energy equations for turbulent flows to find the relationship between the different forms of turbulent energy.

From the conservation of energy it is known that:

The rate of increase of internal energy and kinetic energy in a volume element is equal to:

a. The net rate of flow of energy into the element, plus

b. The rate of work done on the fluid by the surface forces, plus

c. The rate of work done on the fluid by the body forces, plus

d. The rate of heat flow into the element.

So that per unit volume we have (in tensor notation):

$$\frac{\partial \rho e}{\partial t} + \frac{\partial}{\partial t}\left(\frac{\rho u_i u_i}{2}\right) = -\frac{\partial}{\partial x_k}(\rho u_k e) - \frac{\partial}{\partial x_k}\left(\rho u_k \frac{u_i u_i}{2}\right) - \frac{\partial}{\partial x_k}(\rho u_k) + \frac{\partial}{\partial x_k}(u_i \sigma_{ik}) + \rho u_i X_i + \frac{\partial}{\partial x_k}\left(K \frac{\partial T}{\partial x_k}\right) \qquad (2.00)$$

where: ρ = mass density of fluid.

e = internal energy of fluid per unit mass

u_i = velocity in x_1, x_2, x_3 direction

x_k = direction x_1, x_2, x_3 (coordinate)

p = pressure intensity

σ_{ik} = shear stress

X_i = body force per unit mass on x_1, x_2, x_3 direction

K = thermal conductivity

T = temperature

t = time

From the continuity equation for compressible flow:

$$\frac{\partial \rho}{\partial t} + \frac{\partial}{\partial x_k}(\rho u_k) = 0$$

Considering the above equation, equation 2.00 may be expressed as:

$$\rho\left[\frac{\partial e}{\partial t} + \frac{\partial}{\partial t}\left(\frac{u_i u_i}{2}\right)\right] = -\rho\left[u_k \frac{\partial e}{\partial x_k} + u_k \frac{\partial}{\partial x_k}\left(\frac{u_i u_i}{2}\right)\right] - \frac{\partial}{\partial x_i}(\rho u_i) + \frac{\partial}{\partial x_k}(u_i \sigma_{ik}) + \rho u_i X_i + \frac{\partial}{\partial x_i}\left(K \frac{\partial T}{\partial x_i}\right) \qquad (2.01)$$

which is the general energy equation for compressible flow.

Assuming incompressibility the continuity equation becomes:

$$\frac{\partial u_i}{\partial x_i} = 0$$

Substituting $u_i = U_i + u_i'$ (where u_i' is the fluctuation component) we get:

$$\frac{\partial (U_i + u_i')}{\partial x_i} = 0 \qquad \text{or} \qquad \frac{\partial U_i}{\partial x_i} + \frac{\partial u_i'}{\partial x_i} = 0$$

Taking the mean we find:

$$\frac{\partial U_i}{\partial x_i} = 0 \qquad \therefore \quad \frac{\partial u_i'}{\partial x_i} = 0$$

without even the mean.

Substituting:

$e = \bar{e} + e'$, $\quad \rho = P + \rho'$, $\quad u_i = U_i + u_i'$, $\quad \sigma_{ik} = \tau_{ik} + \tau_{ik}'$,

$T = T + T'$ in equation 2.01 we get:

$$\rho\left\{\overline{\frac{\partial(\bar{e}+e')}{\partial t}}+\overline{\frac{\partial}{\partial t}\frac{(v_i+u_i')(v_i+u_i')}{2}}\right\}=-\left\{\rho\,\overline{(v_k+u_k')\frac{\partial(\bar{e}+e')}{\partial x_k}}\right.$$

$$\left.+\overline{(v_k+u_k')\frac{\partial}{\partial x_k}\frac{(v_i+u_i')(v_i+u_i')}{2}}\right\}-\overline{\frac{\partial}{\partial x_i}(p+p')(v_i+u_i')}$$

$$+\overline{\frac{\partial}{\partial x_k}\left[(v_i+u_i')(\tau_{ik}+\tau_{ik}')\right]}+\rho\overline{(v_i+u_i')X_i}+\overline{\frac{\partial}{\partial x_i}k\frac{\partial}{\partial x_i}(T+T')}$$

Expanding and putting all terms of first order with respect to the fluctuations equal to zero, we find:

$$\rho\left\{\frac{\partial\bar{e}}{\partial t}+v_k\frac{\partial\bar{e}}{\partial x_k}+\overline{u_k'\frac{\partial e'}{\partial x_k}}\right\}+\frac{\rho}{2}\left\{\frac{\partial v_iv_i}{\partial t}+\frac{\partial\overline{u_i'u_i'}}{\partial t}+v_k\frac{\partial v_iv_i}{\partial x_k}\right.$$

$$\left.+v_k\frac{\overline{\partial u_i'u_i'}}{\partial x_k}+2\overline{u_k'\frac{\partial v_iu_i'}{\partial x_k}}+\overline{u_k'\frac{\partial u_i'u_i'}{\partial x_k}}\right\}=$$

$$=-\left[\frac{\partial}{\partial x_i}(pv_i)+\frac{\partial}{\partial x_i}\overline{(p'u_i')}\right]+\left[\frac{\partial}{\partial x_k}(v_i\tau_{ik})+\frac{\partial}{\partial x_k}\overline{(u_i'\tau_{ik}')}\right]$$

$$+\rho v_iX_i+\frac{\partial}{\partial x_i}\left(k\frac{\partial T}{\partial x_i}\right)$$

Expanding and rearranging terms we get the following after adding and subtracting $v_i\frac{\partial\tau_{ik}^*}{\partial x_k}$ in the second member:

$$\rho\left\{\frac{\partial\bar{e}}{\partial t}+v_k\frac{\partial\bar{e}}{\partial x_k}+\overline{u_k'\frac{\partial e'}{\partial x_k}}\right\}+\rho\left\{\frac{\partial}{\partial t}\left(\frac{v_iv_i}{2}\right)+v_k\frac{\partial}{\partial x_k}\left(\frac{v_iv_i}{2}\right)\right\}$$

$$+\rho\left\{\frac{\partial}{\partial t}\left(\overline{\frac{u_i'u_i'}{2}}\right)+v_k\frac{\partial}{\partial x_k}\left(\overline{\frac{u_i'u_i'}{2}}\right)\right\}+\rho\left\{\overline{u_k'\frac{\partial}{\partial x_k}\left(\frac{u_i'u_i'}{2}\right)}+\overline{u_k'\frac{\partial v_iu_i'}{\partial x_k}}\right\}=$$

$$= -U_i\frac{\partial P}{\partial x_i} + U_i\frac{\partial \tau_{ik}}{\partial x_k} + \rho U_i X_i + U_i\frac{\partial \tau^*_{ik}}{\partial x_k}$$

$$+ \frac{\partial}{\partial x_i}\left(k\frac{\partial T}{\partial x_i}\right) - \overline{\frac{\partial p' u_i'}{\partial x_i}} + \tau_{ik}\frac{\partial U_i}{\partial x_k} \qquad (2.02)$$

$$+ \left[\overline{u_i'\frac{\partial \tau_{ik}'}{\partial x_k}} + \overline{\tau_{ik}'\frac{\partial u_i'}{\partial x_k}}\right] - U_i\frac{\partial \tau^*_{ik}}{\partial x_k}$$

The momentum equation can be written,

$$\rho\left(\frac{\partial u_i}{\partial t} + u_k\frac{\partial u_i}{\partial x_k}\right) = -\frac{\partial p}{\partial x_i} + \rho X_i + \frac{\partial \sigma_{ik}}{\partial x_k}$$

or $$\rho\left(\frac{\partial U_i}{\partial t} + U_k\frac{\partial U_i}{\partial x_k}\right) = -\frac{\partial P}{\partial x_i} + \rho X_i + \frac{\partial \tau^{(R)}_{ik}}{\partial x_k}$$

where: $\tau^{(R)}_{ik} = \tau_{ik} + \tau^*_{ik}$ and $\tau^*_{ik} = -\rho\overline{u_i' u_k'}$

Multiplying by U_1, U_2, U_3 respectively and adding we find

$$\rho\left(U_i\frac{\partial U_i}{\partial t} + U_i U_k\frac{\partial U_i}{\partial x_k}\right) = -U_i\frac{\partial P}{\partial x_i} + \rho U_i X_i + U_i\left(\frac{\partial \tau_{ik}}{\partial x_k} + \frac{\partial \tau^*_{ik}}{\partial x_k}\right)$$

or

$$\rho\left\{\frac{\partial}{\partial t}\left(\frac{U_i U_i}{2}\right) + U_k\frac{\partial}{\partial x_k}\left(\frac{U_i U_i}{2}\right)\right\} =$$

$$= -U_i\frac{\partial P}{\partial x_i} + \rho U_i X_i + U_i\left(\frac{\partial \tau_{ik}}{\partial x_k} + \frac{\partial \tau^*_{ik}}{\partial x_k}\right) \qquad (2.03)$$

Substituting equation 2.03 into equation 2.02 we find:

$$\rho\left\{\frac{\partial \bar{e}}{\partial t}+U_k\frac{\partial \bar{e}}{\partial x_k}+\overline{u_k'\frac{\partial e'}{\partial x_k}}\right\}+\rho\left\{\frac{\partial}{\partial t}\bar{E}+U_k\frac{\partial}{\partial x_k}\bar{E}\right\}$$

$$+\rho\left\{\overline{u_k'\frac{\partial}{\partial x_k}E}+\overline{u_k'\frac{\partial U_i u_i'}{\partial x_k}}\right\}=-\frac{\partial}{\partial x_i}\overline{(p'u_i')} \qquad (2.04)$$

$$+\phi_L+\overline{u_i'\frac{\partial \tau_{ik}'}{\partial x_k}}+\phi_T-U_i\frac{\partial \tau_{ik}^*}{\partial x_k}+\frac{\partial}{\partial x_i}\left(\kappa\frac{\partial T}{\partial x_i}\right)$$

where: $E=\frac{u_i'u_i'}{2}$, $\phi_L=\tau_{ik}\frac{\partial U_i}{\partial x_k}$ and $\phi_T=\overline{\tau_{ik}'\frac{\partial u_i'}{\partial x_k}}$

Expanding the term:

$$\overline{\rho u_k'\frac{\partial U_i u_i'}{\partial x_k}}=\rho\overline{u_k'u_i'}\frac{\partial U_i}{\partial x_k}+\rho U_i\overline{u_k'\frac{\partial u_i'}{\partial x_k}}$$

$$=-\tau_{ik}^*\frac{\partial U_i}{\partial x_k}+\rho U_i\frac{\partial}{\partial x_k}\overline{u_i'u_k'}$$

in which

$$\rho U_i\frac{\partial \overline{u_i'u_k'}}{\partial x_k}=U_i\frac{\partial \overline{\rho u_i'u_k'}}{\partial x_k}=-U_i\frac{\partial \tau_{ik}^*}{\partial x_k}$$

$$\therefore\quad \overline{\rho u_k'\frac{\partial U_i u_i'}{\partial x_k}}=-\tau_{ik}^*\frac{\partial U_i}{\partial x_k}-U_i\frac{\partial \tau_{ik}^*}{\partial x_k}$$

Substituting in equation 2.04 and rearranging terms we get:

$$\rho\left\{\frac{\partial \bar{e}}{\partial t}+U_k\frac{\partial \bar{e}}{\partial x_k}+\overline{u_k'\frac{\partial e'}{\partial x_k}}\right\}-\phi-\frac{\partial}{\partial x_i}\left(\kappa\frac{\partial T}{\partial x_i}\right)+\rho\left\{\frac{\partial \bar{E}}{\partial t}+U_k\frac{\partial \bar{E}}{\partial x_k}\right\}=$$

$$=\tau_{ik}^*\frac{\partial U_i}{\partial x_k}+\overline{u_i'\frac{\partial \tau_{ik}'}{\partial x_k}}-\rho\overline{u_k'\frac{\partial E}{\partial x_k}}-\frac{\partial}{\partial x_i}\overline{p'u_i'} \qquad (2.05)$$

where $\phi = \phi_L + \phi_T = \tau_{ik}\frac{\partial U_i}{\partial x_k} + \overline{\tau'_{ik}\frac{\partial u'_i}{\partial x_k}}$

Expanding further the terms:

$$\overline{u'_i\frac{\partial \tau_{ik}}{\partial x_k}} = \mu\,\overline{u'_i\frac{\partial}{\partial x_k}\left(\frac{\partial u'_i}{\partial x_k}+\frac{\partial u'_k}{\partial x_i}\right)} = \mu\,\overline{u'_i\frac{\partial}{\partial x_k}\left(\frac{\partial u'_i}{\partial x_k}\right)} + \mu\,\overline{u'_i\frac{\partial}{\partial x_k}\left(\frac{\partial u'_k}{\partial x_i}\right)}$$

$$= \mu\left\{\frac{\partial}{\partial x_k}\overline{\left(u'_i\frac{\partial u'_i}{\partial x_k}\right)} - \overline{\left(\frac{\partial u'_i}{\partial x_k}\right)\left(\frac{\partial u'_i}{\partial x_k}\right)}\right\} + \mu\,\overline{u'_i\frac{\partial^2 u'_k}{\partial x_k \partial x_i}}$$

$$= \mu\frac{\partial^2}{\partial x_k \partial x_k}\left(\frac{\overline{u'_i u'_i}}{2}\right) - \mu\overline{\left(\frac{\partial u'_i}{\partial x_k}\right)\left(\frac{\partial u'_i}{\partial x_k}\right)} + \mu\,\overline{u'_i\frac{\partial}{\partial x_i}\left(\frac{\partial u'_k}{\partial x_k}\right)}^{\,0}$$

$$\overline{\frac{\partial \rho' u'_i}{\partial x_i}} = \overline{u'_i\frac{\partial \rho'}{\partial x_i}} + \overline{\rho'\left(\frac{\partial u'_i}{\partial x_i}\right)}^{\,0}$$

$$\overline{\rho u'_k\frac{\partial E}{\partial x_k}} = \rho\frac{\partial}{\partial x_k}\overline{(u'_k E)} - \rho\,\overline{E\left(\frac{\partial u'_k}{\partial x_k}\right)}^{\,0}$$

Consequently, substituting the above expressions in equation 2.05 we find:

$$\rho\left\{\frac{\partial \bar{e}}{\partial t} + U_k\frac{\partial \bar{e}}{\partial x_k} + \overline{u'_k\frac{\partial e'}{\partial x_k}}\right\} - \Phi - \frac{\partial}{\partial x_i}\left(K\frac{\partial T}{\partial x_i}\right) + \rho\frac{\partial \bar{E}}{\partial t}$$

$$+\rho U_k\frac{\partial \bar{E}}{\partial x_k} = \tau^*_{ik}\frac{\partial U_i}{\partial x_k} + \left\{\mu\frac{\partial^2 \bar{E}}{\partial x_k \partial x_k} - \mu\overline{\left(\frac{\partial u'_i}{\partial x_k}\right)\left(\frac{\partial u'_i}{\partial x_k}\right)}\right\}$$

$$-\rho\overline{\frac{\partial u'_k E}{\partial x_k}} - \overline{u'_i\frac{\partial p'}{\partial x_i}}$$

Rearranging terms, we get the general energy equation for incompressible turbulent flow.

$$\rho\left\{\frac{\partial \bar{e}}{\partial t}+U_k\frac{\partial \bar{e}}{\partial x_k}+\overline{u_k'\frac{\partial e'}{\partial x_k}}\right\}-\phi-\nabla\cdot(k\nabla T)+\rho\left(\frac{\partial \bar{E}}{\partial t}+U_k\frac{\partial \bar{E}}{\partial x_k}\right)=$$

$$=\tau_{ik}^{*}\frac{\partial U_i}{\partial x_k}-\mu\overline{\left(\frac{\partial u_i'}{\partial x_k}\right)\left(\frac{\partial u_i'}{\partial x_k}\right)}-\rho\frac{\partial}{\partial x_k}\left[\overline{u_k'\left(E+\frac{p'}{\rho}\right)}\right]+\mu\nabla^2\bar{E} \qquad (2.06)$$

From the Mechanical Energy Equation for incompressible flow, i.e. equation 2.13 derived in the next article:

$$\rho\left(\frac{\partial \bar{E}}{\partial t}+U_k\frac{\partial \bar{E}}{\partial x_k}\right)=\tau_{ik}^{*}\frac{\partial U_i}{\partial x_k}-\mu\overline{\left(\frac{\partial u_i'}{\partial x_k}\right)\left(\frac{\partial u_i'}{\partial x_k}\right)}-\rho\frac{\partial}{\partial x_k}\left[\overline{u_k'\left(E+\frac{p'}{\rho}\right)}\right]+\mu\nabla^2\bar{E}$$

Consequently substituting the above equation into equation 2.06 we get:

$$\rho\left\{\frac{\partial \bar{e}}{\partial t}+U_k\frac{\partial \bar{e}}{\partial x_k}+\overline{u_k'\frac{\partial e'}{\partial x_k}}\right\}=\phi+\nabla\cdot(k\nabla T)$$

or

$$\rho\frac{De}{Dt}=\phi+\nabla\cdot(k\nabla T) \qquad (2.07)$$

where: $e=\bar{e}+e'$, $\frac{D}{Dt}=\frac{\partial}{\partial t}+U_k\frac{\partial}{\partial x_k}$, $E=\frac{u_i'u_i'}{2}$

and

$$\phi=\tau_{ik}\frac{\partial U_i}{\partial x_k}+\overline{\tau_{ik}'\frac{\partial u_i'}{\partial x_k}}=\frac{\mu}{2}\left\{\left(\frac{\partial U_i}{\partial x_k}+\frac{\partial U_k}{\partial x_i}\right)^2+\overline{\left(\frac{\partial u_i'}{\partial x_k}+\frac{\partial u_k'}{\partial x_i}\right)^2}\right\}$$

Equation 2.07 describes the thermodynamical energy law, that the rate of increase of the internal energy e, is equal to the dissipation function ϕ, plus the heat added by conduction.

The same equation is derived in any textbook for equilibrium thermodynamics in a different way. There the flow is considered laminar and the fluid compressible. However in that case the entropy rather than the internal energy appears on the left-hand side member of the equation.

B. Mechanical Energy Equation for Incompressible Flow

The mechanical energy equation is derived from the momentum equation, which can be written in the following form[4]:

$$\rho \frac{\partial u_i}{\partial t} + \rho u_k \frac{\partial u_i}{\partial x_k} = -\frac{\partial p}{\partial x_i} + \rho X_i + \frac{\partial \sigma_{ik}}{\partial x_k}$$

where: σ_{ik} is the instantaneous shear stress:

$$\sigma_{ik} = \mu \left(\frac{\partial u_i}{\partial x_k} + \frac{\partial u_k}{\partial x_i} \right)$$

u_i is the instantaneous velocity component in the x_i direction and $u_i = U_i + u_i'$

After some algebraic manipulations we get:

$$\rho \frac{\partial u_i}{\partial t} + \rho u_k \frac{\partial u_i}{\partial x_k} = -\frac{\partial p}{\partial x_i} + \rho X_i + \mu \nabla^2 u_i \qquad (2.08)$$

Multiplying the three momentum equations 2.08 by u_1, u_2, u_3 respectively and adding we find:

$$\rho u_i \frac{\partial u_i}{\partial t} + u_k u_i \frac{\partial u_i}{\partial x_k} = -u_i \frac{\partial p}{\partial x_i} + \rho u_i X_i + \mu u_i \nabla^2 u_i \qquad (2.09)$$

Now the terms of equation 2.09 may be rewritten as follows:

First of all:

$$u_i \frac{\partial u_i}{\partial t} = \frac{\partial}{\partial t}\left(\frac{u_i u_i}{2}\right),$$

from

$$u_i \frac{\partial u_i}{\partial x_k} = \frac{\partial}{\partial x_k}\left(\frac{u_i u_i}{2}\right) = \frac{1}{2}\frac{\partial}{\partial x_k}(u_i u_i)$$

Multiplying both sides by u_k we get,

$$u_k u_i \frac{\partial u_i}{\partial x_k} = \frac{1}{2} u_k \frac{\partial u_i u_i}{\partial x_k}$$

or

$$\frac{1}{2} u_k \frac{\partial u_i u_i}{\partial x_k} = \frac{1}{2}\frac{\partial u_k u_i u_i}{\partial x_k} - \frac{1}{2} u_i u_i \frac{\partial u_k}{\partial x_k}$$

and from the continuity equation for incompressible flow: $\frac{\partial u_k}{\partial x_k} = 0$

there results:

$$u_k u_i \frac{\partial u_i}{\partial x_k} = \frac{1}{2}\frac{\partial (u_k u_i u_i)}{\partial x_k}$$

Similarly:

$$u_i \frac{\partial p}{\partial x_i} = \frac{\partial u_i p}{\partial x_i} - p \cancel{\frac{\partial u_i}{\partial x_i}}^{\,0}$$

And:

$$u_i \frac{\partial^2 u_i}{\partial x_k \partial x_k} = u_i \frac{\partial}{\partial x_k}\left(\frac{\partial u_i}{\partial x_k}\right) = \frac{\partial}{\partial x_k}\left(u_i \frac{\partial u_i}{\partial x_k}\right) - \left(\frac{\partial u_i}{\partial x_k}\right)\left(\frac{\partial u_i}{\partial x_k}\right)$$

or

$$\frac{\partial}{\partial x_k}\left(u_i \frac{\partial u_i}{\partial x_k}\right) = \frac{\partial}{\partial x_k}\left[\frac{\partial}{\partial x_k}\left(\frac{u_i u_i}{2}\right)\right] = \frac{1}{2}\frac{\partial^2 (u_i u_i)}{\partial x_k \partial x_k}$$

Consequently equation 2.09 becomes:

$$\rho\frac{\partial}{\partial t}\left(\frac{u_i u_i}{2}\right) + \frac{1}{2}\rho\frac{\partial}{\partial x_k}(u_i u_i u_k) = -\frac{\partial}{\partial x_i}(u_i p) + \rho u_i X_i + \frac{\mu}{2}\frac{\partial^2(u_i u_i)}{\partial x_k \partial x_k} - \mu\left(\frac{\partial u_i}{\partial x_k}\right)\left(\frac{\partial u_i}{\partial x_k}\right) \tag{2.10}$$

Introducing the velocity fluctuations: $u_i = U_i + u_i'$ and taking the means the above mechanical energy equation becomes:

$$\rho\frac{\partial}{\partial t}\frac{\overline{(U_i+u_i')(U_i+u_i')}}{2} + \frac{1}{2}\rho\frac{\partial\,\overline{(U_i+u_i')(U_i+u_i')(U_i+u_i')}}{\partial x_k} =$$

$$= \rho\overline{(U_i+u_i')}X_i - \frac{\partial}{\partial x_i}\overline{(P+p')(U_i+u_i')}$$

$$+ \frac{1}{2}\mu\frac{\partial^2}{\partial x_j \partial x_j}\overline{(U_i+u_i')(U_i+u_i')} - \mu\overline{\left(\frac{\partial(U_i+u_i')}{\partial x_j}\right)\left(\frac{\partial(U_i+u_i')}{\partial x_j}\right)}$$

Since the mean value of the terms of first order with respect to turbulent fluctuations are zero, expanding the terms of the above equation one obtains:

$$\rho\left\{\frac{\partial}{\partial t}\left(\frac{U_i U_i}{2}\right) + \frac{\partial}{\partial t}\left(\frac{\overline{u_i' u_i'}}{2}\right)\right\} + \frac{\rho}{2}\left\{\frac{\partial U_i U_i U_k}{\partial x_k} + \frac{2\partial U_i\,\overline{u_i' u_k'}}{\partial x_k} + \frac{\partial U_k\,\overline{u_i' u_i'}}{\partial x_k} + \frac{\partial\,\overline{u_i' u_i' u_k'}}{\partial x_k}\right\} = \rho U_i X_i - \left\{\frac{\partial P U_i}{\partial x_i} + \frac{\partial\,\overline{p' u_i'}}{\partial x_i}\right\} +$$

$$+\tfrac{1}{2}\mu\left\{\frac{\partial^2 U_i U_i}{\partial x_J \partial x_J}+\frac{\partial^2 \overline{u_i' u_i'}}{\partial x_J \partial x_J}\right\}-\mu\left\{\left(\frac{\partial U_i}{\partial x_J}\right)\left(\frac{\partial U_i}{\partial x_J}\right)+\overline{\left(\frac{\partial u_i'}{\partial x_J}\right)\left(\frac{\partial u_i'}{\partial x_J}\right)}\right\}$$

or

$$\rho\left\{\frac{\partial}{\partial t}\left(\frac{U_i U_i}{2}\right)+\frac{\partial}{\partial t}\left(\frac{\overline{u_i' u_i'}}{2}\right)\right\}+\rho\left\{\frac{\partial}{\partial x_K} U_K \frac{U_i U_i}{2}+\frac{\partial}{\partial x_K} U_K \frac{\overline{u_i' u_i'}}{2}\right\}$$

$$+\rho\left\{U_i \frac{\partial \overline{u_i' u_K'}}{\partial x_K}+\overline{u_i' u_K'}\frac{\partial U_i}{\partial x_K}\right\}+\rho\left\{\frac{\partial}{\partial x_K} u_K' \frac{\overline{u_i' u_i'}}{2}\right\}=$$

$$=\rho U_i X_i-\left[\frac{\partial}{\partial x_i} P U_i+\frac{\partial}{\partial x_i}\overline{p' u_i'}\right]+\mu\left[\frac{\partial^2 \frac{U_i U_i}{2}}{\partial x_J \partial x_J}+\frac{\partial^2 \frac{\overline{u_i' u_i'}}{2}}{\partial x_J \partial x_J}\right]$$

$$-\mu\left\{\left(\frac{\partial U_i}{\partial x_J}\right)\left(\frac{\partial U_i}{\partial x_J}\right)+\overline{\left(\frac{\partial u_i'}{\partial x_J}\right)\left(\frac{\partial u_i'}{\partial x_J}\right)}\right\}$$

Replacing $-\rho\overline{u_i' u_J'}$ by τ_{iJ}^*, the mechanical energy equation becomes:

$$\rho\left\{\frac{\partial}{\partial t}\left(\frac{U_i U_i}{2}\right)+\frac{\partial}{\partial t}\left(\frac{\overline{u_i' u_i'}}{2}\right)\right\}+\rho\frac{\partial}{\partial x_K}\left\{U_K\left(\frac{U_i U_i}{2}+\frac{\overline{u_i' u_i'}}{2}\right)\right\}-\left(U_i\frac{\partial \tau_{iK}^*}{\partial x_K}+\tau_{iK}^*\frac{\partial U_i}{\partial x_K}\right)$$

$$+\rho\frac{\partial}{\partial x_K}\overline{u_K'\frac{u_i' u_i'}{2}}=\rho U_i X_i-\frac{\partial}{\partial x_K}\left[P U_K+\overline{p' u_K'}\right]+$$

$$+\mu\frac{\partial^2}{\partial x_J \partial x_J}\left(\frac{U_i U_i}{2}+\frac{\overline{u_i' u_i'}}{2}\right)-\mu\left\{\left(\frac{\partial U_i}{\partial x_J}\frac{\partial U_i}{\partial x_J}\right)+\left(\overline{\frac{\partial u_i'}{\partial x_J}\frac{\partial u_i'}{\partial x_J}}\right)\right\}$$

Rearranging terms, and putting $\frac{\partial}{\partial x_K}(PU_K) = U_K\frac{\partial P}{\partial x_K} + P\left(\frac{\partial U_K}{\partial x_K}\right)^{0}$

$$\rho\frac{\partial}{\partial t}\left(\frac{U_i U_i}{2}\right)+\rho\frac{\partial}{\partial x_K}\left(U_K\frac{U_i U_i}{2}\right)+\rho\frac{\partial}{\partial t}\left(\frac{\overline{u_i' u_i'}}{2}\right)+\rho\frac{\partial}{\partial x_K}\left(U_K\frac{\overline{u_i' u_i'}}{2}\right)=$$

$$=\tau_{iK}^{*}\frac{\partial U_i}{\partial x_K}-\rho\frac{\partial}{\partial x_K}\left\{\overline{u_K'\left(\frac{u_i' u_i'}{2}+\frac{p'}{\rho}\right)}\right\}+\mu\frac{\partial^2\left(\frac{\overline{u_i' u_i'}}{2}\right)}{\partial x_J \partial x_J} \qquad (2.11)$$

$$-\mu\overline{\left(\frac{\partial u_i'}{\partial x_J}\right)\left(\frac{\partial u_i'}{\partial x_J}\right)}+U_i\frac{\partial \tau_{iK}^{*}}{\partial x_K}+\rho U_i X_i-U_K\frac{\partial P}{\partial x_K}$$

$$+\mu\frac{\partial^2}{\partial x_J \partial x_J}\left(\frac{U_i U_i}{2}\right)-\mu\left(\frac{\partial U_i}{\partial x_J}\right)\left(\frac{\partial U_i}{\partial x_J}\right)$$

The equation for the shear stress is

$$\tau_{iK}=\mu\left(\frac{\partial U_i}{\partial x_K}+\frac{\partial U_K}{\partial x_i}\right)$$

Differentiating τ_{iK} with respect to x_K and multiplying by U_i we get: (assuming μ = constant)

$$U_i \frac{\partial}{\partial x_K} \tau_{iK} = U_i \mu \frac{\partial}{\partial x_K}\left(\frac{\partial U_i}{\partial x_K} + \frac{\partial U_K}{\partial x_i}\right)$$

$$= \mu U_i \frac{\partial^2 U_i}{\partial x_K \partial x_K} + \mu U_i \frac{\partial^2 U_K}{\partial x_i \partial x_K}$$

$$= \mu\left\{\frac{\partial^2}{\partial x_K \partial x_K}\left(\frac{U_i U_i}{2}\right) - \frac{\partial U_i}{\partial x_K}\frac{\partial U_i}{\partial x_K}\right\} + \mu U_i \frac{\partial}{\partial x_i}\left(\frac{\partial U_K}{\partial x_K}\right)^{0}$$

Consequently from the above equation and equation 2.03, equation 2.11 for the mechanical energy is reduced to:

$$\rho \frac{\partial}{\partial t}\left(\overline{\frac{u_i' u_i'}{2}}\right) + \rho \frac{\partial}{\partial x_K}\left(U_K \overline{\frac{u_i' u_i'}{2}}\right) = \tau_{iK}^{*} \frac{\partial U_i}{\partial x_K} - \rho \frac{\partial}{\partial x_K}\overline{\left[u_K'\left(\frac{u_i' u_i'}{2} + \frac{p'}{\rho}\right)\right]} \qquad (2.12)$$

$$+ \mu \frac{\partial^2}{\partial x_J \partial x_J}\left(\overline{\frac{u_i' u_i'}{2}}\right) - \mu \overline{\left(\frac{\partial u_i'}{\partial x_J}\right)\left(\frac{\partial u_i'}{\partial x_J}\right)}$$

Rearranging terms and calling $E = \frac{u_i' u_i'}{2}$ we get[5, 6]:

$$\rho\left\{\frac{\partial \bar{E}}{\partial t} + \frac{\partial}{\partial x_K}(U_K \bar{E})\right\} = \tau_{iK}^{*} \frac{\partial U_i}{\partial x_K} - \mu \overline{\left(\frac{\partial u_i'}{\partial x_J}\right)\left(\frac{\partial u_i'}{\partial x_J}\right)} \qquad (2.13)$$

$$- \rho \frac{\partial}{\partial x_K}\overline{\left[u_K'\left(E + \frac{p'}{\rho}\right)\right]} + \mu \nabla^2 \bar{E}$$

Equation 2.13 was first given by von Karman in reference 5. It describes the variation of turbulent energy $\overline{E}$ and is properly called a mechanical energy law as distinguished from the thermodynamic energy law, equation 2.07.

The first term of the right-hand side of equation 2.13 represents the rate at which energy is produced by the turbulent shear stresses. The second represents the rate at which turbulent energy is dissipated by viscous action, and the third term represents the so-called diffusion part of the energy, which is the rate at which turbulent energy is transferred by diffusion.

It is clear that for uniform flow the total variation of the turbulent energy is zero. Consequently the turbulent energy produced is equal to the part which is dissipated plus the part which is diffused. In non-tensor notation equation 2.13 is written as follows:

$$\rho\left(\frac{\partial \overline{E}}{\partial t} + U\frac{\partial \overline{E}}{\partial x} + V\frac{\partial \overline{E}}{\partial y} + W\frac{\partial \overline{E}}{\partial z}\right) =$$

Rate of Total Variation of Turbulent Energy

$$= \tau^*_{xx}\frac{\partial U}{\partial x} + \tau^*_{yy}\frac{\partial V}{\partial y} + \tau^*_{zz}\frac{\partial W}{\partial z} + \tau^*_{xy}\left(\frac{\partial U}{\partial y} + \frac{\partial V}{\partial x}\right)$$

$$+ \tau^*_{xz}\left(\frac{\partial U}{\partial z} + \frac{\partial W}{\partial x}\right) + \tau^*_{yz}\left(\frac{\partial V}{\partial z} + \frac{\partial W}{\partial y}\right)$$

Rate of Energy Withdrawn from Basic Flow or Turbulent Energy Production

$$-\mu\left\{\overline{\left(\frac{\partial u'}{\partial x}\right)^2} + \overline{\left(\frac{\partial u'}{\partial y}\right)^2} + \overline{\left(\frac{\partial u'}{\partial z}\right)^2} + \overline{\left(\frac{\partial v'}{\partial x}\right)^2} + \overline{\left(\frac{\partial v'}{\partial y}\right)^2} +\right.$$

$$+\overline{\left(\frac{\partial v'}{\partial z}\right)^2}+\overline{\left(\frac{\partial w'}{\partial x}\right)^2}+\overline{\left(\frac{\partial w'}{\partial y}\right)^2}+\overline{\left(\frac{\partial w'}{\partial z}\right)^2}\Bigg\}$$

Rate of Dissipation of Turbulent Energy

$$-\rho\left\{\frac{\partial}{\partial x}\overline{u'\left(E+\frac{p'}{\rho}\right)}+\frac{\partial}{\partial y}\overline{v'\left(E+\frac{p'}{\rho}\right)}+\frac{\partial}{\partial z}\overline{w'\left(E+\frac{p'}{\rho}\right)}\right\}$$

$$+\mu\left(\frac{\partial^2\bar{E}}{\partial x^2}+\frac{\partial^2\bar{E}}{\partial y^2}+\frac{\partial^2\bar{E}}{\partial z^2}\right)$$

Rate of Diffusion of Turbulent Energy

Table 1 gives a summary of the energy equations derived in this chapter, articles A and B.

Table 1

Summary of energy equations

1.- COMPRESSIBLE FLOW

$$\rho\left\{\frac{\partial e}{\partial t}+\frac{\partial}{\partial t}\left(\frac{u_i u_i}{2}\right)\right\}=-\rho\left\{u_\kappa\frac{\partial e}{\partial x_\kappa}+u_\kappa\frac{\partial}{\partial x_\kappa}\left(\frac{u_i u_i}{2}\right)\right\}-\frac{\partial p u_i}{\partial x_i}+\frac{\partial u_i \sigma_{i\kappa}}{\partial x_\kappa}+\rho u_i X_i+\frac{\partial}{\partial x_i}\left(\kappa\frac{\partial T}{\partial x_i}\right)$$

Where: $e=\bar{e}+e'$, $u_i=U_i+u_i'$, $\sigma_{i\kappa}=\tau_{i\kappa}+\tau_{i\kappa}'$, $p=P+p'$, $T=\bar{T}+T'$

2.- INCOMPRESSIBLE FLOW

$$\rho\left\{\frac{\partial\bar{e}}{\partial t}+U_\kappa\frac{\partial\bar{e}}{\partial x_\kappa}+\overline{u_\kappa'\frac{\partial e'}{\partial x_\kappa}}\right\}-\left\{\tau_{i\kappa}\frac{\partial U_i}{\partial x_\kappa}+\overline{\tau_{i\kappa}'\frac{\partial u_i'}{\partial x_\kappa}}\right\}-\frac{\partial}{\partial x_i}\left(\kappa\frac{\partial T}{\partial x_i}\right)+\rho\left\{\frac{\partial\bar{E}}{\partial t}+U_\kappa\frac{\partial\bar{E}}{\partial x_\kappa}\right\}+\rho\overline{u_i'u_\kappa'}\frac{\partial U_i}{\partial x_\kappa}+\mu\overline{\frac{\partial u_i'}{\partial x_\kappa}\cdot\frac{\partial u_i'}{\partial x_\kappa}}+\rho\frac{\partial}{\partial x_\kappa}\left\{\overline{u_\kappa'\left(E+\frac{p'}{\rho}\right)}\right\}-\mu\nabla^2\bar{E}=0$$

3.- MECHANICAL ENERGY FOR INCOMPRESSIBLE FLOW

$$\rho\left\{\frac{\partial\bar{E}}{\partial t}+U_\kappa\frac{\partial\bar{E}}{\partial x_\kappa}\right\}=-\rho\overline{u_i'u_\kappa'}\frac{\partial U_i}{\partial x_\kappa}-\mu\overline{\frac{\partial u_i'}{\partial x_\kappa}\cdot\frac{\partial u_i'}{\partial x_\kappa}}-\rho\frac{\partial}{\partial x_\kappa}\left\{\overline{u_\kappa'\left(E+\frac{p'}{\rho}\right)}\right\}+\mu\nabla^2\bar{E}$$

4.- NON-TENSOR NOTATION OF 3

$$\rho\left\{\frac{\partial\bar{E}}{\partial t}+U\frac{\partial\bar{E}}{\partial x}+V\frac{\partial\bar{E}}{\partial y}+W\frac{\partial\bar{E}}{\partial z}\right\}=$$

TOTAL VARIATION OF TURB. ENERGY

$$=-\rho\left\{\overline{u'^2}\frac{\partial U}{\partial x}+\overline{v'^2}\frac{\partial V}{\partial y}+\overline{w'^2}\frac{\partial W}{\partial z}+\overline{u'v'}\left(\frac{\partial U}{\partial y}+\frac{\partial V}{\partial x}\right)+\overline{u'w'}\left(\frac{\partial U}{\partial z}+\frac{\partial W}{\partial x}\right)+\overline{v'w'}\left(\frac{\partial V}{\partial z}+\frac{\partial W}{\partial y}\right)\right\}-$$ TURB. ENERGY PRODUCTION

$$-\mu\left\{\overline{\left(\frac{\partial u'}{\partial x}\right)^2}+\overline{\left(\frac{\partial u'}{\partial y}\right)^2}+\overline{\left(\frac{\partial u'}{\partial z}\right)^2}+\overline{\left(\frac{\partial v'}{\partial x}\right)^2}+\overline{\left(\frac{\partial v'}{\partial y}\right)^2}+\overline{\left(\frac{\partial v'}{\partial z}\right)^2}+\overline{\left(\frac{\partial w'}{\partial x}\right)^2}+\overline{\left(\frac{\partial w'}{\partial y}\right)^2}+\overline{\left(\frac{\partial w'}{\partial z}\right)^2}\right\}-$$ TURB. ENERGY DISSIPATION

$$-\rho\left\{\frac{\partial}{\partial x}\overline{u'\left(E+\frac{p'}{\rho}\right)}+\frac{\partial}{\partial y}\overline{v'\left(E+\frac{p'}{\rho}\right)}+\frac{\partial}{\partial z}\overline{w'\left(E+\frac{p'}{\rho}\right)}\right\}+\mu\left\{\frac{\partial^2\bar{E}}{\partial x^2}+\frac{\partial^2\bar{E}}{\partial y^2}+\frac{\partial^2\bar{E}}{\partial z^2}\right\}$$ TURB. ENERGY DIFFUSION

C. Sediment Transport

1. General Case of Incompressible Fluid

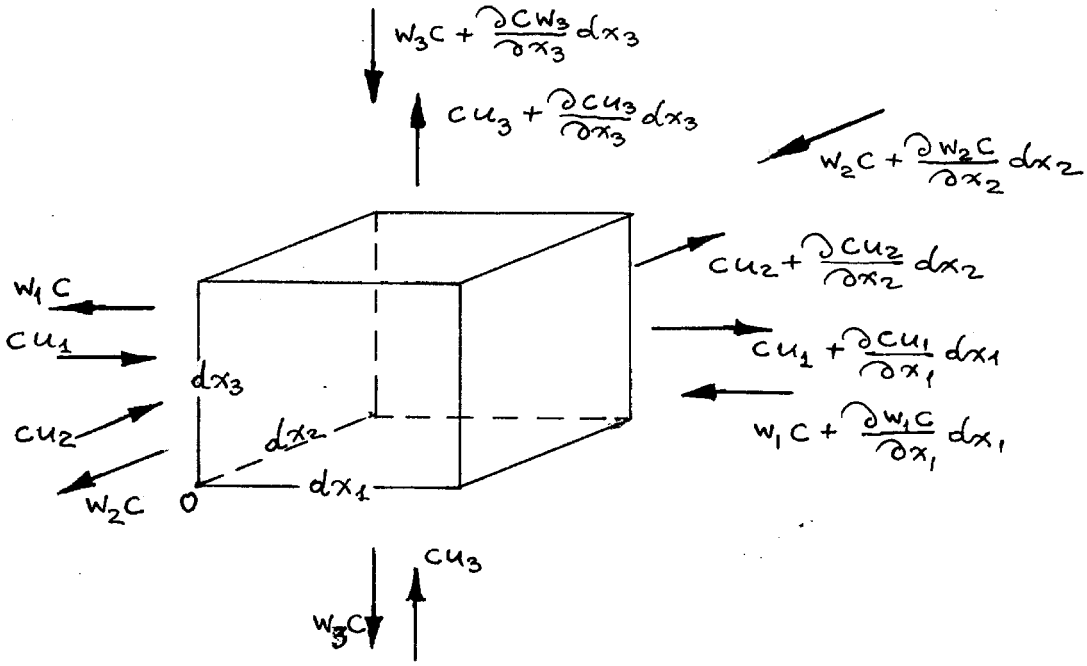

From conservation of matter, the rate of increase of concentration in a volume element is equal to:

The net rate of flow of particles into the element due to the fluid flow, plus

The net rate due to settling velocity.

So that per unit volume we have, (using tensor notation)

$$\frac{\partial c}{\partial t} = -\frac{\partial cu_i}{\partial x_i} + \frac{\partial w_i c}{\partial x_i}$$

or

$$\frac{\partial c}{\partial t} = -\frac{\partial}{\partial x_i} c(u_i - w_i)$$

where: $c = C + c'$, $u_i = U_i + u_i'$, $w_i = W_i + w_i'$

w_i is the settling velocity, and is positive in negative direction $(-x_i)$

C is the concentration of particles

w_i' & c' are the fluctuating components of w_i & C.

Substituting the expressions for c, u_i & w_i into the above equation,

$$\frac{\partial}{\partial t}\overline{(C+c')} + \frac{\partial \overline{(C+c')(U_i+u_i')}}{\partial x_i} = \frac{\partial \overline{(W+w_i')(C+c')}}{\partial x_i}$$

Expanding and putting equal to zero all the terms in first order with respect to the fluctuation,

i.e. $\frac{\partial \overline{c'}}{\partial t} = 0$ $\frac{\partial U_i \overline{c'}}{\partial x_i} = 0$ $\frac{\partial C\overline{u_i'}}{\partial x_i} = 0$

$\frac{\partial W_i \overline{c'}}{\partial x_i} = 0$ $\frac{\partial C\overline{w_i'}}{\partial x_i} = 0$

we find:

$$\frac{\partial C}{\partial t} + \frac{\partial C U_i}{\partial x_i} + \frac{\partial \overline{c'u_i'}}{\partial x_i} = \frac{\partial W_i C}{\partial x_i} + \frac{\partial \overline{w_i'c'}}{\partial x_i}$$

or $$\frac{\partial C}{\partial t} + U_i\frac{\partial C}{\partial x_i} + \frac{\partial \overline{c'u_i'}}{\partial x_i} = W_i\frac{\partial C}{\partial x_i} + C\frac{\partial W_i}{\partial x_i} + \frac{\partial \overline{w_i'c'}}{\partial x_i}$$

From the definition of the diffusion coefficient:

$$-\overline{c'u_i'} = \varepsilon_{①}\frac{\partial C}{\partial x_i}$$

where: The subscript of the diffusion coefficient ε (in a circle) has not the meaning of repetition. Since the correlation between w' and c' is negligible, $\overline{w'c'} \approx 0$ and

$$\frac{\partial C}{\partial t} + U_i \frac{\partial C}{\partial x_i} - \frac{\partial}{\partial x_i}\left(\varepsilon_{(i)} \frac{\partial C}{\partial x_i}\right) = W_i \frac{\partial C}{\partial x_i} + C \frac{\partial W_i}{\partial x_i} \qquad (2.15)$$

This is the equation of diffusion in tensor notation where the subscript of ε (in a circle) has not the meaning of repetition. $w_i = W_i + w_i'$ is the fall velocity, which is positive in the direction of negative coordinates.

2. Steady Incompressible 2-Dimensional Case

Calling from now on c and w the time averages of the concentration and fall velocity respectively we have in the case of steady incompressible two-dimensional flow, (y being the vertical coordinate):

$$\frac{\partial c}{\partial t} = 0 \,, \quad \frac{\partial c}{\partial x} = 0 \,, \quad \frac{\partial c}{\partial z} = 0 \,, \quad \frac{\partial U}{\partial x} = 0 \,, \quad \frac{\partial w}{\partial y} \neq 0$$

$$U_1 = U \neq 0 \,, \quad U_2 = U_3 = 0 \,, \quad w_x = w_z = 0 \,, \quad w_i = w_y = W \neq 0$$

Equation 2.15 then becomes:

$$\frac{\partial \overline{c'u_i'}}{\partial x_i} = w \frac{\partial c}{\partial y} + c \frac{\partial w}{\partial y}$$

$$-\frac{\partial}{\partial x}\left(\varepsilon_x \frac{\partial c}{\partial x}\right)^{0} - \frac{\partial}{\partial y}\left(\varepsilon_y \frac{\partial c}{\partial y}\right) - \frac{\partial}{\partial z}\left(\varepsilon_z \frac{\partial c}{\partial z}\right)^{0} = \frac{\partial}{\partial y}(wc)$$

$$-\frac{\partial}{\partial y}\left(\varepsilon_y \frac{\partial c}{\partial y}\right) = \frac{\partial}{\partial y}(wc) \qquad \text{or} \qquad \frac{\partial}{\partial y}(\overline{c'v'}) = \frac{\partial}{\partial y}(wc)$$

Integrating we find:

$$-\varepsilon_y \frac{\partial c}{\partial y} = wc + \text{constant} \qquad \text{or} \qquad \overline{c'v'} = wc + \text{constant}$$

where the constant is equal to zero, because the flux of the particles going up should be equal to those going down through any surface.

Introducing that the constant is zero we have:

$$\varepsilon_y \frac{\partial c}{\partial y} + wc = 0 \qquad \text{or} \qquad \overline{c'v'} = wc \tag{2.16}$$

This equation is given in reference 12.

For the boundary condition of this differential equation (2.16) it might be assumed that for $y = 0$ the concentration $C = C_o$ = density at the bed.

D. Velocity Profile

The flow field has been considered as consisting of two regions, one very close to the bed, and the other away from the bed.

1. Region I, Very Close to the Bed (Smooth)

For the velocity fluctuations very close to a hydrodynamically smooth wall, Rannie[3] has suggested the relation,

$$-\overline{u'v'} = \kappa_1^2 u^2$$

For shear stress τ = constant in this region:

$$u_*^2 = \kappa_1^2 u^2 + \nu \frac{du}{dy} \qquad \text{where:} \qquad u_* = \sqrt{\frac{\tau_o}{\rho}} = \sqrt{\frac{\tau}{\rho}}$$

or

$$\nu \frac{du}{dy} + \kappa_1^2 u^2 = u_*^2 \tag{2.17}$$

with the boundary condition $u=0$ at $y=0$.

The solution is: $$\frac{u}{u_*} = \frac{1}{\kappa_1} \tanh \kappa_1 y^* \tag{2.18}$$

where $y^* = y \frac{u_*}{\nu}$

And the derivative is: $$\frac{du}{dy^*} = u_* \operatorname{sech}^2 \kappa_1 y^* \tag{2.19}$$

2. Region II Away from the Bed

For the velocity fluctuations in the region away from the wall, Prandtl and von Karman[4] suggested the following:

a. Prandtl's assumption:

$$-\overline{u'v'} = \frac{\tau}{\rho} = \kappa^2 y^2 \left(\frac{du}{dy}\right)^2$$

von Karman's assumption:

$$-\overline{u'v'} = \frac{\tau}{\rho} = \kappa^2 \frac{\left(du/dy\right)^4}{\left(d^2u/dy^2\right)^2}$$

Assuming constant shear stress $\tau=\tau_o$ one obtains:

$$\frac{du}{dy} = \frac{u_*}{\kappa y} \tag{2.20}$$

which is the so-called experimental law of the wall. This also represents a universal turbulent boundary layer flow.

The solution of the above equation is:

$$\frac{u}{u_*} = \frac{1}{\kappa} \ln y^* + B \tag{2.21}$$

where B is constant.

It should be noted that if we assume linear distribution of the shear $\tau = \tau_0\left(1 - \frac{y}{r}\right)$, the solutions of both Prandtl's and von Karman's assumptions for the velocity profiles are not simple and do not fit the experimental data better than the simple law (equation 2.21).

b. For the intermediate region, neither far away from, nor close to the wall, one considers the viscosity of the fluid, so that:

$$\frac{\tau_0}{\rho} = -\overline{u'v'} + \nu \frac{du}{dy} \tag{2.22}$$

Substituting $-\overline{u'v'} = \kappa^2 y^2 \left(\frac{du}{dy}\right)^2$ we get the equation:

$$\kappa^2 y^2 \left(\frac{du}{dy}\right)^2 + \nu \frac{du}{dy} = u_*^2$$

Solving for $\frac{du}{dy}$ and expanding the solution in power series:

$$\frac{du}{dy} = \frac{u_*}{\kappa y} - \frac{\nu}{2\kappa^2 y^2} + \frac{\nu^2}{8 u_* (\kappa y)^3} \cdots$$

$$\text{or} \quad \frac{du}{dy^*} = u_* \left(\frac{1}{\kappa y^*} - \frac{1}{2(\kappa y^*)^2} + \frac{1}{8(\kappa y^*)^3} \cdots \right) \tag{2.23}$$

Integrating we find:

$$\frac{u}{u_*} = \frac{1}{\kappa} \ln y^* + B + \frac{1}{2\kappa^2 y^*} - \frac{1}{4^2 \kappa^3 y^{*2}} \cdots \tag{2.24}$$

It is obvious that the constant B is the same as that of Region II because the terms $\frac{1}{2\kappa^2 y^*} - \frac{1}{4^2 \kappa^3 y^{*2}} - \cdots$ become quite negligible for large values of y^*.

E. Sediment Concentration Profile

From physical considerations and from experimental measurements it is known that the concentration is a continuous function of the distance from the bed y, and increases when y decreases. Since the concentration at $y = 0$ is equal to the density of the sediment resting on the bed, it is deduced that the maximum value of the concentration is at the bed and is equal to the bed density. From experimental measurements[15] it is known that the settling velocity should be a continuous function of the concentration. Consequently the fall velocity will be a continuous function of the distance from the bed.

The theoretical or experimental determination of the above function, $w = w(c)$, will give a formula which for each grain size will go to zero at the bed elevation where $y = 0$. In the experiments of this work the grain size of the sands used was uniform enough to consider the material to be of a single size. Qualitatively the concentration and fall velocity profiles will be of the form shown in fig. 1. It is obvious that the fall velocity decreases

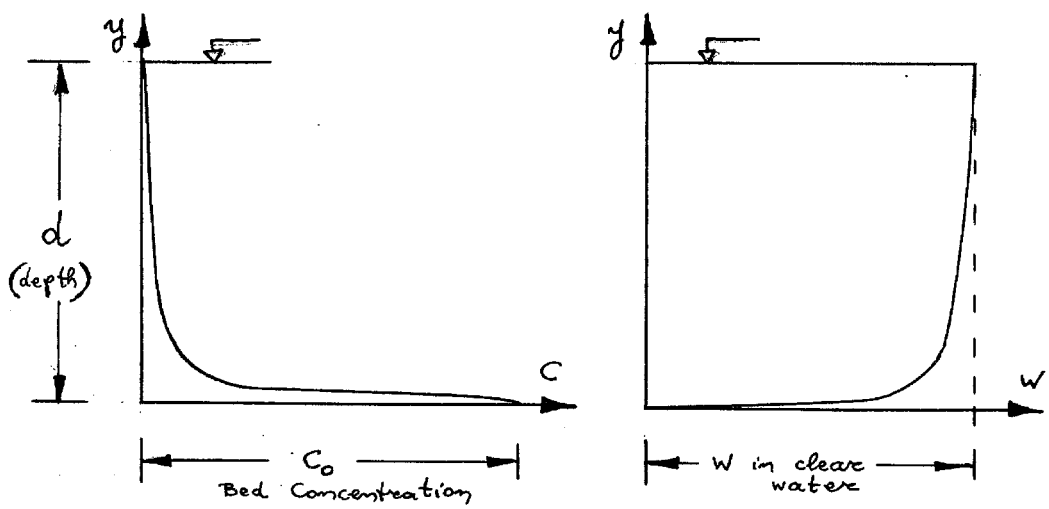

Fig. 1. - Qualitative diagram of the concentration and fall velocity profile

with the depth due to hindered settling from the increase of the concentration.

All the experimental measurements for the main region of flow away from the bed fit reasonably well the theory which has been derived considering a constant fall velocity in equation 2.16. This constant velocity is actually taken to be equal to a reduced value due to hindered settling for the average concentration all over the main region of the flow, as it is outlined in Chapter IV, article D, 2.

However in the very small region at the bed proximity, a mathematical treatment with an average constant fall velocity, gives a singularity at $y = 0$ with infinite concentration at the bed. It is very interesting to mention that if one considers that w = constant and the logarithmic velocity profile is extrapolated to $y = 0$, then even the average concentration for the vertical profile becomes infinity for all the values of $\frac{w}{\beta \kappa u_*} \geq 1$.

On the other hand, it would be very difficult to find or check experimentally any formula for the settling velocity from the concentration profile in such a small region, which actually is of the order of magnitude of the thickness of the so-called laminar sublayer.

From the above discussion it seems reasonable to assume that the settling velocity can be approximated by a continuous function which has the following property: it is almost constant in the region away from the bed and decreases rapidly in the very small region at the bed proximity, becoming equal to zero

at the bed.

A relation was assumed with the above properties such that:

(i) The differential equation for sediment concentration would be easy to integrate in the very small region near the bed.

(ii) The concentration at $y = 0$ would be finite.

(iii) The concentration would approach asymptotically the profile computed for constant fall velocity in the main region of the flow away from the bed, which has already been checked experimentally.

An assumption for w which has been tried and has the above properties is:

$$w = w_o \tanh^n \kappa_1 y^* \tag{2.25}$$

Since κ_1 is of the order $\frac{1}{10}$ and y^* is equal to $y \frac{u_*}{\nu}$, it is obvious that even when the exponent n is of the order 10, the settling velocity w becomes equal to approximately a constant w_o for $y^* > 50$. The thickness of the so-called laminar sublayer corresponds to $y^* = 11.6$.

From the above it is obvious that by computing the exponent n of each particular case in such a way that the concentration profile would satisfy the condition $c = c_o$ at $y = 0$ and $c = c_{md}$ at $y = \frac{d}{2}$, then for $y > 50$ the concentration profile agrees very well with that given by the simplest formula for sediment concentration:

$$\frac{c}{c_{md}} = \left(\frac{d-y}{y}\right)^{z_o}$$

where d is the depth and $z_o = \frac{w_o}{\beta \kappa u_*}$

This corresponds to using $w = w_o =$ constant.

1. Region I, Very Close to the Bed

Assuming that Rannie's hypothesis holds: $-\overline{u'v'} = \kappa_1^2 u^2$,

equation 2.17 gives:

$$u = \frac{u_*}{\kappa_1} \tanh \kappa_1 y^*$$

and its derivative with respect to y is:

$$\frac{du}{dy} = \frac{u_*^2}{\nu} \operatorname{sech}^2 \kappa_1 y^* \tag{2.26}$$

From: $-\overline{u'v'} = \kappa_1^2 u^2 = u_*^2 \tanh^2 \kappa_1 y^*$ one obtains,

$$-\frac{\overline{u'v'}}{du/dy} = \nu \sinh^2 \kappa_1 y^*$$

Assuming that "Reynolds' Analogy" holds, it follows that:

$$-\frac{\overline{u'v'}}{du/dy} = \varepsilon_m \,, \qquad -\frac{\overline{c'v'}}{dc/dy} = \varepsilon_s$$

and

$$\beta \frac{\overline{u'v'}}{du/dy} = \frac{\overline{c'v'}}{dc/dy} \tag{2.27}$$

$$\beta \varepsilon_m = \varepsilon_s$$

where $\beta \simeq 1$.

Thus the differential equation for sediment concentration, equation 2.16, becomes:

$$\beta \nu \sinh^2 \kappa_1 y^* \frac{dc}{dy} + wc = 0$$

or:

$$\frac{dc}{c} = \frac{-w\,dy}{\beta \nu \sinh^2 \kappa_1 y^*} \tag{2.28}$$

where $w = w(c)$.

Assuming that $w = w(y)$ we make the solution of the differential equation easier. Substituting equation 2.25 for w in equation 2.28 one obtains

$$\frac{dc}{c} = -\frac{w_o \tanh^n K_1 y^*}{\beta \nu \sinh^2 K_1 y^*}\, dy$$

Integrating we find:

$$\frac{c}{c_o} = e^{-\frac{\Im_1}{n-1}\tanh^{n-1} K_1 y^*} \qquad (2.29)$$

where $c_o = c_{bed}$ is the concentration at $y^* = 0$,

$$\Im_1 = \frac{w_o}{\beta K_1 u_*}$$

2. Region II Away from the Bed

a. Universal Turbulent Boundary Layer Flow and Linear Shear Distribution

From the so-called experimental law of the wall, or universal turbulent boundary layer flow we have that: (ref. 7)

$$\frac{du}{dy} = \frac{u_*}{\kappa y} \qquad (2.20)$$

For linear shear distribution:

$$-\overline{u'v'} = u_*^2 (1 - y/h)$$

or

$$-\frac{\overline{u'v'}}{du/dy} = \frac{u_*^2}{du/dy}(1 - y/h) = u_* \kappa y (1 - y/h)$$

Assuming that the "Reynolds' Analogy" holds: $\varepsilon_s = \beta \varepsilon_m$ where $\beta \simeq 1$ and

$$\frac{\overline{c'v'}}{dc/dy} = \beta \frac{\overline{u'v'}}{du/dy}$$

Thus the differential equation for sediment concentration, equation 2.16 becomes:

$$\beta u_* \kappa y \left(1 - \frac{y}{R}\right) \frac{dc}{dy} + wc = 0$$

or:

$$\frac{dc}{c} = - \frac{w dy}{\beta u_* \kappa y (1 - y/R)} \qquad (2.30)$$

where $w = w(c)$.

It should be noted that for the velocity profile the universal boundary layer flow or law of the wall was applied, $\frac{du}{dy} = \frac{u_*}{\kappa y}$ (which can also be derived from Prandtl's or Karman's assumption with constant shear), and for the concentration profile the shear was considered linearly distributed.

Substituting equation 2.25 for w in equation 2.30 one obtains

$$\frac{dc}{c} = - \frac{w_o}{\beta \kappa u_*} \frac{\tanh^n \kappa_1 y^*}{y(1 - y/R)} dy$$

Integrating we find:

$$\ln \frac{c}{c_a} = - \frac{w_o}{\beta \kappa u_*} \left\{ \int_{\omega_a}^{\omega_y} \frac{\tanh^n \omega}{\omega} d\omega + \int_{\omega_a}^{\omega_y} \frac{\tanh^n \omega}{\kappa_1 R^* - \omega} d\omega \right\} \qquad (2.31)$$

where $\omega = \kappa_1 y^*$.

Since $\omega > 1$ we can try to integrate by expanding $\tanh^n \omega$ in asymptotic series.

$$\tanh^n \omega = \left(1 - \frac{2}{e^{2\omega}} + \frac{2}{e^{4\omega}} - \frac{2}{e^{6\omega}} + \ldots\right)^n$$

$$\tanh^n \omega \simeq 1 - \frac{2n}{e^{2\omega}} + \frac{2n^2}{e^{4\omega}} - \ldots\ldots$$

And the above integral equation 2.31 is approximated by:

$$\ln \frac{c}{c_a} \simeq -\frac{w_o}{\beta K u_*} \left\{ \int_{\omega_a}^{\omega_y} \left(\frac{1}{\omega} - \frac{2n}{\omega} e^{-2\omega} + \frac{2n^2}{\omega} e^{-4\omega} \ldots\ldots + \right.\right.$$

$$\left.\left. + \frac{1}{K_1 R^* - \omega} - \frac{2n}{K_1 R^* - \omega} e^{-2\omega} + \frac{2n^2}{K_1 R^* - \omega} e^{-4\omega} \ldots\ldots \right) d\omega \right\}$$

which when integrated becomes:

$$\ln \frac{c}{c_a} \simeq \ln \left(\frac{K_1 R^* - K_1 y^*}{K_1 y^*} \right)^{\beta_0} \Bigg|_{a^*}^{y^*} + 2n\beta_0 \left\{ \int_{2K_1 a^*}^{2K_1 y^*} \frac{e^{-\varphi}}{\varphi} d\varphi - \frac{1}{e^{2K_1 R^*}} \int_{2K_1 (R^* - a^*)}^{2K_1 (R^* - y^*)} \frac{e^{+\varphi}}{\varphi} d\varphi \right\}$$

$$- 2n^2 \beta_0 \left\{ \int_{4K_1 a^*}^{4K_1 y^*} \frac{e^{-\varphi}}{\varphi} d\varphi - \frac{1}{e^{4K_1 R^*}} \int_{4K_1 (R^* - a^*)}^{4K_1 (R^* - y^*)} \frac{e^{+\varphi}}{\varphi} d\varphi \right\}$$

From the ordinary exponential integrals existing in tables:

$$\int_x^{\infty} \frac{e^{-\varphi}}{\varphi} d\varphi = E_i(x) \quad \not\equiv \quad \int_{x_1}^{x_2} \frac{e^{-\varphi}}{\varphi} d\varphi = E_i(x_1) - E_i(x_2)$$

$$\int_{-\infty}^{x} \frac{e^{+\varphi}}{\varphi} d\varphi = I_i(x) \quad \not\equiv \quad \int_{x_1}^{x_2} \frac{e^{+\varphi}}{\varphi} d\varphi = I_i(x_2) - I_i(x_1)$$

the integral equation reduces to:

$$\frac{c}{c_a} \simeq \left(\frac{R-y}{y}\cdot\frac{a}{R-a}\right)^{\beta_0} \cdot \left\{ \frac{e^{2n\beta_0\left\{E_i(2K_1a^*)-E_i(2K_1y^*)\right\}}}{e^{2n\beta_0 e^{-2K_1R^*}\times\left\{I_i\left[2K_1(R^*-y^*)\right]-I_i\left[2K_1(R^*-a^*)\right]\right\}}} \cdot \right.$$

$$\left. \cdot \frac{e^{-2n^2\beta_0\left\{E_i(4K_1a^*)-E_i(4K_1y^*)\right\}}}{e^{-2n^2\beta_0 e^{-4K_1R^*}\times\left\{I_i\left[4K_1(R^*-y^*)\right]-I_i\left[4K_1(R^*-a^*)\right]\right\}}} \right\} \qquad (2.32)$$

where $\beta_0 = \frac{w_0}{\beta K u_*}$.-

From $\frac{c}{c_0} = \left(\frac{c}{c_1}\right)_{II}\left(\frac{c_1}{c_0}\right)_{I} = \left(\frac{c}{c_1}\right)_{\text{Region II}}\left(\frac{c_1}{c_0}\right)_{\text{Region I}}$ we get:

$$\frac{c}{c_0} \simeq \left(\frac{R-y}{y}\,\frac{y_1}{R-y_1}\right)^{\beta_0} \left\{ \frac{e^{2n\beta_0\left[E_i(2K_1y_1^*)-E_i(2K_1y^*)\right]}}{e^{2n\beta_0 e^{-2K_1R^*}\times\left[I_i\{2K_1(R^*-y^*)\}-I_i\{2K_1(R^*-y_1^*)\}\right.}} \right.$$

$$\left. \cdot \frac{e^{-2n^2\beta_0\left[E_i(4K_1y_1^*)-E_i(4K_1y^*)\right]-\frac{\beta_1}{n-1}\tan R^{n-1}K_1y_1^*}}{e^{-2n^2\beta_0 e^{-4K_1R^*}\left[I_i\{4K_1(R^*-y^*)\}-I_i\{4K_1(R^*-y_1^*)\}\right]}} \right\} \qquad (2.33)$$

where $\beta_0 = \frac{w_0}{\beta K u_*}$ and $\beta_1 = \frac{w_0}{\beta K_1 u_*}$.-

By neglecting the terms with I_i since they are multiplied with $e^{-2K_1R^*}$ or $e^{-4K_1R^*}$ which is very small we have that equations 2.32 and 2.33 become:

$$\frac{c}{c_a} \simeq \left(\frac{R-y}{y}\,\frac{a}{R-a}\right)^{\beta_0} \cdot \frac{e^{2n\beta_0\left\{E_i(2K_1a^*)-E_i(2K_1y^*)\right\}}}{e^{2n^2\beta_0\left\{E_i(4K_1a^*)-E_i(4K_1y^*)\right\}}} \qquad (2.34)$$

And the general formula for $\frac{c}{c_o}$ becomes,

$$\frac{c}{c_o} \simeq \left(\frac{h-y}{y}\cdot\frac{y_1}{h-y_1}\right)^{z_o} \frac{e^{2n z_o\left\{E_i(2k_1y_1^*)-E_i(2k_1y^*)\right\}-\frac{z_1}{n-1}\tanh^{n-1}k_1y_1^*}}{e^{2n^2 z_o\left\{E_i(4k_1y_1^*)-E_i(4k_1y^*)\right\}}} \qquad (2.35)$$

b. Approximation

If we consider w constant in the differential equation for Region II:

$$\frac{dc}{c} = -\frac{w\,dy}{\beta k u_* y(1-y/h)} \qquad (2.30)$$

and if we substitute in the solution $w = w_o$, then we find the following: (refs. 8 and 9)

$$\frac{c}{c_a} = \left(\frac{h-y}{y}\cdot\frac{a}{h-a}\right)^{z_o} \qquad (2.36)$$

where α is any reference level in region II.

The general formula for $\frac{c}{c_o}$ becomes:

$$\frac{c}{c_o} = \left(\frac{h-y}{y}\frac{y_1}{h-y_1}\right)^{z_o} e^{-\frac{z_1}{n-1}\tanh^{n-1}k_1y_1^*} \qquad (2.37)$$

As it is discussed in Chapter VI, article D, equation 2.35 becomes approximately identical with equation 2.37 for $y^* > 50$.

Table 2 gives a summary of sediment load formulae derived in this chapter, article E.

Table 2

Summary of proposed sediment load formulae

ASSUMPTION $w = w_0 \tanh^n K_1 y^*$

REGION Nº	APPROX. Nº	RATIO c/c_0
I		$e^{-\frac{Z_1}{n-1}\tanh^{n-1} K_1 y^*}$
II		$\left(\frac{R-y}{y}\cdot\frac{y_1}{R-y_1}\right)^{Z_0} \frac{e^{2nZ_0\left[\left\{E_i(2K_1y_1^*)-E_i(2K_1y^*)\right\}-n\left\{E_i(4K_1y_1^*)-E_i(4K_1y^*)\right\}\right]-\frac{Z_1}{n-1}\tanh^{n-1}K_1y_1^*}}{e^{\left\{\frac{2nZ_0}{2K_1R^*}\right\}\left[\left\{I_i\left[2K_1(R^*-y^*)\right]-I_i\left[2K_1(R^*-y_1^*)\right]\right\}-\frac{n}{2K_1R^*}\left\{I_i\left[4K_1(R^*-y^*)\right]-I_i\left[4K_1(R^*-y_1^*)\right]\right\}\right.}}$
	FORMULA USED	$\left(\frac{R-y}{y}\cdot\frac{y_1}{R-y_1}\right)^{Z_0} \frac{e^{2nZ_0\left\{E_i(2K_1y_1^*)-E_i(2K_1y^*)\right\}-\frac{Z_1}{n-1}\tanh^{n-1}K_1y_1^*}}{e^{2n^2Z_0\left\{E_i(4K_1y_1^*)-E_i(4K_1y^*)\right\}}}$
	APPROX.	$\left(\frac{R-y}{y}\cdot\frac{y_1}{R-y_1}\right)^{Z_0} e^{-\frac{Z_1}{n-1}\tanh^{n-1}K_1y_1^*}$

F. Average Sediment Concentrations

1. Average Sediment Concentration Profile

The average profile concentration is given by:

$$\overline{C} = \frac{1}{R}\int_0^R c\,dy$$

For the assumption $w = w_0 \tanh^n \kappa_1 y^*$, equation 2.25, made for the fall velocity of the particles, the above equation can be evaluated. Substituting the approximate equations, equation 2.29 and 2.35, for the concentration in regions I and II respectively, into the equation for the average profile concentration and integrating we get:

$$\overline{C} = \frac{1}{R}\int_0^{y_1} c\,dy + \frac{1}{R}\int_{y_1}^{R} c\,dy$$

$$\overline{C} = \frac{c_0}{\omega_R}\int_0^{\omega_1} e^{-\frac{3_1}{n-1}\tanh^{n-1}\omega}\,d\omega + \frac{c_{md}}{\omega_R}\int_{\omega_1}^{\omega_R}\left(\frac{\omega_R-\omega}{\omega}\right)^{3_0}\frac{e^{-2n3_0 E_i(2\omega)}}{e^{-2n^2 3_0 E_i(4\omega)}}\,d\omega$$

where $\omega = \kappa_1 y^*$, $\omega_1 = \kappa_1 y_1^*$, $\omega_R = \kappa_1 R^*$

or
$$\overline{C} = c_0\,\Phi'(\omega_1) + c_{md}\,H(\omega_1, \omega_R) \qquad (2.38)$$

where

$$\Phi'(\omega_1) = \frac{1}{\omega_R}\int_0^{\omega_1} e^{-\frac{3_1}{n-1}\tanh^{n-1}\omega}\,d\omega$$

and

$$H(\omega_1, \omega_R) = \frac{1}{\omega_R}\int_{\omega_1}^{\omega_R}\left(\frac{\omega_R-\omega}{\omega}\right)^{3_0}\frac{e^{-2n3_0 E_i(2\omega)}}{e^{-2n^2 3_0 E_i(4\omega)}}\,d\omega$$

Since the integration of $H(\omega_1, \omega_k)$ is not simple, and the factor:

$$e^{-2n\beta_0\{E_i(2\omega) - n E_i(4\omega)\}}$$

is very close to 1

e.g. for $\omega=\omega_1$ it is $\sim .8$

and for $\omega \gg 5\omega_1$ it is ~ 1

we neglect the error and put it equal to 1, which corresponds to using equation 2.36, i.e. $w = w_o \equiv$ constant.

Thus, we have

$$H(\omega_1, \omega_k) \simeq \frac{1}{\omega_k} \int_{\omega_1}^{\omega_k} \left(\frac{\omega_k - \omega}{\omega}\right)^{\beta_0} d\omega$$

and substituting η for $\frac{y}{k} = \frac{\omega}{\omega_k}$ we get,

$$H(\eta_1) = \int_{\eta_1}^{1} \left(\frac{1-\eta}{\eta}\right)^{\beta_0} d\eta$$

so that equation 2.38 becomes,

$$\bar{C} \simeq c_o \mathcal{I}'(\omega_1) + c_{md} H(\eta_1) \qquad (2.39)$$

Tables for integral $H(\eta_1)$ may be found in ref. 10. The integral $\mathcal{I}'(\omega_1)$ might be calculated numerically. Its contribution to $\bar{C}$ is not negligible.

2. Average Sediment Transport Concentration

The average transport concentration is given by

$$\bar{C}_T = \frac{1}{Uk} \int_0^k cu\, dy$$

With the assumption $w = w_o \tanh^n K_1 y^*$, equation 2.25, for the fall velocity of the particles, and substituting equations 2.29 and 2.35 for the concentration and equations 2.18 and 2.24 for the velocity in the regions I and II respectively, and integrating one obtains the following:

$$\bar{C}_T = \frac{1}{Uh}\int_0^{y_1} c u dy + \frac{1}{Uh}\int_{y_1}^{h} c u dy$$

Making the same approximations as those in the preceding article one gets

$$\bar{C}_T \simeq \frac{c_o}{U}\frac{u_x}{K_1}\,\mathcal{Q}_T(\omega_1) + \frac{c_{md}}{U}\left\{u_{max} H(\eta_1) - \frac{u_*}{K} L(\eta_1)\right\} \qquad (2.40)$$

where:

$$\mathcal{Q}_T(\omega_1) = \frac{1}{\omega_h}\int_0^{\omega_1} e^{-\frac{z_1}{n-1}\tanh^{n-1}\omega} \cdot \tanh\omega\, d\omega$$

$$H(\eta_1) = \int_{\eta_1}^{1}\left(\frac{1-\eta}{\eta}\right)^{z_o} d\eta$$

$$L(\eta_1) = \int_1^{\eta_1}\left(\frac{1-\eta}{\eta}\right)^{z_o} \ln\eta\, d\eta$$

Tables for the last two integrals are in ref. 10. The integral $\mathcal{Q}_T(\omega_1)$ might be calculated numerically. Its contribution to $\bar{C}_T$ is small, becoming negligible for small values of $\frac{u_x}{U}$.

G. Turbulent Energy Production

1. Energy Withdrawn from Basic Flow

The rate at which turbulent energy is withdrawn from

the basic flow is given by, (ref. 5),

$$P_\tau = \tau^* \frac{du}{dy}$$

where $\tau^* = -\rho\overline{u'v'}$, and P_τ is the rate of turbulent energy production per unit volume per unit time.

Substituting $\tau - \mu \frac{du}{dy}$ for τ^* we get,

$$P_\tau = \left(\tau - \mu \frac{du}{dy}\right) \frac{du}{dy} \tag{2.41}$$

For constant shear the above equation becomes,

$$P_\tau = \frac{\rho u_*^2}{\nu} \left(u_* - \frac{du}{dy^*}\right) \frac{du}{dy^*} \tag{2.42}$$

and for linear shear distribution it becomes,

$$P_\tau = \frac{\rho u_*^2}{\nu} \left\{\left(1 - \frac{y^*}{R^*}\right) \cdot u_* - \frac{du}{dy^*}\right) \frac{du}{dy^*} \tag{2.43}$$

a. Region I. $(y^* < y_1^*)$

For Region I, near the bed, the velocity profile is approximated by equations 2.18 and 2.19 derived in article D of this chapter. Assuming that the shear is constant in region I, $\tau \simeq \tau_o$, and introducing equations 2.18 and 2.19 into equation 2.42 we find,

$$P_{\tau_I} = \frac{\rho u_*^4}{\nu} \tanh^2 \kappa_1 y^* \operatorname{sech}^2 \kappa_1 y^* \tag{2.44}$$

where P_{τ_I} is the rate of turbulent energy production per unit volume and unit time in region I.

Multiplying by the factor $\frac{\nu}{\rho u_*^4}$ to make it dimensionless:

$$(Pc_I)_\tau = \tanh^2 k_1 y^* \operatorname{sech}^2 k_1 y^* \qquad (2.45)$$

where $(Pc_I)_\tau = \frac{\nu}{\rho u_*^4} Pc_I$

b. Region II. $(y^* > y_1^*)$.

For Region II the velocity profile is approximated by equations 2.23 and 2.24 derived in article D of this chapter. Introducing these equations into equation 2.43 we find,

$$Pc_{II} = \rho \frac{u_*^2}{\nu}\left\{\left(1-\frac{y^*}{R^*}\right)\cdot u_* - u_*\left(\frac{1}{ky^*} - \frac{1}{2(ky^*)^2} + \frac{1}{8(ky^*)^3}\cdots\right)\right\} u_*\left(\frac{1}{ky^*} - \frac{1}{2(ky^*)^2} + \frac{1}{8(ky^*)^3}\cdots\right)$$

Rearranging and factoring terms we get,

$$Pc_{II} = \frac{\rho u_*^4}{\nu}\left\{-\frac{1}{kR^*} + \left(1+\frac{1}{2kR^*}\right)\frac{1}{ky^*} - \left(\frac{3}{2}+\frac{1}{8kR^*}\right)\frac{1}{(ky^*)^2} + \frac{9}{8}\frac{1}{(ky^*)^3} - \frac{1}{4(ky^*)^4} + \frac{1}{64(ky^*)^6}\right\}$$

$$\text{or} \quad Pc_{II} = \frac{\rho u_*^4}{\nu}\left\{-\frac{1}{kR^*} + \left(1+\frac{1}{2kR^*}\right)\frac{1}{ky^*} - \left(\frac{3}{2}+\frac{1}{8kR^*}\right)\frac{1}{(ky^*)^2} + \frac{9}{8(ky^*)^3}\cdots\right. \qquad (2.46)$$

Multiplying by $\frac{\nu}{\rho u_*^4}$ to make it dimensionless

$$(Pc_{II})_\tau = -\frac{1}{kR^*} + \left(1+\frac{1}{2kR^*}\right)\frac{1}{ky^*} - \left(\frac{3}{2}+\frac{1}{8kR^*}\right)\frac{1}{(ky^*)^2} + \frac{9}{8}\frac{1}{(ky^*)^3}\cdots$$

or

$$(Pc_{II})_\tau \simeq -\frac{1}{kR^*} + \frac{1}{ky^*} - \frac{3}{2}\frac{1}{(ky^*)^2} + \frac{9}{8}\frac{1}{(ky^*)^3} \qquad (2.47)$$

2. Average Production of Turbulent Energy

The average rate of production of turbulent energy is given by:

$$\overline{P_\varepsilon} = \frac{1}{h}\int_0^h P_\varepsilon \, dy = \frac{1}{h}\int_0^{y_1} P_{\varepsilon_I} dy + \frac{1}{h}\int_{y_1}^h P_{\varepsilon_{II}} dy = \overline{P_{\varepsilon_I}} + \overline{P_{\varepsilon_{II}}}$$

where h is the depth and $\overline{P_\varepsilon}$ = average production of turbulent energy

a. Region I

$$\overline{P_{\varepsilon_I}} = \frac{1}{h}\int_0^{y_1} P_{\varepsilon_I} dy$$

Substituting equation 2.44 in this equation we get:

$$\overline{P_{\varepsilon_I}} = \frac{1}{K_1 h^*}\int_0^{K_1 y_1^*} \frac{\rho u_*^4}{\nu} \tanh^2 K_1 y^* \operatorname{sech}^2 K_1 y^* \, d(K_1 y^*)$$

which integrated gives:

$$\overline{P_{\varepsilon_I}} = \frac{\rho u_*^3}{3K_1 h} \tanh^3 K_1 y_1^* \qquad (2.48)$$

Multiplying by $\frac{\nu}{\rho u_*^4}$ to make it dimensionless:

$$\left(\overline{P_{\varepsilon_I}}\right)_\tau = \frac{1}{3K_1 h^*} \tanh^3 K_1 y_1^* \qquad (2.49)$$

b. Region II.

$$\overline{P_{\varepsilon_{II}}} = \frac{1}{h}\int_{y_1}^h P_{\varepsilon_{II}} dy$$

Substituting equation 2.46 in this equation we get:

$$\overline{P_{\varepsilon_{II}}} = \frac{1}{h^*}\int_{y_1^*}^{h^*} \frac{\rho u_*^4}{\nu}\left\{-\frac{1}{Kh^*} + \left(1 + \frac{1}{2Kh^*}\right)\frac{1}{Ky^*}\right.$$

$$\left. -\left(\frac{3}{2} + \frac{1}{8Kh^*}\right)\frac{1}{(Ky^*)^2} + \frac{9}{8}\frac{1}{(Ky^*)^3} \cdots\right\} dy^*$$

Integrating and neglecting the terms of order $\frac{1}{R^*}$ we get:

$$\overline{Pr}_{II} \simeq \frac{\rho u_*^4}{\tau} \frac{1}{\kappa R^*} \left\{ \ln \frac{R^*}{y_1^*} - 1 - \frac{3}{2\kappa y_1^*} + \frac{9}{16(\kappa y_1^*)^2} \right\} \tag{2.50}$$

Multiplying by $\frac{\tau}{\rho u_*^4}$ to make it dimensionless:

$$\left(\overline{Pr}_{II}\right)_\tau \simeq \frac{1}{\kappa R^*} \left\{ \ln \frac{R^*}{y_1^*} - 1 - \frac{3}{2\kappa y_1^*} + \frac{9}{16(\kappa y_1^*)^2} \right\} \tag{2.51}$$

so that the average for the whole profile becomes:

$$\overline{Pr} \simeq \frac{\rho u_*^4}{\tau} \left\{ \frac{1}{3\kappa_1 R^*} \tanh^3 \kappa_1 y_1^* + \frac{1}{\kappa R^*} \left(\ln \frac{R^*}{y_1^*} - 1 - \frac{3}{2\kappa y_1^*} + \frac{9}{16(\kappa y_1^*)^2} \right) \right\} \tag{2.52}$$

and in dimensionless form:

$$\left(\overline{Pr}\right)_\tau \simeq \frac{1}{3\kappa_1 R^*} \tanh^3 \kappa_1 y_1^* + \frac{1}{\kappa R^*} \left(\ln \frac{R^*}{y_1^*} - 1 - \frac{3}{2\kappa y_1^*} + \frac{9}{16(\kappa y_1^*)^2} \right) \tag{2.53}$$

H. Dissipation of Energy by Suspended Sediment

1. Dissipation of Energy by Sediment

The rate of dissipation of energy due to settling of sediment is given by, (ref. 11),

$$W_s = c w \left(1 - \frac{\gamma_w}{\gamma_s}\right) \tag{2.54}$$

where W_s is the rate of dissipation of energy by suspended sediment per unit volume per unit time,

C is the sediment concentration,

w is the settling velocity of the particles,

γ_s is the specific weight of the particles, and

γ_w is the specific weight of the water.

a. Region I

Substituting w and C from equations 2.25 and 2.29 into equation 2.54 we get the following for region I,

$$W_{s_I} = C_o w_o \left(1 - \frac{\gamma_w}{\gamma_s}\right) \tanh^n \kappa_1 y^* \cdot e^{-\frac{z_1}{n-1} \tanh^{n-1} \kappa_1 y^*} \tag{2.55}$$

Multiplying it by $\frac{\nu}{\rho u_*^4}$ to make it dimensionless:

$$\left(W_{s_I}\right)_\tau = \frac{C_o w_o \nu}{\rho u_*^4} \left(1 - \frac{\gamma_w}{\gamma_s}\right) \tanh^n \kappa_1 y^* \cdot e^{-\frac{z_1}{n-1} \tanh^{n-1} \kappa_1 y^*} \tag{2.56}$$

b. Region II

Substituting w and C from equations 2.25 and 2.35 into equation 2.54 one obtains the following for region II,

$$W_{s_{II}} = C_o w_o \left(1 - \frac{\gamma_w}{\gamma_s}\right) \tanh^n \kappa_1 y^* \cdot \left(\frac{h-y}{y} \frac{y_1}{h-y_1}\right)^{z_0} \cdot \cdot \frac{e^{2nz_0\left\{E_i(2\kappa_1 y_1^*) - E_i(2\kappa_1 y^*)\right\} - \frac{z_1}{n-1} \tanh^{n-1} \kappa_1 y_1^*}}{e^{2n^2 z_0\left\{E_i(4\kappa_1 y_1^*) - E_i(4\kappa_1 y^*)\right\}}} \tag{2.57}$$

And expressing it in terms of C_{md} (mid-depth concentration) one finds,

$$W_{s_{II}} = c_{md}\, w_o \left(1 - \frac{\gamma_w}{\gamma_s}\right) \tanh^n \kappa_1 y^* \left(\frac{h-y}{y}\right)^{z_o} \cdot \cdot \frac{e^{-2nz_o E_i(2\kappa_1 y^*)}}{e^{-2n^2 z_o E_i(4\kappa_1 y^*)}} \qquad (2.58)$$

Multiplying it by $\frac{\nu}{\rho u_*^4}$ we make it dimensionless.

$$\left(W_{s_{II}}\right)_\tau = c_{md}\, \frac{\nu w_o}{\rho u_*^4} \left(1 - \frac{\gamma_w}{\gamma_s}\right) \tanh^n \kappa_1 y^* \left(\frac{h-y}{y}\right)^{z_o} \cdot \cdot \frac{e^{-2nz_o E_i(2\kappa_1 y^*)}}{e^{-2n^2 z_o E_i(4\kappa_1 y^*)}} \qquad (2.59)$$

where: $\left(W_{s_{II}}\right)_\tau = W_{s_{II}} \frac{\nu}{\rho u_*^4}$

And for $\kappa_1 y^* > 5$

$$\left(W_{s_{II}}\right)_\tau \approx \frac{\nu}{\rho u_*^4} c_{md}\, w_o \left(1 - \frac{\gamma_w}{\gamma_s}\right) \left(\frac{h-y}{y}\right)^{z_o} \qquad (2.60)$$

which corresponds to using $w = w_o$ i.e. constant.

2. Average Sediment Energy Dissipation

The average rate of dissipation of energy by suspended sediment is given by:

$$\overline{W_s} = \frac{1}{h} \int_o^h W_s \, dy$$

where $\overline{W_s}$ is the average rate of dissipation of energy by suspended sediment and h is the depth.

$$\overline{W_s} = \overline{W_{s_I}} + \overline{W_{s_{II}}} = \frac{1}{h} \int_o^{y_1} W_{s_I} \, dy + \frac{1}{h} \int_{y_1}^h W_{s_{II}} \, dy$$

a. Region I

Substituting W_{S_I} from equation 2.55 we find:

$$\overline{W}_{S_I} = \frac{1}{k_1 h^*} \int_0^{k_1 y_1^*} c_0 w_0 \left(1 - \frac{\gamma_w}{\gamma_s}\right) e^{-\frac{3_1}{n-1} \tanh^{n-1} k_1 y^*} \cdot \tanh^n k_1 y^* \, d(k_1 y^*)$$

or

$$\overline{W}_{S_I} = \frac{c_0 w_0}{\omega_h} \left(1 - \frac{\gamma_w}{\gamma_s}\right) \int_0^{\omega_1} e^{-\frac{3_1}{n-1} \tanh^{n-1} \omega} \cdot \tanh^n \omega \, d\omega$$

or

$$\overline{W}_{S_I} = c_0 w_0 \left(1 - \frac{\gamma_w}{\gamma_s}\right) \Phi(\omega_1) \tag{2.61}$$

where $$\Phi(\omega_1) = \frac{1}{\omega_h} \int_0^{\omega_1} e^{-\frac{3_1}{n-1} \tanh^{n-1} \omega} \cdot \tanh^n \omega \, d\omega$$

b. Region II

Substituting $W_{S_{II}}$ from equation 2.58 into the equation for the average dissipation one finds

$$\overline{W}_{S_{II}} = c_{md} w_0 \left(1 - \frac{\gamma_w}{\gamma_s}\right) \frac{1}{\omega_h} \int_{\omega_1}^{\omega_h} \left(\frac{\omega_h - \omega}{\omega}\right)^{3_0} \cdot \cdot \frac{e^{-2n 3_0 E_i(2\omega)}}{e^{-2n^2 3_0 E_i(4\omega)}} \cdot \tanh^n \omega \, d\omega \tag{2.62}$$

which is approximated by:

$$\overline{W}_{S_{II}} \simeq c_{md} w_0 \left(1 - \frac{\gamma_w}{\gamma_s}\right) H(\eta_1) \tag{2.63}$$

because: $$\frac{e^{-2n 3_0 E_i(2\omega)}}{e^{-2n^2 3_0 E_i(4\omega)}} \tanh^n \omega \simeq 1$$

This corresponds to using $w = w_o$ i.e. constant.

Thus the average $\overline{W_s}$ for the whole profile becomes:

$$\overline{W_s} \simeq w_o \left(1 - \frac{\gamma_w}{\gamma_s}\right) \left\{ c_o \, \Omega(\omega_1) + c_{md} \, H(\eta_1) \right\} \qquad (2.64)$$

and in dimensionless form

$$\left(\overline{W_s}\right)_\tau \simeq \frac{\varkappa}{\rho u_*^4} w_o \left(1 - \frac{\gamma_w}{\gamma_s}\right) \left\{ c_o \, \Omega(\omega_1) + c_{md} \, H(\eta_1) \right\} \qquad (2.65)$$

Table 3 gives a summary of formulae for average concentration, rate of turbulent energy production and rate of dissipation of energy by sediment in suspension, derived in this chapter, articles F, G and H.

Table 3

Summary of formulae for average concentration, rate of turbulent energy production and rate of dissipation of energy by suspended sediment

1.- AVERAGE CONCENTRATION

PROFILE: $\bar{C} = \frac{1}{R}\int_0^R c\,dy$ $\qquad \bar{C} \simeq c_o\,\Omega'(\omega_1) + c_{md}\,H(\eta_1)$

TRANSPORT: $\bar{C}_T = \frac{1}{UR}\int_0^R cu\,dy$ $\qquad \bar{C}_T \simeq \frac{c_o}{U}\frac{u_*}{\kappa_1}\Omega_T(\omega_1) + \frac{c_{md}}{U}\left\{u_{max}H(\eta_1) - \frac{u_*}{\kappa}L(\eta_1)\right\}$

2.- TURBULENT ENERGY PRODUCTION

REGION I: $\qquad (P_\varepsilon)_\tau = \tanh^2\kappa_1 y^*\,\mathrm{sech}^2\kappa_1 y^*$

REGION II: $\qquad (P_\varepsilon)_\tau = -\frac{1}{\kappa R^*} + \frac{1}{\kappa y^*}\left(1+\frac{1}{2\kappa R^*}\right) - \frac{1}{(\kappa y^*)^2}\left(\frac{3}{2}+\frac{1}{8\kappa R^*}\right) + \frac{1}{(\kappa y^*)^3}\cdot\frac{9}{8}\cdots\cdots$

$$(P_\varepsilon)_\tau \simeq -\frac{1}{\kappa R^*} + \frac{1}{\kappa y^*} - \frac{1.5}{(\kappa y^*)^2} + \frac{1.125}{(\kappa y^*)^3}\cdots\cdots$$

AVERAGE: $\overline{(P_\varepsilon)_\tau} = \frac{1}{R}\int_0^R (P_\varepsilon)_\tau\,dy = \frac{1}{3\kappa_1 R^*}\tanh^3\kappa_1 y_1^* + \frac{1}{\kappa R^*}\left\{\ln\frac{R^*}{y_1^*} - 1 - \frac{3}{2\kappa y_1^*} + \frac{9}{(4\kappa y_1^*)^2}\cdots\cdots\right\}$

3.- SEDIMENT ENERGY DISSIPATION

REGION I: $\qquad (W_s)_\tau = \frac{c_o w_o \nu}{\rho u_*^4}\left(1-\frac{\gamma_w}{\gamma_s}\right)\tanh^n\kappa_1 y^*\cdot e^{-\frac{z_1}{n-1}\tanh^{n-1}\kappa_1 y^*}$

REGION II: $\qquad (W_s)_\tau = \frac{c_{md} w_o \nu}{\rho u_*^4}\left(1-\frac{\gamma_w}{\gamma_s}\right)\tanh^n\kappa_1 y^*\cdot\left(\frac{R-y}{y}\right)^{z_o}\frac{e^{-2nz_o}E_i(2\kappa_1 y^*)}{e^{-2n^2 z_o}E_i(4\kappa_1 y^*)}$

$$(W_s)_\tau \simeq \frac{c_{md} w_o \nu}{\rho u_*^4}\left(1-\frac{\gamma_w}{\gamma_s}\right)\left(\frac{R-y}{y}\right)^{z_o}$$

AVERAGE: $\overline{(W_s)_\tau} = \frac{1}{R}\int_0^R (W_s)_\tau\,dy = w_o\left(1-\frac{\gamma_w}{\gamma_s}\right)\left\{c_o\,\Omega(\omega_1) + c_{md}\,H(\omega_1,\omega_R)\right\}\frac{\nu}{\rho u_*^4}$

$$\overline{(W_s)_\tau} \simeq w_o\left(1-\frac{\gamma_w}{\gamma_s}\right)\left\{c_o\,\Omega(\omega_1) + c_{md}\,H(\eta_1)\right\}\frac{\nu}{\rho u_*^4}$$

CHAPTER III

OBJECTIVE OF EXPERIMENTS

The main objective of the experiments carried out in this investigation was to study the resistance characteristics of streams flowing over a bed of loose granular material. In particular it was of interest to study the cases where the transportation rate of sediment is high and appreciable amount of material is carried in suspension.

Since two of the most important characteristics of a flow are von Karman's constant k of the velocity profile and the friction factor, f, the effect of suspended sediment on both k and f was investigated. It was attempted to relate both k and f to the ratio of the average rate of dissipation of energy by the sediment in suspension to the average rate of turbulent energy production in the flow.

For the evaluation of the rate of energy dissipation by suspended sediment it was necessary to measure the sediment concentration profile of the flow. For the evaluation of the rate of turbulent energy production the velocity profile and the bed shear were measured. Since both von Karman's k and friction factor f depend on the turbulent energy balance of the flow in a very small region near the wall, measurements were taken as close to the bed as possible. However it was not made possible to measure either velocities or sediment concentrations in the very small region close to the bed.

CHAPTER IV

EQUIPMENT AND PROCEDURE

A. Apparatus

1. 40 Foot Flume

The experiments were carried out in the 40-foot tilting flume shown in figure 2. This flume has a closed circuit system with a 4-inch diameter return-pipe, so that both the sediment and the water were recirculated, without significant sand deposition in the return circuit.

The pump placed under the downstream of the flume end (figure 3) was an axial flow type with a 9-inch impeller. It was driven by a standard commercial electric motor with a variable ratio V-belt transmission, so that the speeds could be varied from 120 rpm to 1050 rpm.

The bottom of the flume was made of a steel plate and the sides were made of 10-inch structural channels placed $10\frac{1}{2}$ inches apart. The inside surfaces were painted with a bitumastic paint and were very smooth. Through a 50-inch long transparent lucite tube installed in the middle of the return pipe, it was easy to observe the flow and sediment deposition, if any, in the return circuit. The whole system was supported by a stiff truss, pivoted at one end and having a jack at the other for the adjustment of its slope.

2. Entrance and Exit Conditions

The entrance to the flume was equipped with an adjustable

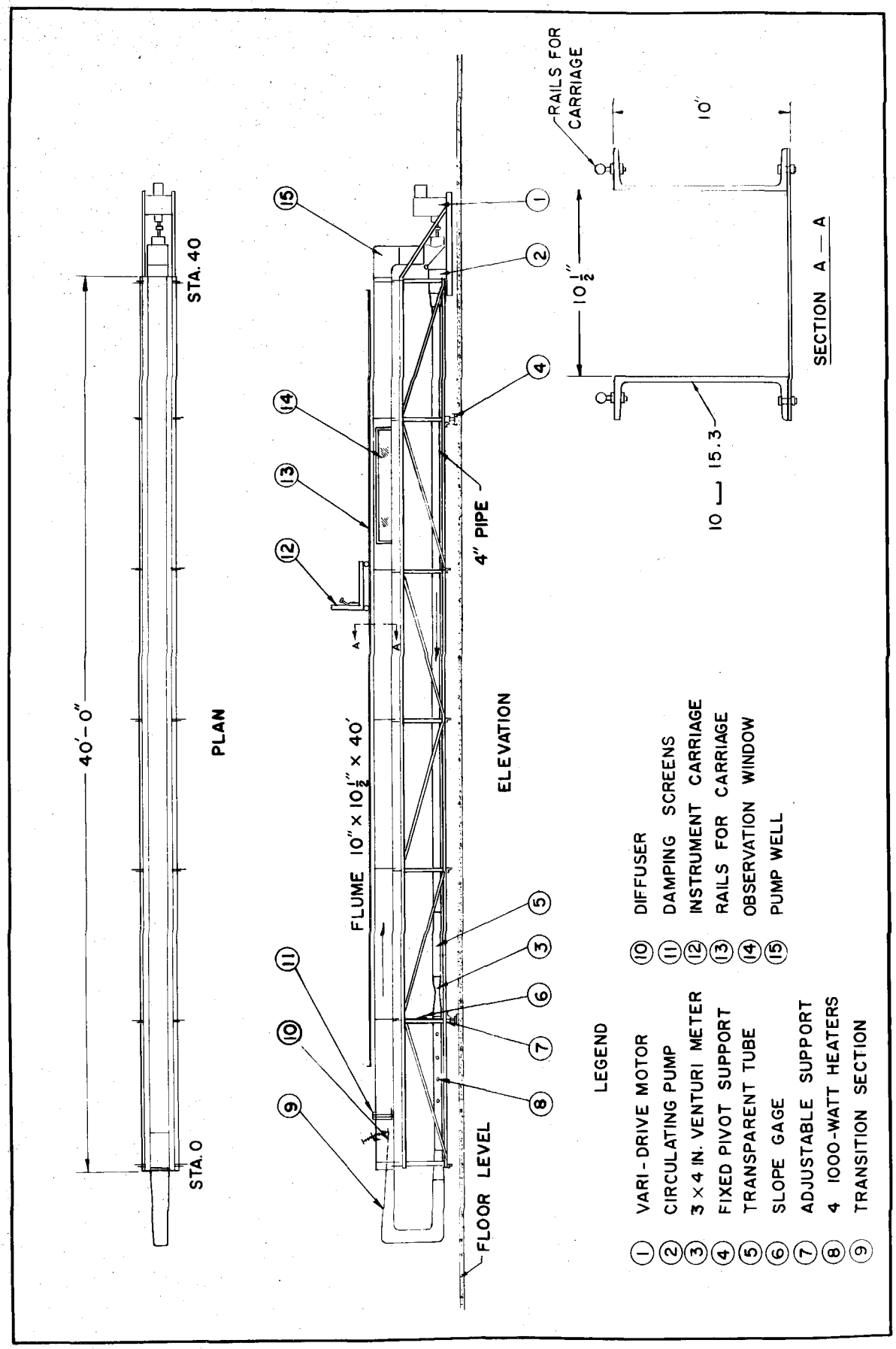

Fig. 2 - Diagram of the flume

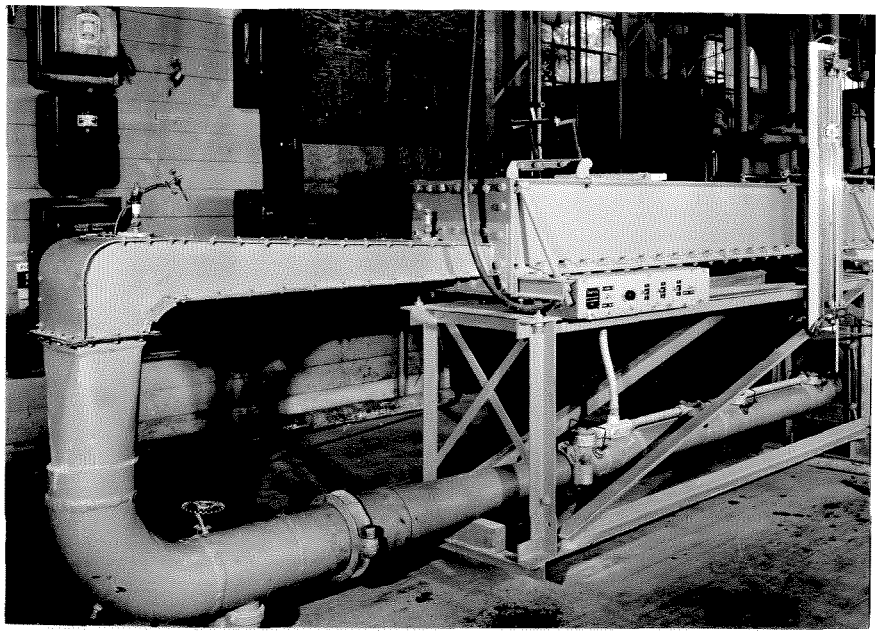

(a) Upstream end of flume showing inlet section, heaters for controlling water temperature, and manometer for venturi meter to measure flow rate.

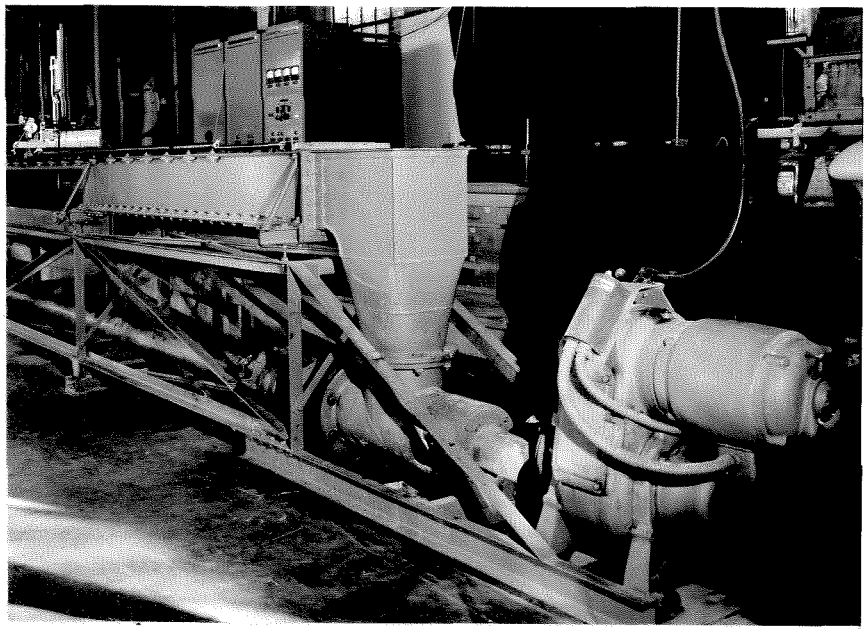

(b) Downstream end of flume with pump, and electric motor with V-belt transmission.

Fig. 3 - Upstream and downstream ends of the flume.

horizontal diffuser lid which permitted the control of the inlet depth of the flow. In addition to this, one or two fine or coarse screens of 16 or 5 openings per inch were inserted vertically in the flow right after the diffuser lid. By damping the turbulence induced by the inlet section they were effective in establishing uniform conditions of the flow in a much shorter length in the flume.

Similarly one fine or coarse screen at the downstream end was effective in establishing stable exit conditions and uniform flow at the working section of the flume, by regulating the depth at the edge of the pump well and damping the small oscillations created by the pump so that they did not travel upstream.

3. Venturi Meter

The venturi meter was placed in the return pipe, fig. 4, under the flume downstream from the lucite tube, far away from the pump, so that uniform pipe flow would have been established before entering the meter.

For the evaluation of the discharge coefficient C of the meter, the velocity was measured in many points of a cross section using a pitot tube. Then the discharge was computed using the Simpson rule of integration, and the following equation was applied:

$$Q = C \frac{A_2 \sqrt{2gh_v}}{\sqrt{1-\left(\frac{D_2}{D_1}\right)^4}}$$

where:

Q = Discharge

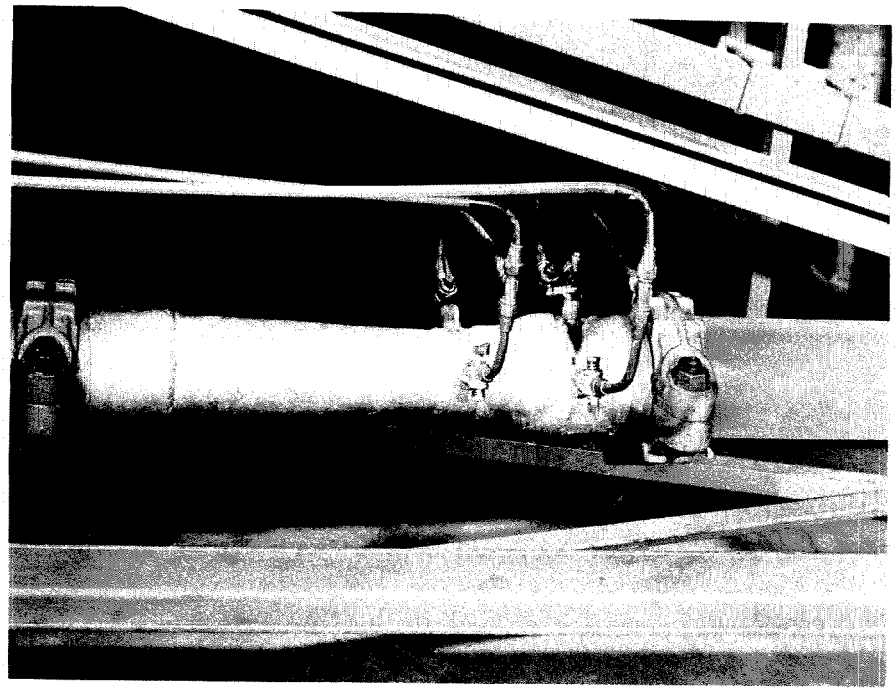

Fig. 4 - 3 x 4 in. venturi meter.

A_2 = Area of contracted section

h_v = Differential piezometric head

D_1 = Diameter of approach = 4.044 in.

D_2 = Diameter of contraction = 2.988 in.

C = Discharge coefficient

Substituting the measured values $Q = .397$ cfs, $h_v = .737$ ft. and $A_2 = .0487$ ft^2 in the above equation one gets $C = .99$.

4. Heaters

The temperature of the water was controlled by four 1000-watt immersion heaters, installed in the return pipe under the upstream end of the flume, right after the venturi meter. Three of the heaters could be switched to 250 or 1000 watts giving an arrangement for the regulation of the power input from 250 to 4000 watts. In this way the temperature of the water was easily controlled within 0.1°C.

5. Carriage-Point Gage and Flume Slope

A movable carriage supported on small rails on the top flange of the side channels of the flume could roll from Station 6 to 37, (feet from upstream end of the flume). It was equipped with a vertical and a transverse mechanism, so that a point gage mounted on it could reach any point in the cross section. The point gage could be easily interchanged with a pitot tube or point sampler using identical mounting brackets. The scales giving the vertical and horizontal position of the instrument on the carriage could be read to 0.001 ft. by means of a vernier.

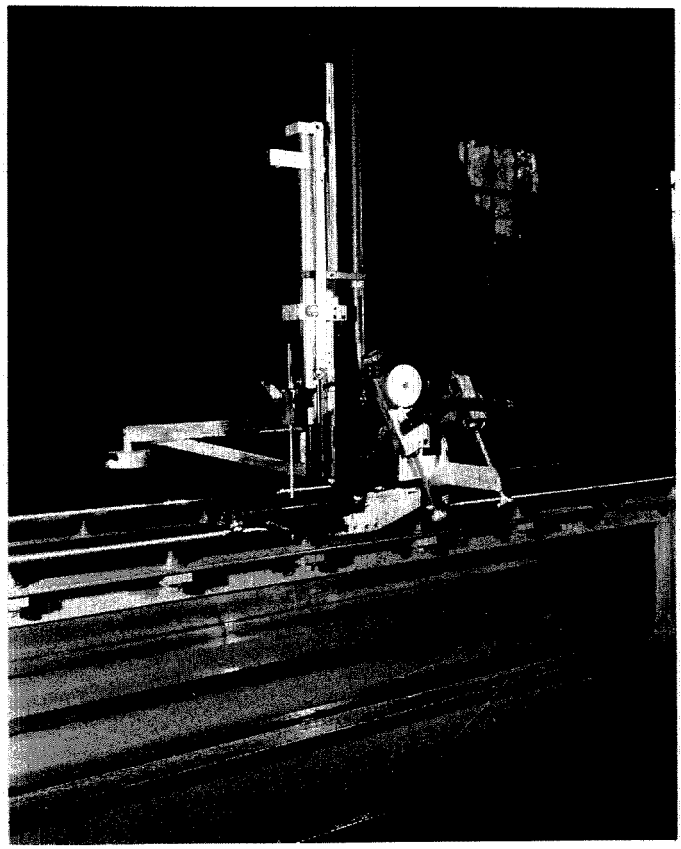

Fig. 5 - Instrument carriage and point gage.

The scale for the slope of the flume was read to the nearest .00001 with a vernier located on the truss close to the upstream end of the flume. The calibration of the slope scale, as well as the level of the small rails on the top flange of the side channels of the flume had been obtained with static water surface and the bed plate of the flume. The mounting of the flume itself and the carriage rails on it were so adjusted that when the reading of the slope scale was zero the point gage of the carriage showed the same reading for the surface of static water in the flume at every point along and across the flume.

B. Measurements

1. Velocity Measurements

The point velocities away from the bed were measured with a 3/16-inch Prandtl type pitot-static tube with a coefficient of 1.00, using an air to water vertical differential manometer which could be read to .001 ft. The difference of the mass density of the water in the manometer and the sediment mixture, introduced a very negligible error in the readings of the velocity head.

For the velocities at points close to the bed a 0.032-inch outside diameter pitot tube was used connected to a Model P5 Statham gage, which is a pressure transducer with a maximum capacity of 0.3 p.s.i. The pressure readings were made using an electronic potentiometer as shown in fig. 7 and fig. 8. Since the strain gage is very sensitive it responded to the velocity fluctuations and small capillary tubes had to be used to damp the high frequency

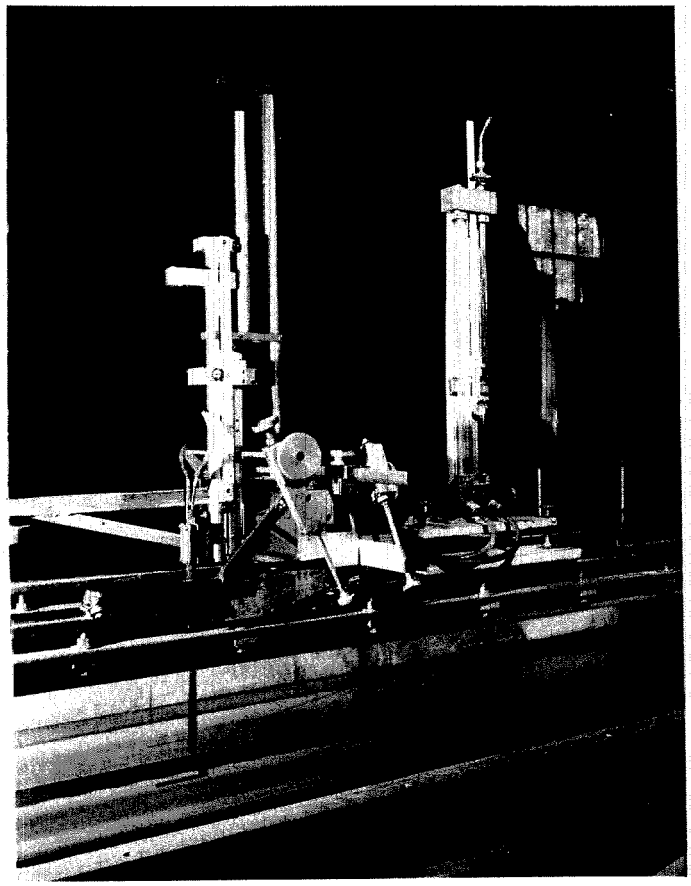

Fig. 6 - Pitot static tube and manometer used for velocity measurements.

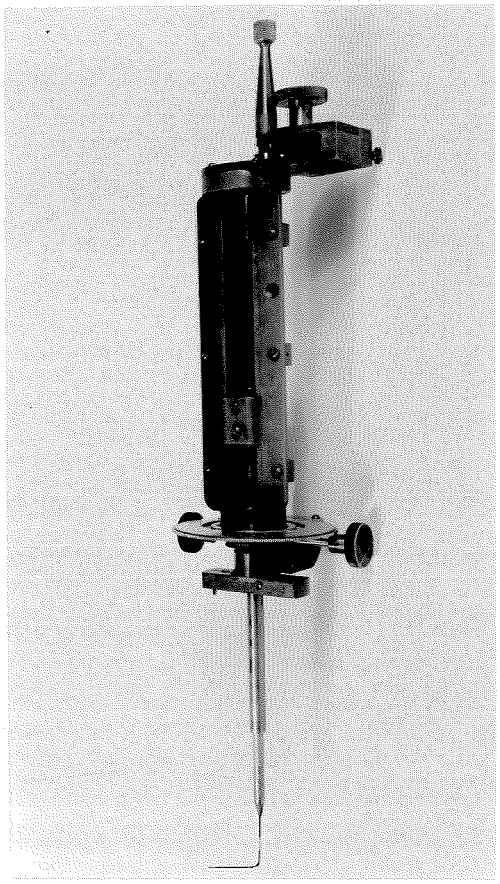

(a) Pitot tube with probe holder (outside diameter = .032 in., inside diameter = .020 in.)

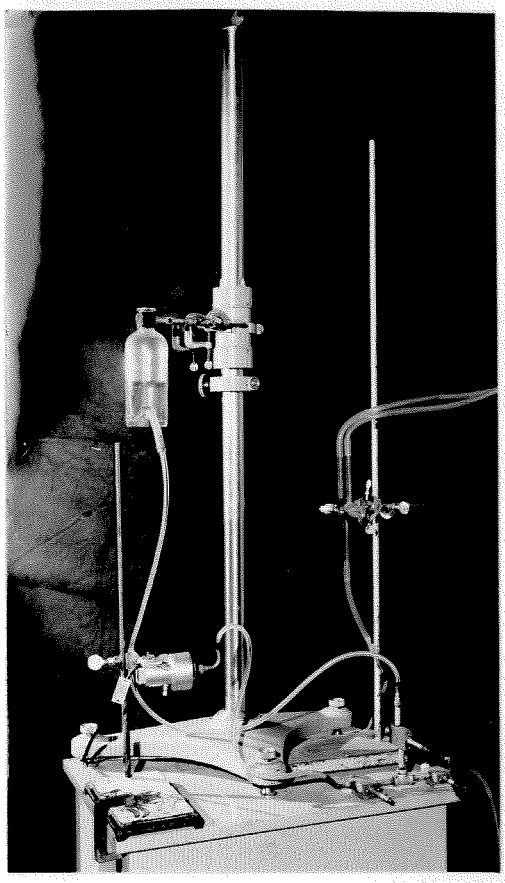

(b) Strain gage (accuracy 1% of 0.3 psi) and Cathetometer used for the calibration of the gage.

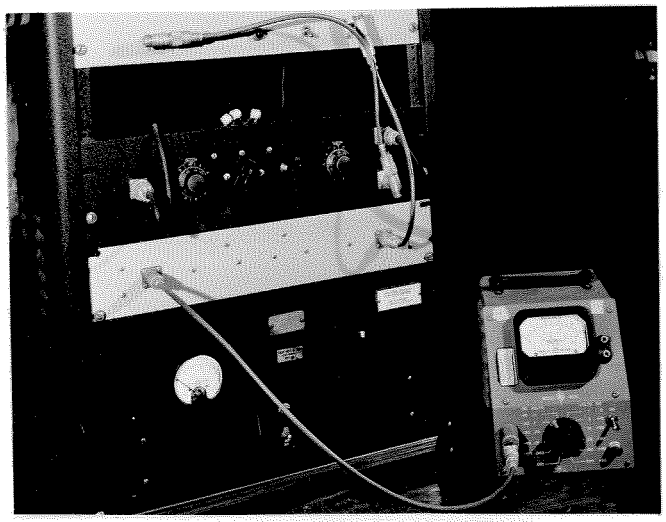

(c) Electronic potentiometer.

Fig. 7 - Equipment for measuring velocities close to the bed.

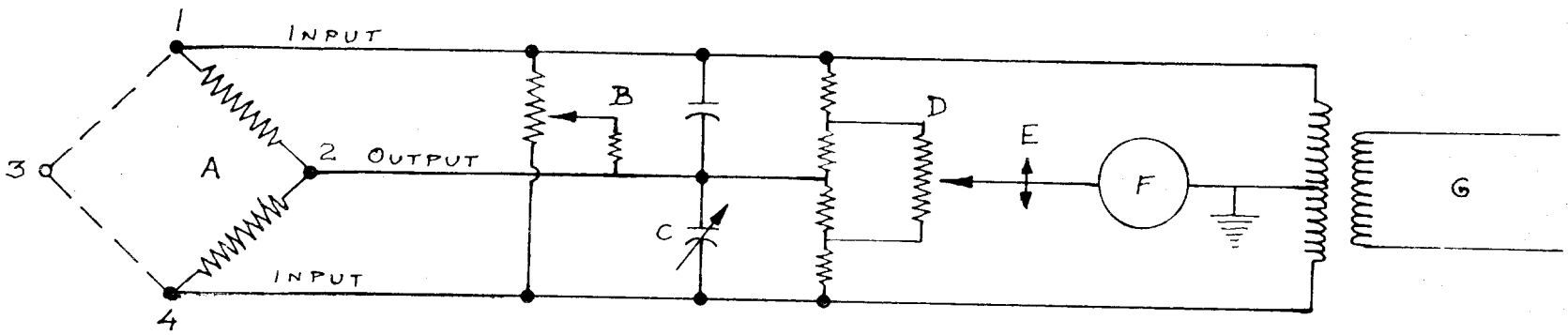

A	Statham gage (strain gage)
B	Initial resistance balance adjustment
C	Reactive balance adjustment
D	Helipot
E	Dial on helipot
F	Null detector (amplifier, band pass filter, vacuum tube voltmeter)
G	1000 c.p.s. oscillator

Fig. 8 - Schematic diagram of pressure instrumentation used for measuring velocity.

turbulent fluctuations so that only the mean fluctuation velocity of the order 1 cps was measured. The measurements were averaged by eye for two minutes for a reliable average velocity at each point of the profile. The calibration of the strain gage was carried out before and after each velocity profile, because long time intervals and large temperature variations changed the calibration of the gage. A cathetometer was used for the accurate readings of the water head during the calibration of the strain gage.

To avoid air bubbles in the strain gage system deaerated distilled water was used to fill the tubing, so that there would not be any small amount of air entrained in the water. Special care was also taken to avoid any slight leakage, which would completely upset the readings.

2. Sediment Concentration Measurements

The concentration of suspended sediment was measured by siphoning from the flow 3 or 6 samples of one liter each in groups from each point of the profile and by weighing the oven-dried sand residue after filtration.

The point sampler used in the experiments is shown in fig. 9. It was made of a 3/16-inch outside diameter brass tube flattened at the end so that the tip opening was .040 in. x .217 in. The tube was bent in a right angle much like a pitot tube. The horizontal part of the tube was 2-3/4 in. long and the vertical part of the tube was mounted on the movable carriage. The average velocity in the sampler at the tip was made to be the same as the stream

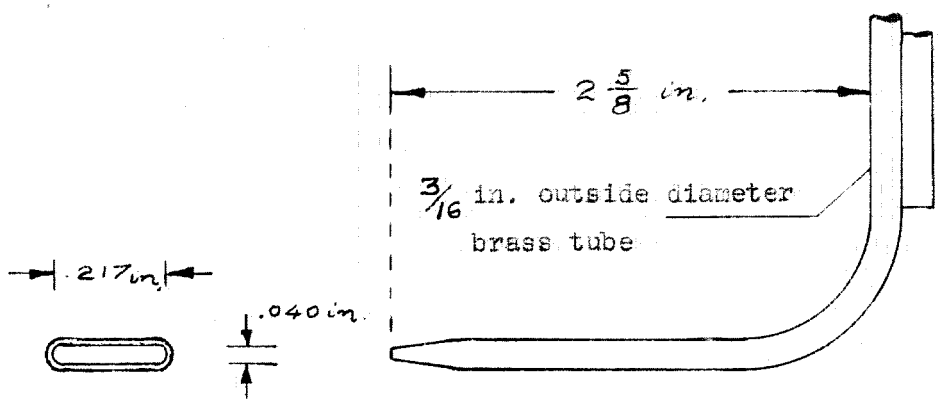

(a) Point sampler (for sediment)

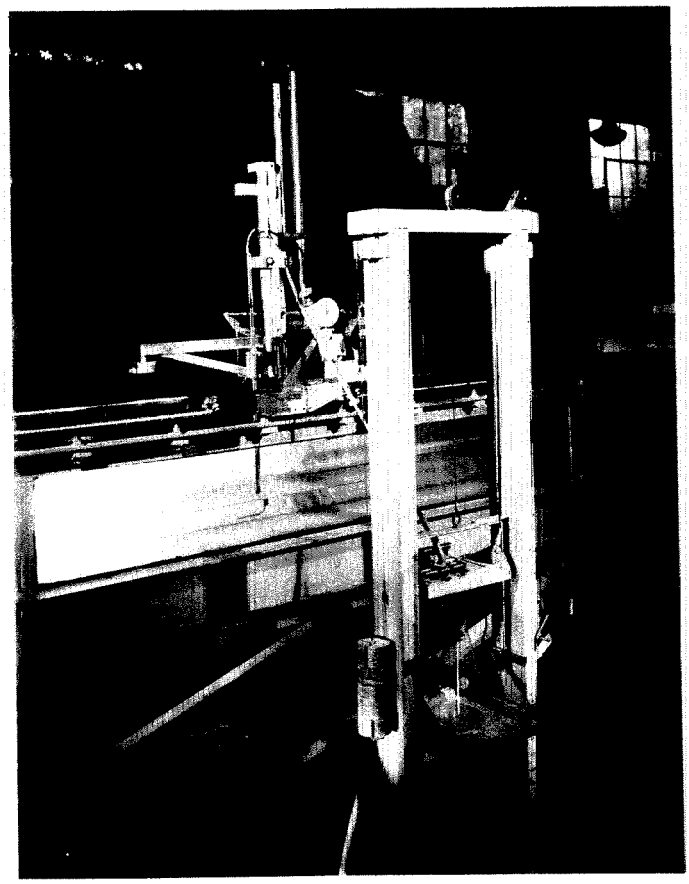

(b) Set-up for point sampling (sediment)

Fig. 9. Sampling equipment (for sediment)

velocity at the same point by adjusting the head of the siphon.

The sediment transport sampler used was a 0.302-inch inside diameter brass tube with a half loop at the end so that the inlet was facing upwards when the sampler was held vertical during sampling. The samples were taken at the downstream end of the flume in the pump well about 20 inches below the surface of the water. During the sampling the tip was moved continuously around to different parts of the cross section.

The use of a screen at the downstream end of the flume prevented the irregular sloughing of small blobs of sand from the bed at the edge of the pump well and therefore tended to minimize the fluctuations in sediment concentration in the pump well.

3. Water Surface and Bed Elevation Measurements

The water surface and bed elevations were measured to the nearest 0.001 ft. over the entire length of the flume, using the point gage mounted on the movable carriage.

For the water surface profile the average elevation was found over a short distance by moving the carriage back and forth.

For the bed profile it was necessary to stop the flow and level the dunes in a short reach. This was done with an adjustable double-bladed scraper, mounted on the rails. Once the sand of the given reach was redistributed making a perfectly flat surface, its elevation was measured on the center line using an intense oblique beam of light from a flashlight to light the bed when the measurement was made. By lowering the point gage until the point just touched its shadow in the sand bed accurate bed elevation measurements could be made.

C. Bed Shear and Friction Factor

1. Bed Shear

In turbulent flows the shear at the bed, like that at any point of the stream, varies with time because of the velocity fluctuations. Since the time average shear depends only on the mean flow characteristics we define as bed shear the resultant of all time averaged stresses acting on the bed in the direction of flow, averaged over a relatively large area.

For a two-dimensional channel (very wide) with uniform flow, the shear on the bed is equal to the component of the weight of the water along the flow direction (ref. 12), i.e.,

$$\tau_o = \gamma d S \tag{4.01}$$

where d is the depth of the stream, S the slope, and γ the specific weight of the water.

For a channel of finite width the average shear is equal to

$$\overline{\tau_o} = \gamma r S \tag{4.02}$$

where r is the hydraulic radius of the stream cross section. The shear distribution on the boundaries can be determined, using the logarithmic formula and measuring the velocity profile on lines perpendicular to the boundaries. The logarithmic profile is:

$$\frac{u}{u_*} = \frac{1}{K} \ln y^* + B = \frac{2.3}{K} \log_{10} y^* + B \tag{4.03}$$

where: $y^* = y \frac{u_*}{\nu}$

K is von Karman's constant

$\mathcal{B}$ is a constant.

For clear water flow in pipes with hydrodynamically smooth walls the constant $\mathcal{B}$ is equal to 5.5.

For rough walls $$\mathcal{B} = A_s - \frac{1}{\kappa} \ln \kappa_s^* \tag{4.04}$$

where $\kappa_s^* = \kappa_s \frac{u_*}{\nu}$

κ_s is the equivalent roughness

A_s is a constant.

When the velocity u is plotted against $\log_{10} y$ the slope m of the straight line profile in units of velocity per cycle of 10 is:

$$m = \frac{2.3\, u_*}{\kappa} \tag{4.05}$$

So by measuring m and knowing u_* we compute κ i.e.

$$\kappa = \frac{2.3 \times u_*}{m} \tag{4.06}$$

If the value of u_* is unknown, then we first find κ by averaging the shear τ_o all over the boundaries of the cross section, i.e.

From: $$\tau_o = \rho u_*^2 = \rho \frac{\kappa^2 m^2}{(2.3)^2}$$

Averaging: $$\overline{\tau_o} = \rho \frac{\kappa^2 \overline{m^2}}{(2.3)^2}$$

Solving for κ : $$\kappa = \frac{2.3\, U_*}{\sqrt{\overline{m^2}}} \tag{4.07}$$

where U_* is the average shear velocity of the total cross section.

And assuming that κ is constant for the total cross section we compute u_* for any point on the boundary as:

$$u_* = \frac{\kappa m}{2.3} \tag{4.08}$$

2. Friction Factor

The friction factor, f, defined by the Darcy-Weisbach relation is such that

$$\bar{\tau}_o = \frac{f}{4} \rho \frac{U^2}{2} \tag{4.09}$$

Solving for f and substituting ρU_*^2 for $\bar{\tau}_o$ we get

$$f = 8 \frac{U_*^2}{U^2} \tag{4.10}$$

where: U_* is the average shear velocity, and

U is the average flow velocity.

For the derivation of the friction factor of the bed, f_b, the following procedure is followed, used by Brooks[13], which is based largely on a procedure outlined by Johnson[19]. Assuming that the cross section could be divided into a bed section and a wall section, with average velocities equal to that of the entire cross section we get:

$$\bar{\tau}_b = \frac{f_b}{4} \rho \frac{U^2}{2} \qquad \text{and} \qquad \bar{\tau}_w = \frac{f_w}{4} \rho \frac{U^2}{2} \tag{4.11}$$

where $\bar{\tau}_b = \rho U_{*b}^2$ is the mean bed shear stress, and

$\bar{\tau}_w = \rho U_{*w}^2$ is the mean side-wall shear stress

Also

$$U_{*b} = \sqrt{g r_b S} \qquad \text{and} \qquad U_{*w} = \sqrt{g r_w S} \tag{4.12}$$

where r_b is the bed hydraulic radius, and

r_w is the wall hydraulic radius

Substituting $\bar{\tau}_b$ & $\bar{\tau}_w$ in equations 4.11 and solving for f_b and f_w one gets:

$$f_b = 8\left(\frac{U_{*b}}{U}\right)^2 \quad \text{and} \quad f_w = 8\left(\frac{U_{*w}}{U}\right)^2 \tag{4.13}$$

The Reynolds numbers are respectively:

$$Re_b = \frac{4Ur_b}{\nu}, \quad Re_w = \frac{4Ur_w}{\nu} \quad \text{and} \quad Re = \frac{4Ur}{\nu}$$

where r is the hydraulic radius of the total cross section. Taking the ratios of the above Reynolds numbers we get:

$$\frac{Re_b}{r_b} = \frac{Re_w}{r_w} = \frac{Re}{r}$$

Introducing equations 4.11 and 4.12 for the friction factors we get:

$$\frac{Re_b}{f_b} = \frac{Re_w}{f_w} = \frac{Re}{f} \tag{4.14}$$

Thus, when we know the friction factor f and the Reynolds number Re we can find the ratio $\frac{Re_w}{f_w}$.

For smooth walls we use fig. 10, based on the graph of f vs. Re given in standard text books to determine the f_w corresponding to the above computed ratio $\frac{Re}{f}$.

Now, from the fact that the total shear force is equal to:

$$p\bar{\tau}_o = p_b\bar{\tau}_b + p_w\bar{\tau}_w$$

where: p is the total wetted perimeter of the cross section

p_b is the wetted perimeter of the bed section

p_w is the wetted perimeter of the wall section

introducing the equations 4.11 for the shears we get:

$$fp = f_b p_b + f_w p_w$$

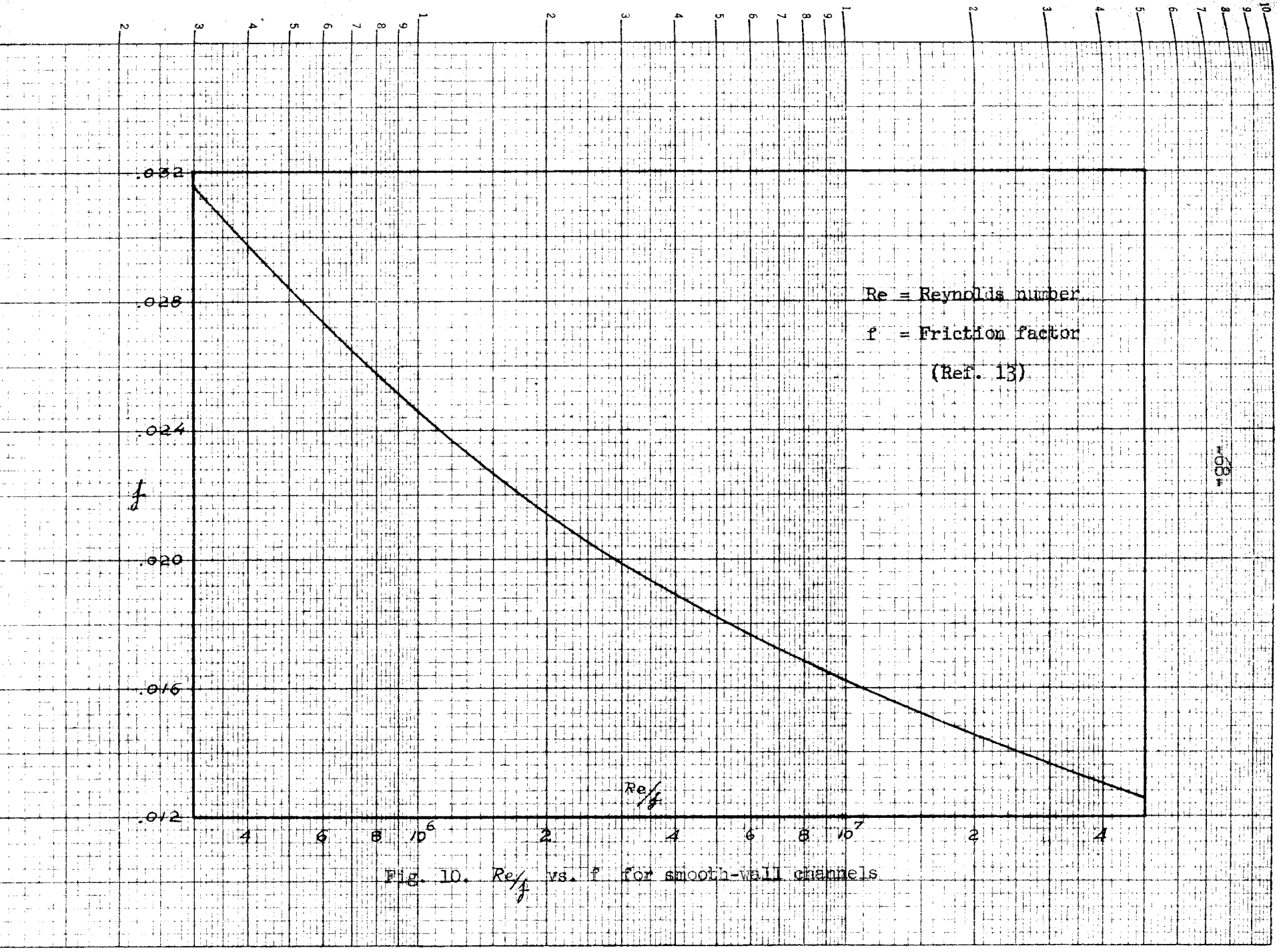

Fig. 10. Re/f vs. f for smooth-wall channels

and solving for f_b :

$$f_b = \frac{p}{p_b} f - \frac{p_w}{p_b} f_w \qquad (4.15)$$

For rectangular channels, where $p = b+2d$, $p_b = b$, $p_w = 2d$ the above equation becomes:

$$f_b = f + \frac{2d}{b}(f - f_w) \qquad (4.16)$$

3. Bed Shear at Centerline

As suggested by Brooks[13] u_* at the centerline can be calculated approximately from:

(i) A measured velocity profile at $\mathcal{L}$, from which the mean velocity $\bar{u}_{\mathcal{L}}$ is read at $y/d = 1/e$ or $y = .37d$, and

(ii) The friction factor for the bed f_b.

Substituting in the Darcy-Weisbach formula we get:

$$u_{*\mathcal{L}} = \bar{u}_{\mathcal{L}} \sqrt{\frac{f_b}{8}} \qquad (4.17)$$

Under any circumstances $u_{*\mathcal{L}}$ should always be less or at most equal to the two-dimensional shear velocity $u_{*_{2-D}} = \sqrt{gdS}$.

D. Sand Characteristics

1. Sand Preparation

The sands used in the experiments were prepared by grading silica sands in a wind-tunnel classifier. This device[14], shown in fig. 11 is arranged so that the sand is dropped into the stream near the upstream end of the horizontal wind stream in a sheet extending over the full width of the tunnel. The sand grains

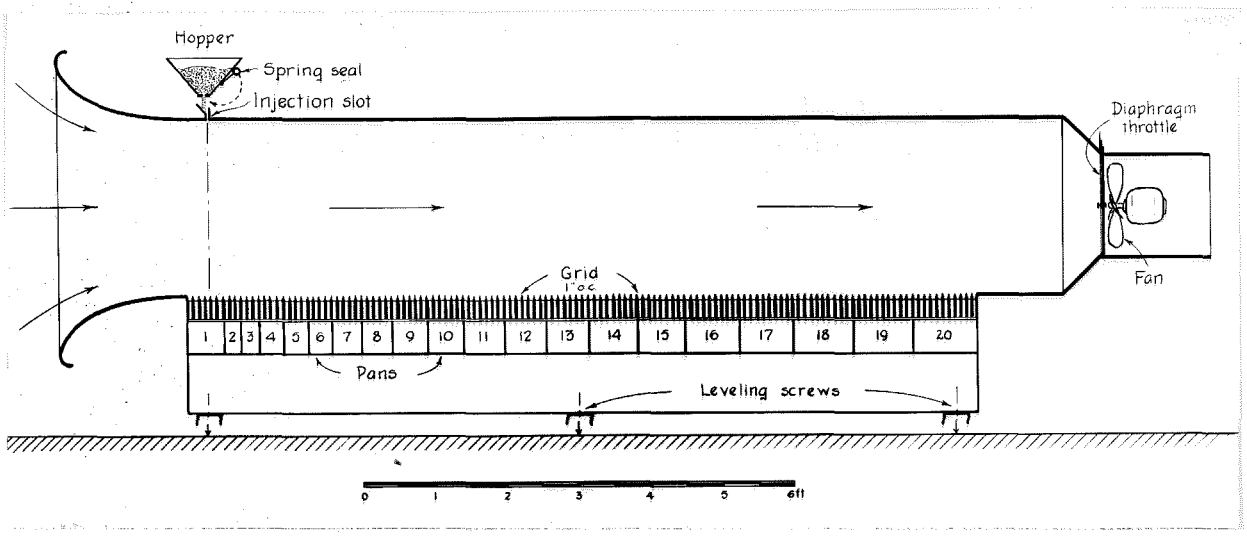

(a) Profile diagram of tunnel.

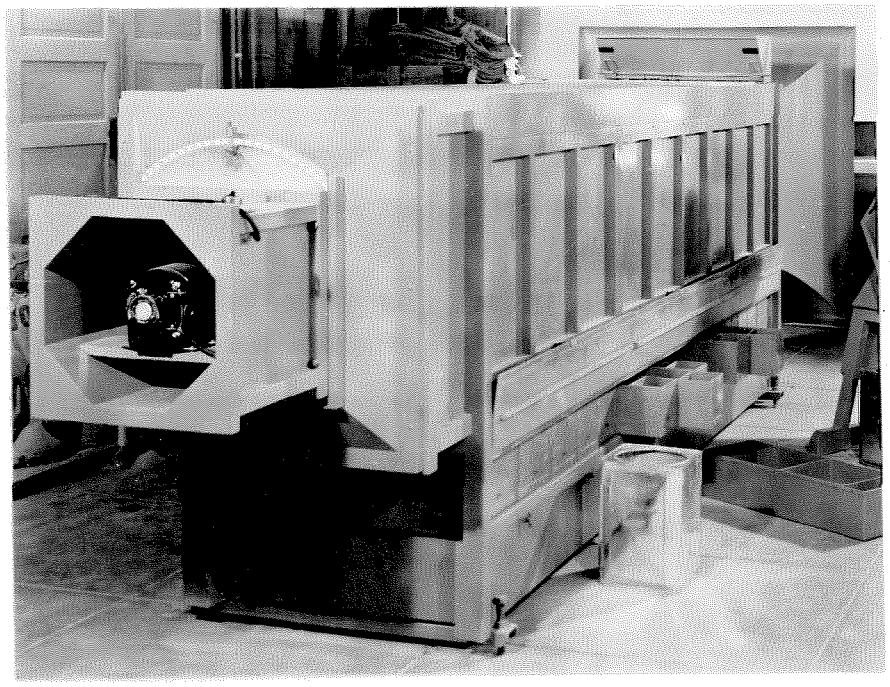

(b) Photograph, looking toward outlet end.

Fig. 11 - Wind tunnel classifier for sorting sand.

are collected in pans along the bottom of the stream, being separated into a number of size fractions according to their settling velocities, with the finer grains settling further downstream. One thickness of cheesecloth stretched over the face of the nozzle at the inlet end of the tunnel decreased the dispersion in size separation by damping out eddies that caused fluctuations of the velocity.

After sorting, the sediment was washed in water with a small amount of sodium oxalate, used as a peptizer to loosen the dust and dirt which adhered to the grains.

2. Fall Velocity

Since all three sands used in the experiments were predominantly quartz (specific gravity 2.65), the calculation of their settling velocity was based on their sedimentation diameter, or the diameter of quartz spheres with identical fall velocity. A chart prepared by Rouse for the fall velocity of quartz spheres and derived from the diagram of drag coefficient of spheres vs. Reynolds number was used.

The interference of the flow patterns due to an increased concentration of the particles, decreased the fall velocity of the grains. This so-called hindered settling was taken into account in the analysis of the experimental results as a function of the concentration, using Table 4 based on McNown and Lin[15].

3. Mean Sedimentation Diameter

The mean sedimentation diameter of a mixture was determined by computing its mean fall velocity from Table 5, based on

TABLE 4 - Effect of concentration on the fall velocity of quartz spheres in water.
(based on McNown and Lin, ref. 15)

Diameter = .105 mm Temperature = 25° C

Concent. grms/lit.	Fall Vel. ft/sec	Reduction per cent
0	.0310	0
.1	.0309	.2
1	.0300	3
5	.0284	8
10	.0273	12
20	.0259	16
30	.0250	19

TABLE 5 - Relation between sedimentation diameter and sieve diameter.
(based on Vanoni for Nevada white sand, ref. 8)

Tyler Sieve No. retained on	Sieve Opening next above	Sieve Opening retained on	Mean Sieve diam.	D_{Si} Mean Sediment diam.	W_i Fall Velocity at 20° C	W_i Fall Velocity at 25° C
no.	mm	mm	mm	mm	fps	fps
50	.351	.295	.323	.323*		.158*
60	.295	.246	.270	.270*		.125*
70	.246	.208	.227	.227*		.098*
80	.208	.175	.191	.198	.078	.083
100	.175	.147	.161	.168	.061	.066
115	.147	.124	.135	.153	.053	.058
150	.124	.104	.114	.128	.038	.042
170	.104	.088	.096	.107	.029	.032
200	.088	.074	.081	.096	.024	.027
250	.074	.061	.0675	.086	.020	.022
Pan	.061	.040*	.050*	.070*	.014*	.016*

Note: * Estimated value.

Vanoni's experiments[8] for the relation of the fall velocity to the sieve diameter of standard Tyler laboratory sieves.

By averaging the fall velocity we get:

$$w = \sum_i w_i p_i$$

where p_i is the fraction of the weight of sand retained in the i^{th} sieve fraction

and $\sum_i p_i = 1$

From the mean fall velocity w the mean sedimentation diameter d_s is found from a chart prepared by Rouse for the fall velocity of quartz spheres as outlined in the preceding article.

4. Mechanical Analysis

The size distribution of the three sands used and their photomicrographs are shown in fig. 12. The first was a well-sorted white silica sand with geometric mean sieve diameter $d_g \simeq .091$ mm and geometric standard deviation $\sigma_g \simeq 1.16$, prepared from a foundry sand and obtained from a local foundry supply company. The second was a well-sorted pink stained sand with the same characteristics as the first, prepared from the sand used before in laboratory studies at the Institute by Brooks[13] and Ismail[16]. The third was a well-sorted white sand with geometric mean sieve diameter $d_g \simeq .148$ mm and geometric standard deviation $\sigma_g \simeq 1.16$, prepared from a molding sand and obtained from a local firm.

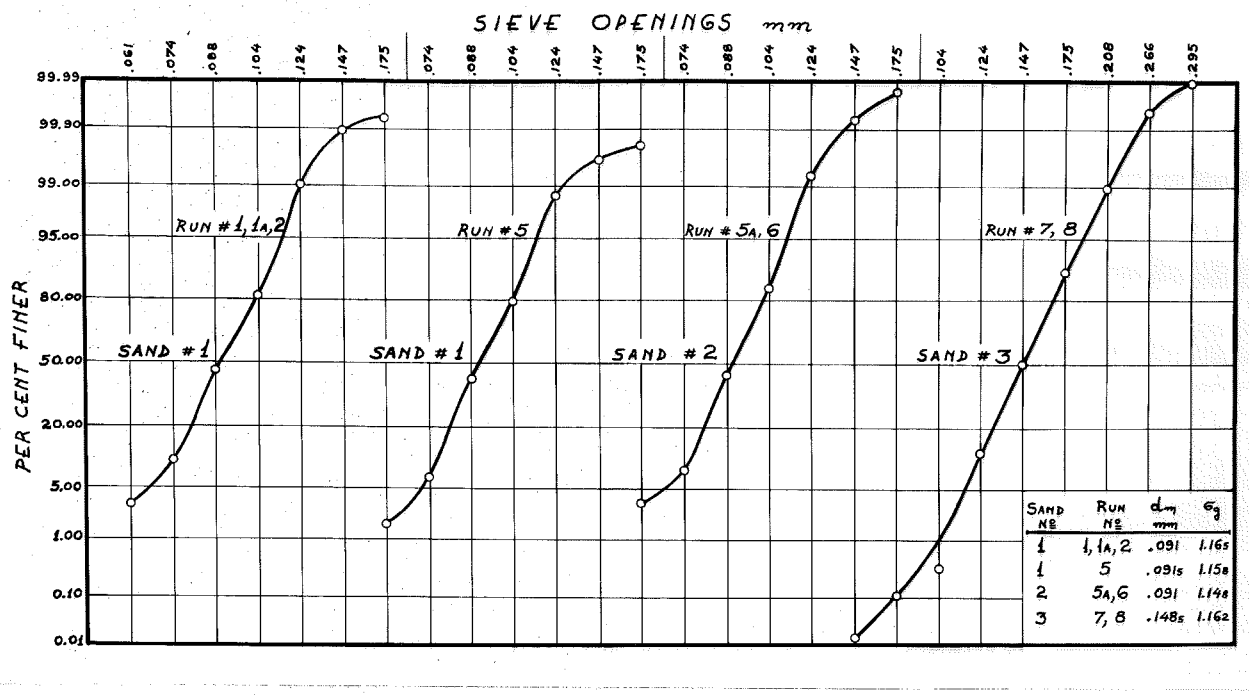

Sieve analysis of sands.

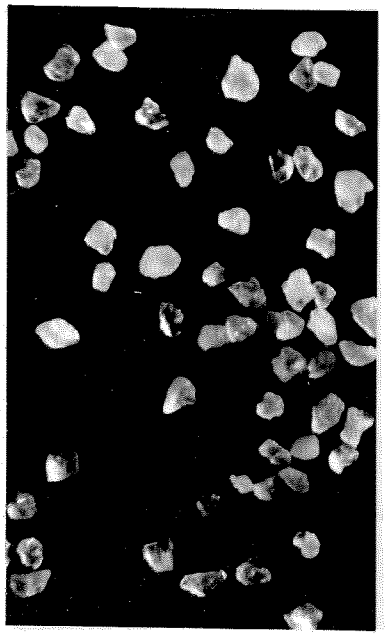

No. 1 sand
(.10mm)

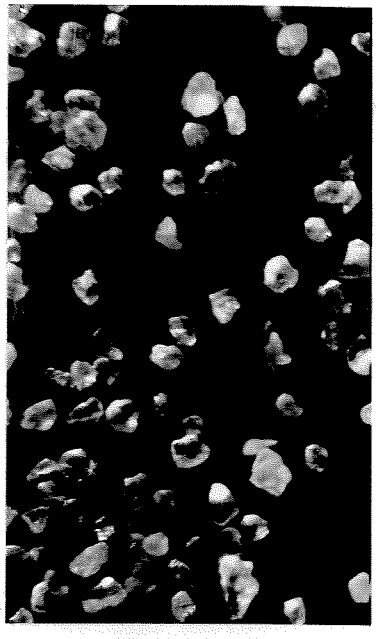

No. 2 sand
(.10mm)

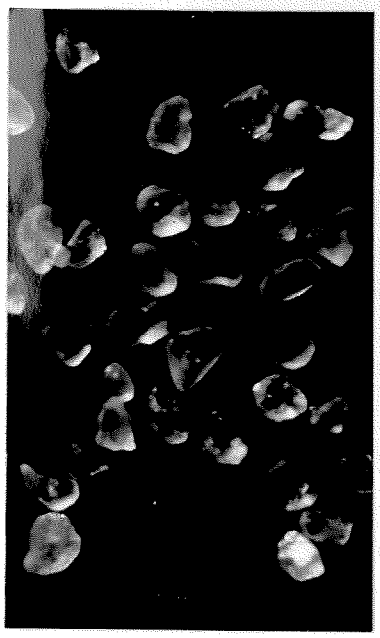

No. 3 sand
(.16mm)

Fig. 12 - Sieve analysis and photomicrographs of sands.
(Magnification - 35 times)

Summary of Sand Properties

Table 6

Sand No.	Sand #1	Sand #1	Sand #2	Sand #3
Set of Experiments	I, II	Part of III	III	IV
Geometric Mean Diameter d_g (mm)	.091	.091	.0915	.1485
Geometric Standard Deviation σ_g	1.165	1.160	1.158	1.163
Mean Sed. Diam. d_s (mm)	.105	.106	.106	.161
Mean Settling Vel. at 25°C w(fps)	.0311	.0318	.0310	.0623

E. Stabilization of Sand Bed

One of the most important factors for the success of the experiments carried out was the selection of a good stabilization method. Numerous tests on methods of stabilizing a sand bed in place were conducted using chemical grouts but very few were completely successful.

At the beginning and for the first two sets of experiments with low velocities, a method was developed involving use of solutions of calcium chloride and sodium silicate as well as waterproof synthetic varnish. This method was not adequate for prolonged submergence and when the velocity became higher in the third set of experiments it failed completely.

Therefore, a second method, developed to resist higher velocities, was used for the last two sets of experiments. It involved chemical grouts of sodium aluminate and sodium silicate as well as calcium chloride and synthetic varnish.

1st Method

In this method the following technique was evolved:

Step 1: The water was drained carefully from the natural bed configuration and allowed to dry for 24 to 48 hours at room temperature, so that its moisture content would be approximately 10% by weight.

Step 2: Calcium chloride solution with specific gravity 1.2 was sprayed gently on the surface of the sand bed with a paint sprayer. The amount used was about 5% by weight of sand, or enough to make the surface show signs of saturation.

Step 3: Approximately the same amount of sodium silicate solution with specific gravity 1.2 (24° Be in 80°F) was sprayed immediately after the calcium chloride on the sand bed and it was left to set for 24 hours.

Step 4: Synthetic varnish manufactured by Krylon, Incorporated, Philadelphia, Pa., called "Krylon Acrylic" was sprayed on 24 hours after the sodium silicate, giving a strong waterproof surface. The amount used was about half that of calcium chloride.

2nd Method

In this method the following steps were evolved:

Step 1: Same as in the first method.

Step 2: A mixture was sprayed of the following (percentages by volume):

68% sodium aluminate, 2% solution by weight,

22% sodium silicate solution of spec. grav. 1.2,
10% distilled water

The amount used was about 10% by weight of sand and it was sprayed all at once at the same location until signs of saturation would appear.

Step 3: After drying, about 12 hours, a light coat of calcium chloride solution of specific gravity 1.2 was applied.

Step 4: Finally a thin coat of acrylic varnish was sprayed on the surface of the sand the next day.

For the mixing of the solutions of sodium aluminate and sodium silicate it was found easiest to add the latter to the former while constantly stirring. Otherwise there would be an excess of sodium aluminate over sodium silicate at the contact point, thereby speeding the reaction of thickening and forming small globules of jell, which tended to plug the painting gun and did not penetrate into the sand. The addition of the distilled water was necessary so that the mixture would begin to set in about 20 minutes, permitting ample time to spray one small paint-sprayer container on the sand bed before the reaction would thicken the solution in the sprayer. The time required for setting of the mixture used was about one hour.

Since the most important problem in the stabilization process is that of preserving the proper grain roughness of the surface, careful attention was paid to the technique of the application of the chemical grouts, as well as their amounts. Therefore, all

the solutions were sprayed with a paint sprayer. During spraying the air stream was kept parallel to the sand bed, so that the spray would not disturb the surface of the bed.

The moisture of the sand, when the chemicals were applied, was kept low; otherwise the penetration of the chemicals would be small and therefore the structural strength of the stabilized surface inadequate.

The waterproof acrylic varnish formed a very thin skin, which held the sand grains firmly, and prevented them from being scoured from the bed and coming into suspension when clear water flowed over the bed.

F. Procedure

1. Uniform Flow with Movable Bed

In order to establish uniform flow in equilibrium with a movable bed, there should be a constant depth and a surface profile with uniform slope in a reasonably long working section of the flume. By fixing the rate of flow and the depth it was easy to make the adjustment of the slope to achieve uniform flow.

By plotting the energy grade line, as shown in a typical example in fig. 13, it was made sure that the flow was uniform. The specific energy, e_R, in coordinates referred to the rails of the flume, is defined as:

$$e_R = y_w + \frac{v^2}{2g}$$

where: v = mean velocity in the cross section,

y_w = water surface elevation

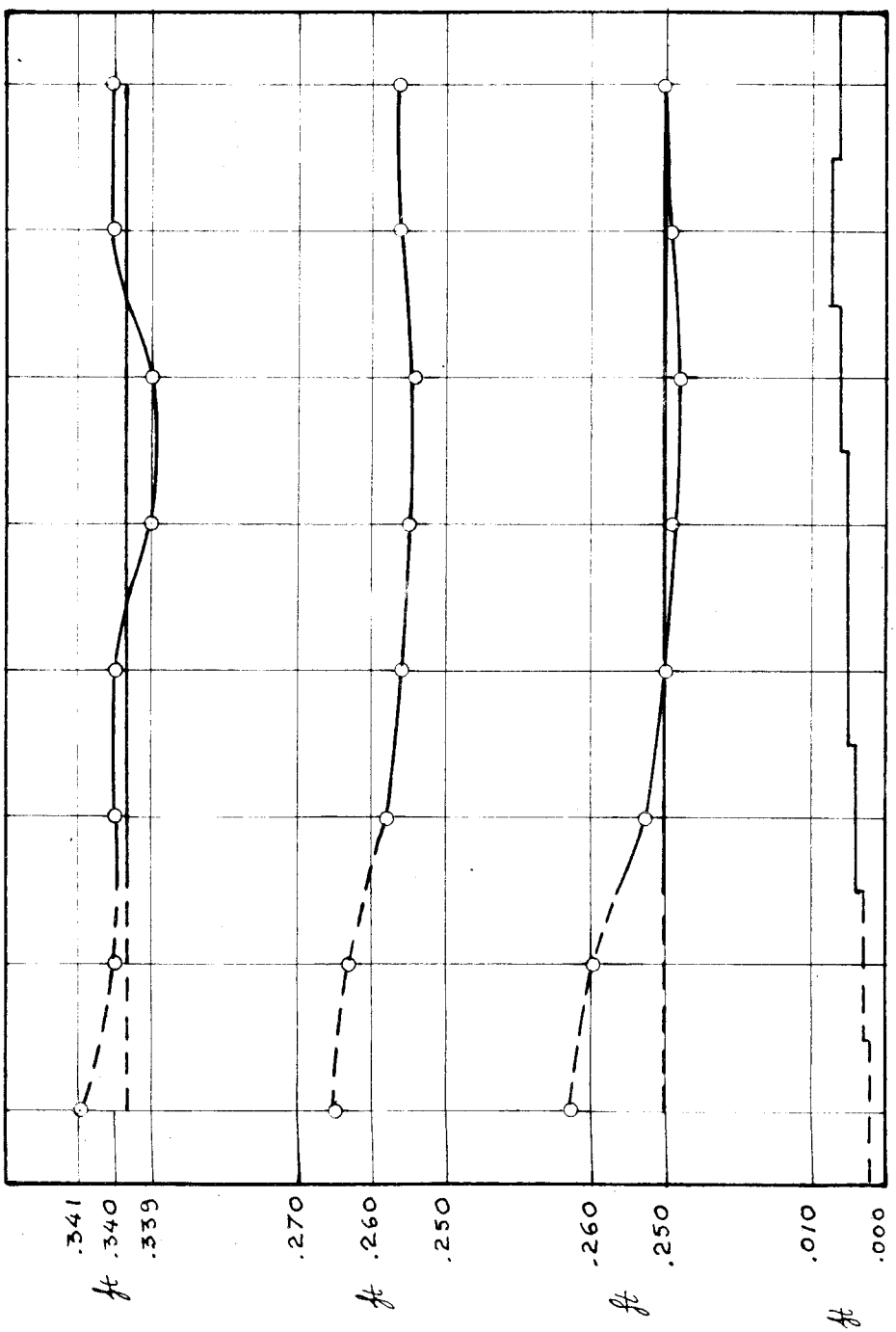

Fig. 13. Typical example of energy grade line

After running the flume for 3 or 4 hours to ensure that the equilibrium conditions had been established, the following measurements were taken, according to procedures outlined in detail in article B of this chapter:

a. The water surface profile along the flume

b. Vertical velocity profile at the centerline near station 24

c. Sediment concentration profile at the centerline of station 24

d. Average sediment transport concentration

e. Bed elevation profile along the flume

Rechecking again the equilibrium of the established flow, the run was repeated; then the pump was stopped and the water drained very carefully, in order to proceed to the stabilization of the top layer of the sand bed, without disturbing its natural form.

2. Stabilization of the Sand Bed

Within one or two days from the time the stabilization procedure described in article E had been completed, the return pipe, pump well, venturi meter, and the diffuser, were dismantled and washed out carefully with water to remove all the sand, deposited when the flow with the movable bed was stopped. Then the entire closed system was connected again, making sure that there was not any loose sand remaining in it.

3. Clear Water Flow on Stabilized Sand Bed

Starting with clear water the same flow as that with the movable bed was reproduced on the stabilized sand bed. The discharge, depth and consequently the mean velocity were all kept

the same (velocity) as those of the movable bed flow. However the slope varied and it was adjusted to establish uniform flow.

When it was made sure that stable equilibrium conditions had been established, the following measurements were made, according to procedures outlined before.

a. The water surface profile along the flume

b. The velocity profile at the centerline of Stat. 24

c. The average sediment transport concentration

d. The elevation of the crests and troughs of the bed dunes in some prescribed places.

It should be stressed that the equilibrium conditions were checked for their stability, at the end of the measurements of each of the above profiles.

4. Sediment Laden Flow on Stabilized Sand Bed

A small amount of loose sediment (with the same characteristics as the sand of the stabilized bed) was added to the clear water flow described in the preceding article. Following the same procedure as outlined in the preceding article, uniform flow was established by adjusting only the slope of the flume. The mean depth and velocity were kept the same as those of the clear water flow. Measurements of the various profiles were taken, checking continually to see that uniform flow was maintained.

Then more sand was added to the system and the same procedure was followed after each addition of sand, establishing uniform flow and taking measurements of the various profiles.

5. Sediment Laden Flow on Smooth Painted Bed

For these experiments, both the bed and the walls of the flume were hydrodynamically smooth, painted carefully with bitumastic paint. First a clear water uniform flow was established and measurements of the profiles outlined in article F3 of this chapter were taken.

Then some of the No. 2 sand was added to the system in many steps and the same procedure was followed, as before, establishing uniform flow and taking measurements of the various profiles, after each addition of sand.

6. Sediment Laden Flow on Sand-coated Bed

For the experiments of series II the side walls were hydrodynamically smooth, as they were for all the runs of this investigation. The bed was coated with sand grains by spreading them on the freshly painted steel bottom of the flume. After three days, when the paint was thoroughly dried, all the loose sand grains were swept away with a hard brush, so that a rough bed was obtained.

Then starting with clear water uniform flow was established. Following the same procedure as that in the preceding articles, measurements of the various profiles were taken for several runs. Runs with sediment of the same size as that used to coat the bed were then made for each flow rate and depth used in the clear water runs.

CHAPTER V

RESULTS

A. Experimental Results

1. Outline of Experiments

From the procedure followed in this study, given in detail in Chapter IV, article F, it is obvious that the experiments may be divided into two series.

The first series includes the first four sets of runs for which the sand bed was stabilized in its natural configuration. Each of the four sets included the following runs:

1. A run with loose sand movable bed.
2. A run of clear water on the stabilized natural sand bed of the preceding run.
3. Runs of sediment laden flows with sand of the same size as that of the bed added in steps.

The second series of experiments includes the runs 9, 10 and 12, for which the bed was smoothly painted, coated with .10 mm sand and .16 mm sand respectively, as outlined previously.

Uniform flow of clear water was first established. Then sand of the same size as that of the coated bed (.10 mm or .16 mm) was added to the system in steps, and sediment laden uniform flows were established, with various concentrations according to the amount of sand added in each step.

2. Summary of Experiments

A summary of the experiments with the most important measured and calculated quantities for each run, are tabulated in Tables 7 and 8. The missing items, either were not measured

Table 7 - Summary of results

Series No.	Set No.	Run No.	Discharge Q cfs	Depth d ft	Hydraulic radius r ft	Mean Velocity U fps	Slope of Energy Grade line S_e	Mean Shear Velocity U_* fps	Mean Friction Factor f	Bed Friction Factor f_b	Shear Vel. at ℄ u_{*C} fps	Karman's Constant at ℄ K_C	Ave.Trans. Concent. $\bar{C}_T$	Froude Number $F_e=U/\sqrt{gd}$	Sand Size mm	Bed Condition
		1	.306	.284	.172	1.23	.0025	.118	.0735	.1058	.151	.369	3.64	.41	.10	dunes
		1A	.306	.284	.172	1.23	.00247	.117	.0727	.1044	.150	.367	3.38	.41	.10	"
		2	.306	.284	.172	1.23	.00262	.121	.0771	.1116	.155		0.00	.41	.10	"
1st	I	2a	.306	.284	.172	1.23	.00257	.119	.0757	.1093	.153		0.31	.41	.10	"
		2b	.306	.284	.172	1.23	.00253	.119	.0744	.1071	.152		0.47	.41	.10	"
		2c	.306	.284	.172	1.23	.00249	.118	.0733	.1054	.151		0.60	.41	.10	"
		2d	.306	.284	.172	1.23	.00247	.117	.0727	.1044	.150		0.83	.41	.10	"
		3	.433	.244	.157	2.02	.0020	.101	.0198	.0211	.110	.265	4.60	.72	.10	small dunes
		4	.433	.244	.157	2.02	.0025	.112	.0246	.0283			0.00	.72	.10	"
1st	II	4a	.433	.244	.157	2.02	.0023	.108	.0226	.0253			1.71	.72	.10	"
		4b	.433	.244	.157	2.02	.0021	.103	.0207	.0225			3.44	.72	.10	"
		4c	.433	.244	.157	2.02	.0020	.101	.0198	.0211			3.63	.72	.10	"
		5	.509	.257	.162	2.26	.00206	.1035	.0169	.0170	.111	.223	6.92	.78	.10	plane
		5A	.509	.255	.161	2.28	.00206	.1035	.0165	.0165	.109	.219	8.08	.79	.10	"
1st	III	6	.509	.255	.161	2.28	.00251	.114	.0208	.0229	.136	.384	0.00	.79	.10	"
		6a	.509	.255	.161	2.28	.00227	.1085	.0182	.0189	.116	.255	3.99	.79	.10	"
		6b	.509	.254	.161	2.28	.00227	.1085	.0180	.0187	.116	.236	5.71	.80	.10	"
		6c	.509	.252	.160	2.30	.00210	.104	.0163	.0164	.114	.209	6.82	.81	.10	"
		7	.509	.255	.161	2.28	.00258	.116	.0207	.0227	.135	.299	3.61	.79	.16	plane
		8	.509	.253	.160	2.29	.00293	.123	.0230	.0262	.150	.364	0.00	.80	.16	"
		8B	.509	.253	.160	2.29	.00259	.116	.0203	.0222	.134	.355	0.00	.80	.16	"
1st	IV	8a	.509	.254	.161	2.28	.00259	.116	.0206	.0225	.135	.345	0.51	.80	.16	"
		8b	.509	.253	.160	2.29	.00257	.116	.0202	.0219	.133	.330	1.41	.80	.16	"
		8c	.509	.253	.160	2.29	.00257	.116	.0202	.0219	.133	.315	2.43	.80	.16	"
		8d	.509	.253	.160	2.29	.00259	.116	.0203	.0222	.134	.310	3.27	.80	.16	"
		9	.509	.255	.161	2.28	.0020	.102	.0160	.0162	.113	.364	0.005	.79	.10	smooth
		9a	.509	.255	.161	2.28	.0020	.102	.0160	.0162	.113	.360	0.05	.79	.10	plane
		9b	.509	.255	.161	2.28	.0020	.102	.0160	.0162	.112	.354	0.13	.79	.10	"
2nd	V	9c	.509	.255	.161	2.28	.0020	.102	.0160	.0162	.112	.348	0.42	.79	.10	"
		9d	.509	.254	.161	2.28	.00205	.103	.0163	.0164	.113	.319	1.02	.80	.10	ripples at walls
		9e	.509	.253	.160	2.29	.00207	.1035	.0163	.0164	.114	.284	2.10	.80	.10	" " "
		9f	.509	.252	.160	2.30	.0021	.104	.0163	.0164	.116	.258	3.46	.81	.10	dunes at walls
		9g	.509	.250	.159	2.32	.0022	.106	.0167	.0169	.119	.227	8.06	.82	.10	" " "
		10	.509	.255	.161	2.28	.0021	.104	.0168	.0170	.113	.348	0.00	.79	.10	.10mm coated
		10a	.509	.255	.161	2.28	.0021	.104	.0168	.0170	.113	.326	0.75	.79	.10	plane
2nd	VI	10b	.509	.255	.161	2.28	.0021	.104	.0168	.0170	.113	.307	2.33	.79	.10	ripples at walls
		10c	.509	.255	.161	2.28	.0021	.104	.0168	.0170	.113	.275	5.56	.79	.10	dunes at walls
		10d	.509	.255	.161	2.28	.0021	.104	.0168	.0170	.113	.242	6.28	.79	.10	" " "
		12	.509	.255	.161	2.28	.00222	.107	.0178	.0184	.119	.359	0.00	.79	.16	.16mm coated
		12a	.509	.255	.161	2.28	.00222	.107	.0178	.0184	.120	.335	0.51	.79	.16	plane
2nd	VII	12b	.509	.254	.161	2.28	.00243	.112	.0193	.0206	.127	.328	1.65	.80	.16	ripples at walls
		12c	.509	.254	.161	2.28	.00253	.114	.0201	.0218	.131	.314	2.83	.80	.16	dunes at walls
		12d	.509	.255	.161	2.28	.00255	.115	.0204	.0223	.134	.299	3.26	.79	.16	" " "

Note: The bed was stabilized in runs 2, 4, 6 and 8.-

Table 8

Exponent z of sediment concentration formula $\frac{c}{c_{ad}} = \left(\frac{d-y}{y}\right)^z$

Run No.	$\frac{w}{\kappa u_*} = z$ computed	z measured	$\beta = \frac{z_{comp}}{z_{meas.}}$
1	.528	.526	1.00
3	.983	.970	1.01
5	1.131	1.127	1.00
7	1.510	1.527	.99

or not calculated.

3. Bed Configuration

For almost all of the runs some observations of the movable bed were made and photographs were taken of the bed configuration. Some of them have been grouped together for each set of experiments, giving an overall view of the bed configuration (figs. 14-17).

For relatively low stream velocities the dunes are fairly large with large bed roughness and consequently large friction factor.

For the second and third sets of experiments with .10 mm sand, the concentration of suspended sand was fairly large and the scattering of the light by the grains in suspension was such that it was not possible to observe the bed configuration during the flow.

When the flow was stopped it was observed that small ripples were formed in the upstream part of the flume, though the bed at the middle and downstream part of the flume remained practically plane. Thus one could not be sure if the above small dunes existed

during the flow or were formed while the water decelerated after the pump was stopped.

In the fourth set of runs with .16 mm sand the visibility was much better and it was very easy to observe that the bed was practically plane all along the length of the flume.

When the pump was stopped, a large wave was formed at the pump well and traveled upstream. The water in the flume decelerated slowly until at each point, it was abruptly stopped when the travelling wave passed by. At the far upstream end of the flume, there was a period of about 15 seconds before the arrival of the travelling wave, when the deceleration was gradual. During this short interval small ripples formed on the sand bed at the upstream end of the flume. The sand bed at the downstream end of the flume was practically undisturbed because the velocity of the decelerating flow was still relatively high when the wave passed over stopping the flow.

The following technique was used for the elimination of the bed disturbances from the deceleration of the flow. As soon as the pump was switched off, a board, about 10 inches wide, was inserted into approximately half the depth of the flow, and starting from the middle of the flume, it was moved to the upstream end, making a wave in front of it. Special care was taken so that this wave would be of the right size and speed in

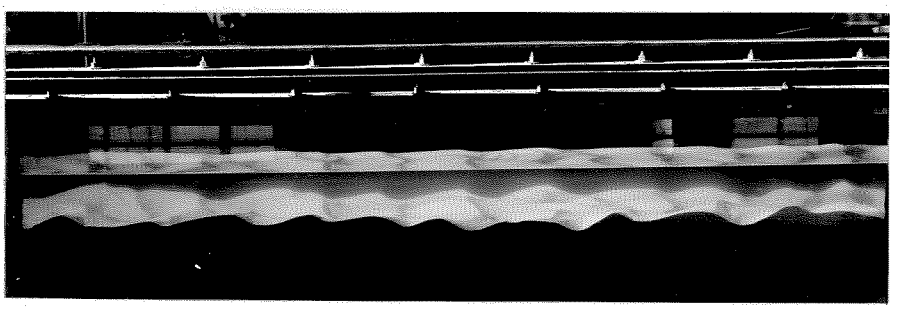

(a) Run No. 1, sideview, loose sand, during flow.

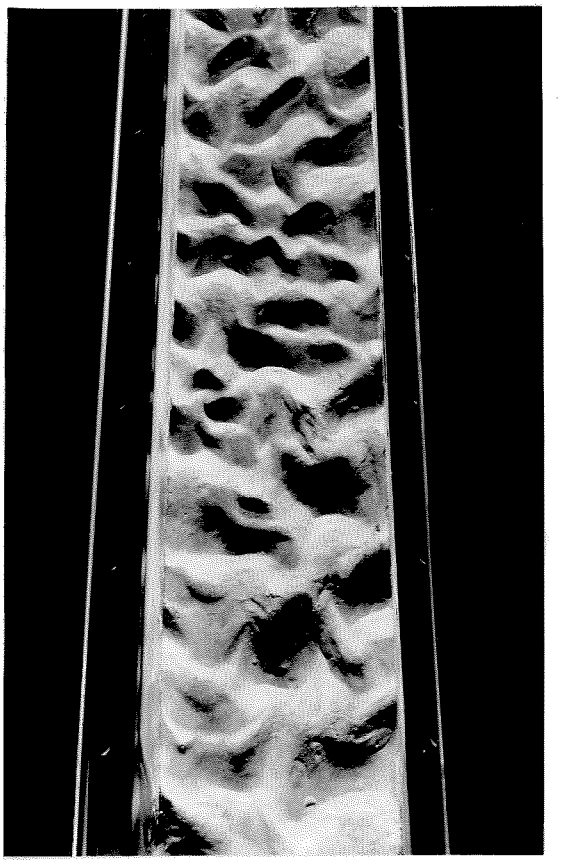

(b) Run No. 2, plan view, stabilized bed, looking upstream, without flow.

Fig. 14 - Bed configuration. Set I, U = 1.23 fps, d = .284 ft.

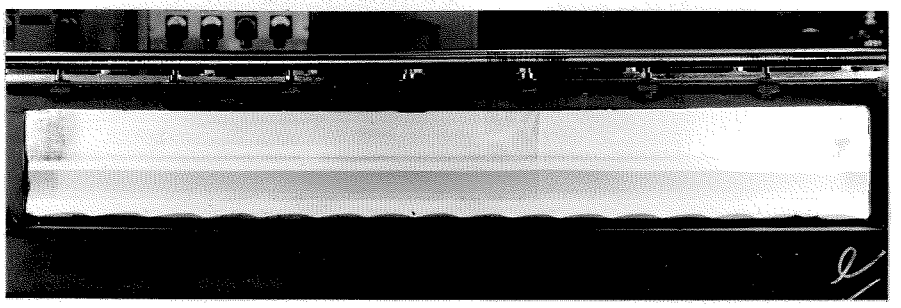

(a) Run No. 3, sideview, loose sand, during flow.

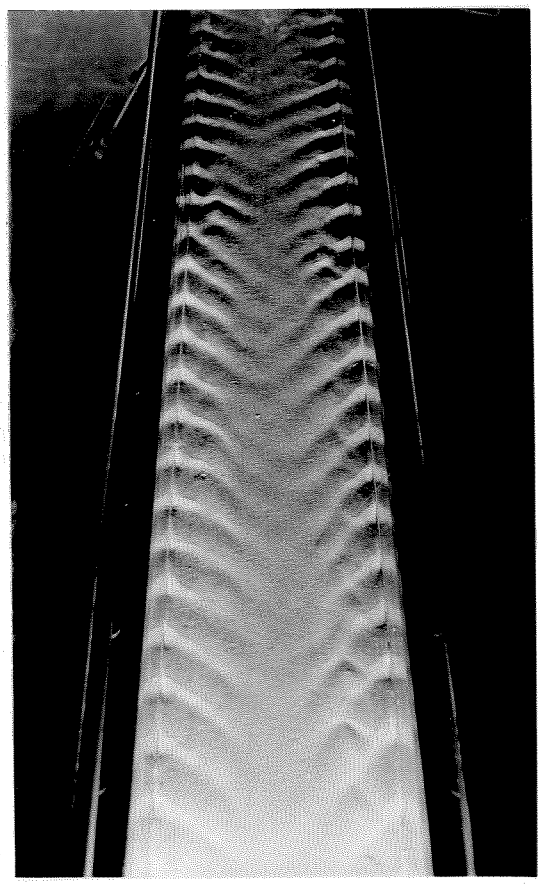

(b) Run No. 4, plan view, stabilized bed, looking upstream, without flow.

Fig. 15 - Bed configuration. Set II, $U = 2.02$ fps, $d = .244$ ft.

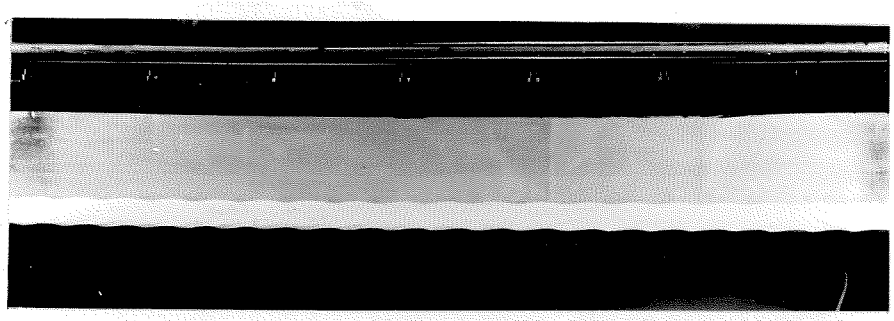

Run No. 5, sideview, loose sand, without flow.

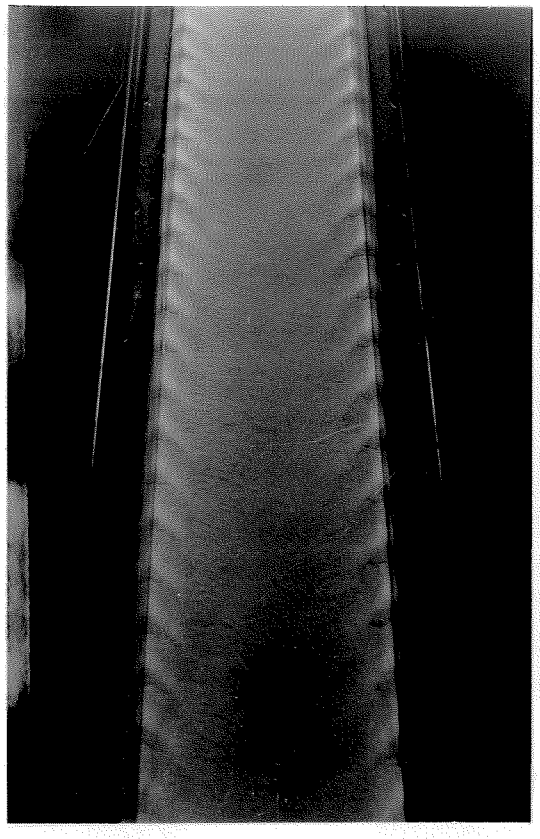

(b) Run No. 5, plan view, looking upstream, loose sand.

Fig. 16 - Bed configuration. Set III, U = 2.28 fps, d = .255 ft.

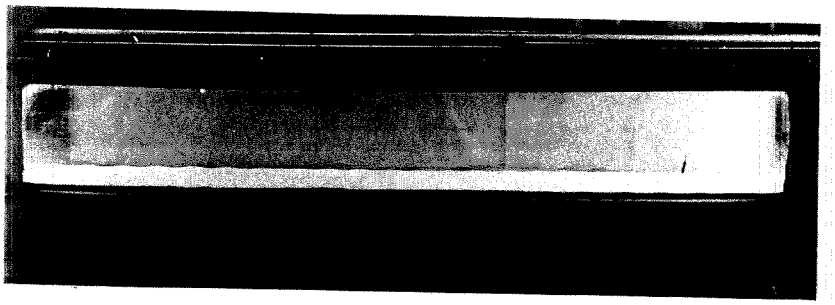

(a) Run No. 9, sideview, C_T= 8.06 grms/liter

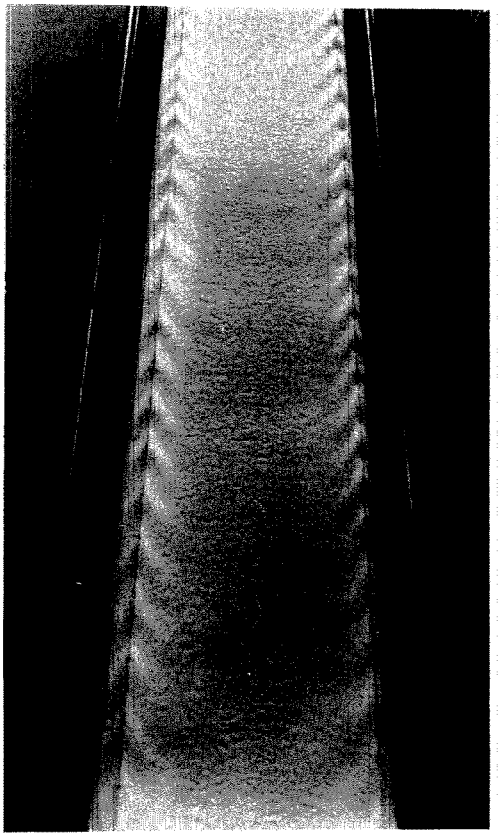

(b) Run No. 10d, looking upstream, C_T= 6.28 grms/liter

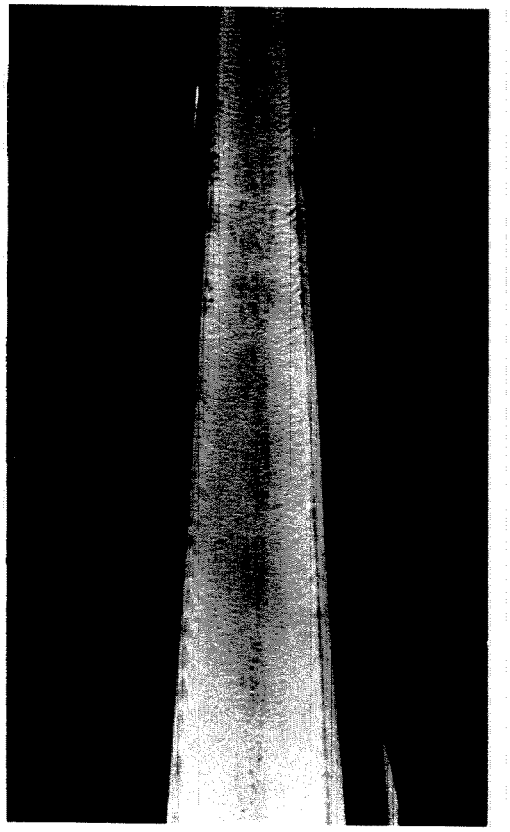

(c) Run No. 12, looking upstream, C_T= 3.26 grms/liter

Fig. 17 - Bed configuration, loose sand, without flow. 2nd series, U = 2.28 fps, d = .255 ft.

order to leave the sand bed undisturbed during its passage.

Using this technique, two waves were moving upstream, one from the pump well and the other from the middle of the flume, bringing the flow to rest in a relatively short time. Thus the bed configuration of the fourth set of runs was practically the same as the natural sand bed formed during the flow, without any noticeable stopping effect.

4. Velocity Profile

The logarithmic law may be fitted very well to the velocity profiles measured at the centerline near station 24. This gives a practical way to calculate von Karman's constant k, from the slope of the profile in a semi-logarithmic graph, as outlined in detail in Chapter IV, article C, 1, using equation 4.06

$$\kappa = \frac{2.3\, u_* \ell}{m}$$

The measured velocity profiles are shown in figs. 18 and 19. The zero elevation of the bed for runs 3, 5 and 7 was checked by stopping the flow and observing the position of the pitot tube with respect to the bottom. For the measurement of the velocity at the closest to the bed point, it was observed that the .032 in. outside diameter pitot tube was approximately .006 in. within the sand of the bed.

As is shown in figs. 18 and 19 the constant k for the velocity profile of runs 3 and 5 with high sediment concentrations has a tendency to increase in a small region close to the bed. But for run 7 it is constant. The results of the measurements of this run are much more reliable than that of the preceding runs,

because of the experience gained in using the 0.3 p.s.i. strain gage to measure very small velocities. Furthermore, the electronic potentiometer had been modified and made more sensitive.

Consequently there is some evidence that for high sediment concentrations the constant k is not the same for the total vertical profile in Region II, away from the wall, where the logarithmic law holds. Nevertheless there is some doubt regarding the above statement, because of the difficulty in determining the bottom of the flow for the velocity profile, when there are high concentrations and because the accuracy of the strain gage (0.01 x 0.3 ≈ .003 p.s.i.) is not satisfactory for very small velocities.

The velocity profiles taken with the 3/16 inch Prandtl type pitot-static tube showed always larger velocity than that of the logarithmic law for small values of the depth y. This happened regardless of the amount of sediment in suspension. Thus this discrepancy seems to be due to the presence of the relatively large diameter tube in the vicinity of the bed. This deviation of the velocity was not observed when a pitot-tube of very small diameter was used, as in runs 6 and 7, provided that the sediment concentrations were not high.

From figs. 18 and 19 it is obvious that the slope m of the velocity profile increased with the average sediment concentration, which means that von Karman's k decreased. The rate of increase of m was such that even if one would assume that the friction velocity u_{*c} at the centerline increased by a small percentage, the k value still must have decreased. As outlined

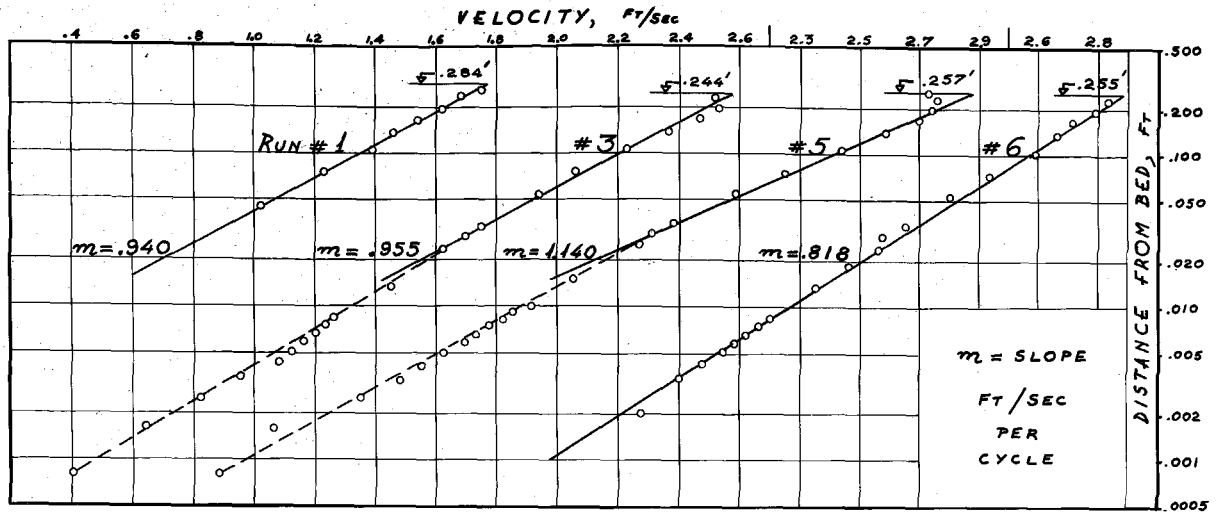

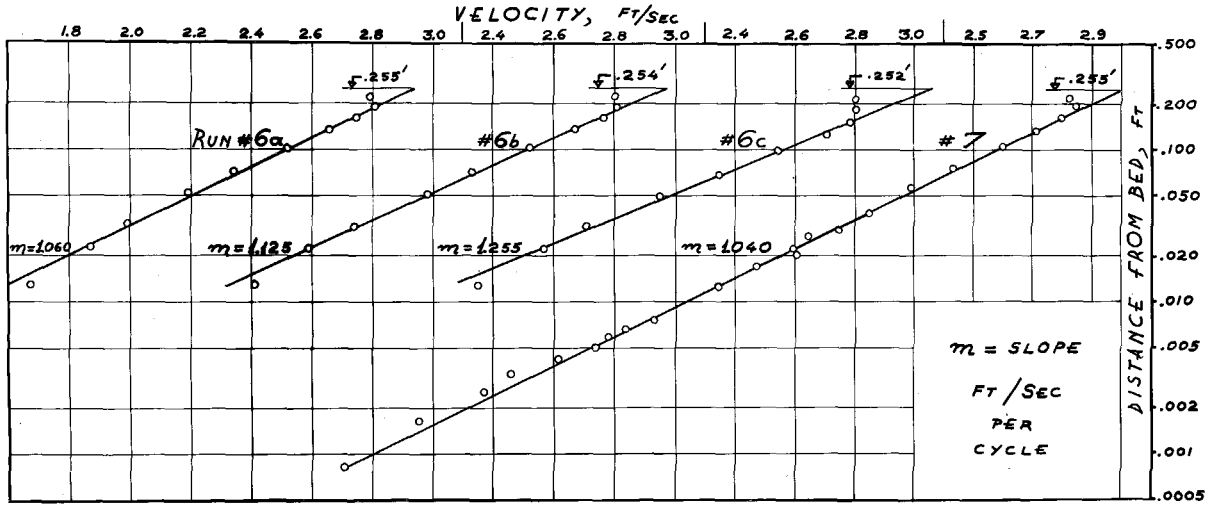

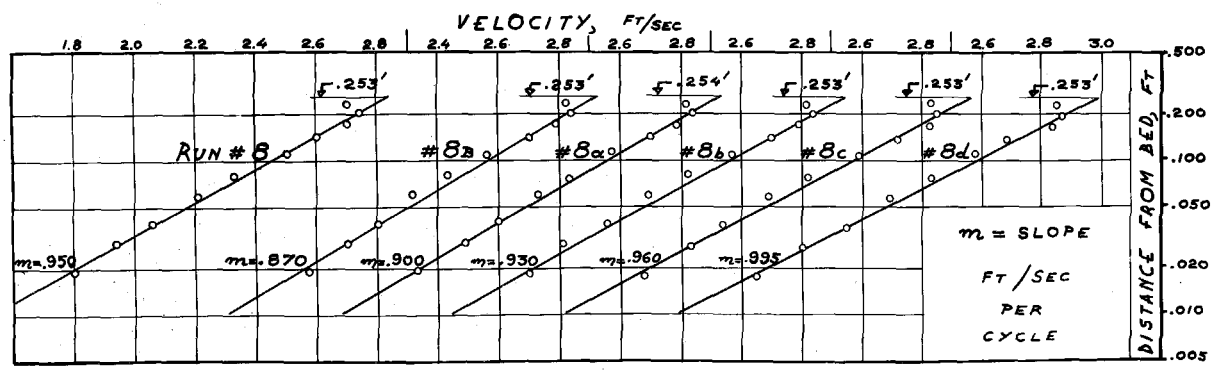

Fig. 18 - Vertical velocity profiles at the centerline of flume

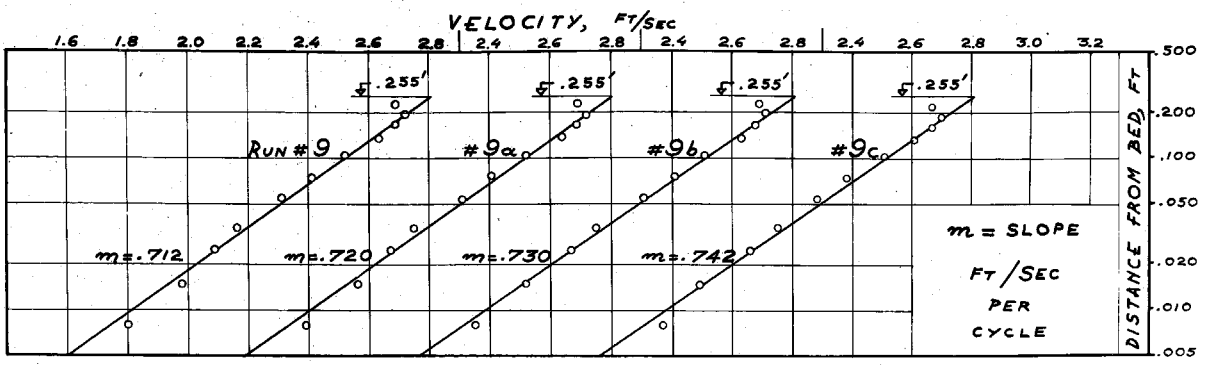

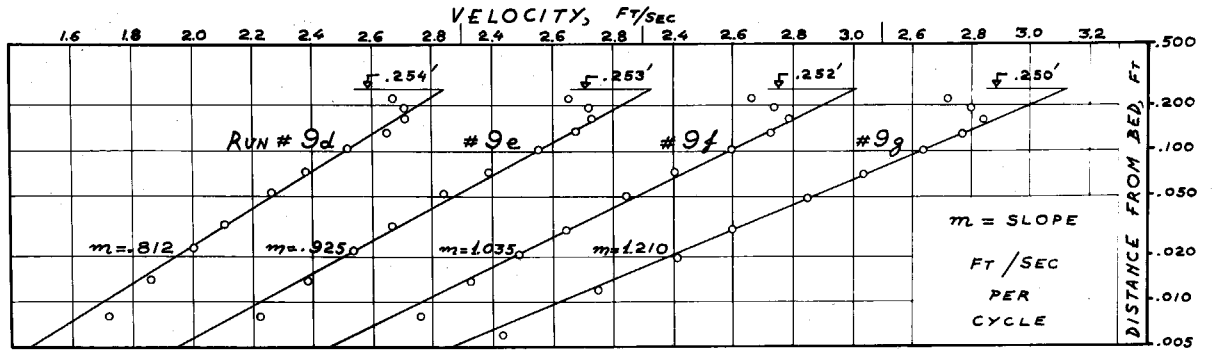

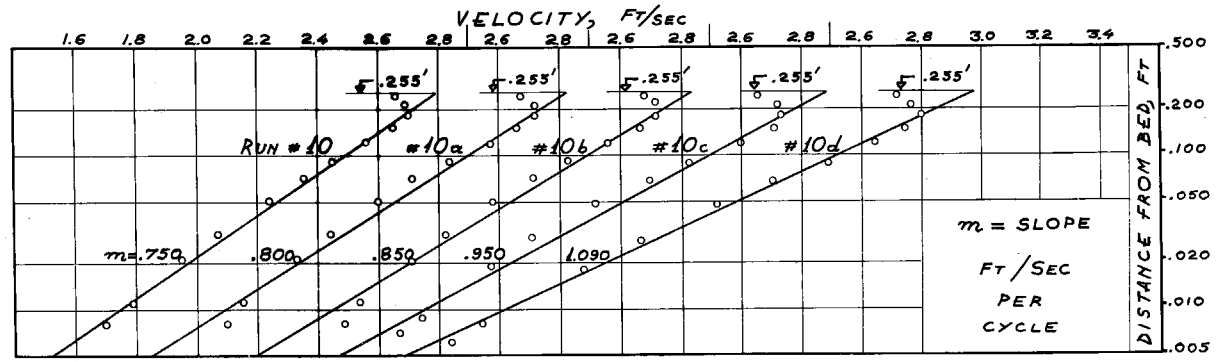

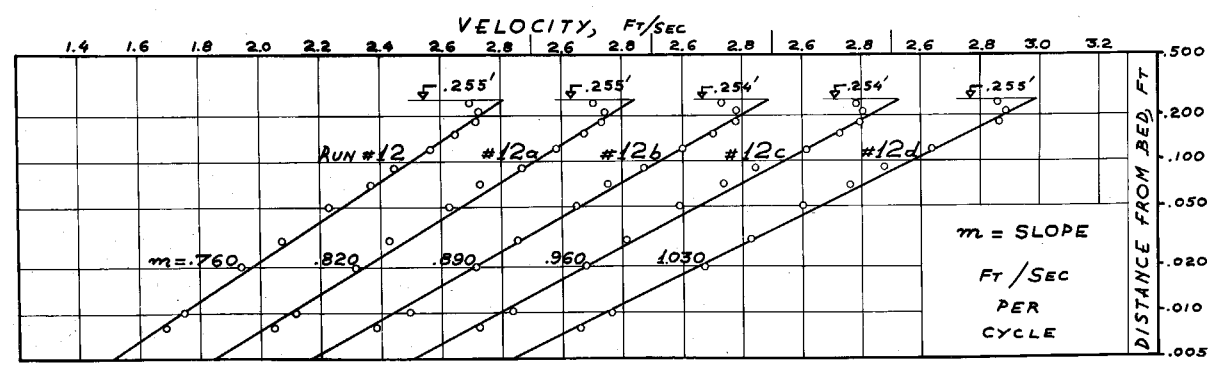

Fig. 19 - Vertical velocity profiles at the centerline of flume

in detail in the next paragraph, the shear velocity u_{*c} not only did not increase, but on the contrary it decreased when the concentration of the sediment in the flow increased. Thus the k value must have decreased.

5. Sediment Concentration Profile

Figure 20 shows logarithmic graphs of sediment concentration c, against $\frac{d-y}{y}$, where y is the distance from the bed. The slope of the profile, z_o, is the number of cycles of c per cycle of $\frac{d-y}{y}$, and is equal to:

$$z_o = \frac{w_o}{\beta k u_*}$$

where β is the ratio of the diffusion coefficient for sediment to that for momentum, and w_o is the settling velocity of the sediment reduced due to hindered settling for the average concentration of the flow. This reduction was outlined in detail in Chapter IV, article D, 2.

The concentration profile of run 5 did not fit the straight line as in the other runs because the concentration was very high and it is not right to express the hindered settling by an average reduction in the fall velocity.

Very close to the surface the concentrations were very small and the fall velocity of the grains was larger than that in regions close to the bed, where the concentrations are high. Since the exponent z of the concentration formula is proportional to the fall velocity of the particles, it is obvious that close to the surface the value of z would be larger than that in regions of smaller depths.

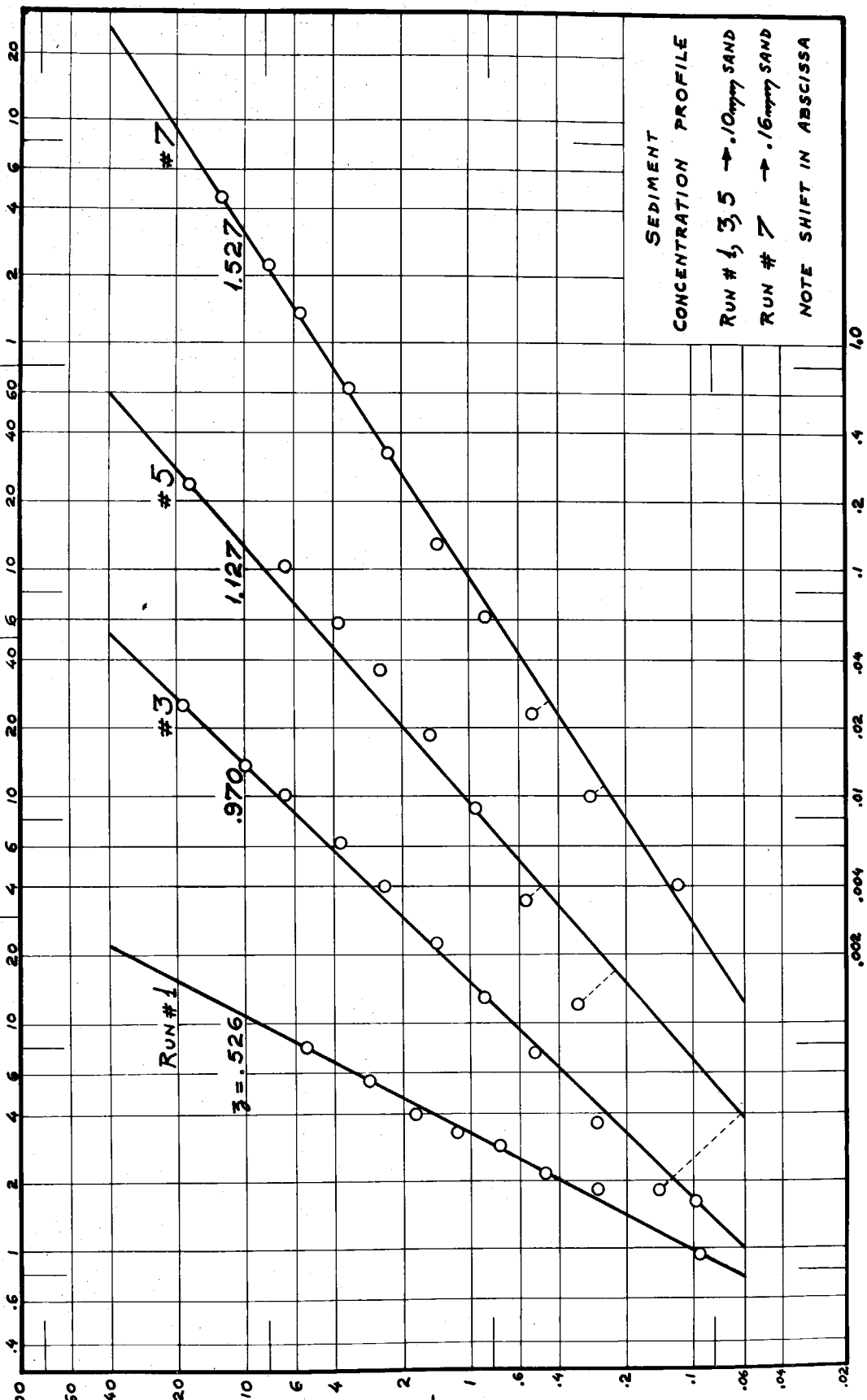

Fig. 20 - Sediment concentration profile at the centerline of flume

Very close to the bed it was not possible to obtain samples of sediment load with the point sampler used in this research, because of the very high concentrations and the very low velocities in that region.

6. Friction Coefficient

From the calculation of the friction factor tabulated in Table 9 it is obvious that the friction coefficient decreased when the sediment concentration increased.

For set IV with .16 mm sand, there are two runs, 8 and 8B, with clear water and different roughnesses, although they had the same mean velocity, discharge and stabilized bed as is shown in Table 7.

Run 8 was made twice (on two different days) and its flow characteristics agreed very closely both times. However when the water had been in the flume for longer than 10 hours (about 5 hours each day) the flow characteristics started changing slowly with time giving the results of the unstable run, 8B.

It is believed that the "Akrylic Spray" used in large quantities in set IV had formed a hard sheet on the surface of the sand bed, covering the grains practically all around without greatly disturbing their roughness. So the first two experiments of run 8 performed on two different days with clear water gave a large increase in the friction factor. However when the water had been in the flume for a long time the varnish sheet became soft, swelling and filling the grain interstices, so that the roughness of the

TABLE 9 - Comparison of friction factors for sediment laden streams with those for clear water flows over stabilized sand beds.

Set No.	Run No.	Depth ft	Bed Cond.	Average Concent. C_T grms/lit.	Friction Factors		Decrease		Decrease %	
					Average f	For Bed f_b	Δf	Δf_b	Δf	Δf_b
I	1	.284	Dunes	3.64	.0735	.1058	.0036	.0058	4.7%	5.0%
	2	.284	"	0	.0771	.1116				
II	3	.244	Small dunes	4.60	.0198	.0211	.0048	.0072	19.5%	25.4%
	4	.244	"	0	.0246	.0283				
III	5A	.255	Plane	8.08	.0165	.0165	.0043	.0064	20.7%	27.9%
	6	.255	"	0	.0208	.0229				
IV	7	.255	Plane	3.61	.0207	.0227	.0023	.0035	10.0%	13.4%
	8	.253	"	0	.0230	.0262				

surface continuously decreased.

To make sure of this, the unstable run, 8B, was repeated three times on three different days, drying the sand bed each day. The change of the friction factor of a uniform flow established in the flume was observed. The first day of run 8B the water was run continuously. The second day the water was added and as soon as the uniform flow had been established, the pump was stopped. After leaving the water in the flume for three hours the run was started again. The flow characteristics and friction factor of the flow were changed by approximately the same amount as they would have been if the water had been running continuously during those three hours without having been stopped. The third day the run 8B of the first day was repeated with approximately the same change in the friction coefficient with time.

Reference to Table 7 shows that all of the runs of set VI, i.e., runs 10 through 10d, gave identical friction factors despite the large variation in the apparent bed roughness. For instance, in run 10, which was made with clear water, the bed was coated with 0.10 mm sand applied to fresh paint. The paint actually coated most of the grains so that the resulting roughness was even less than that of the sand grains alone. In contrast to this, the bed in run 10d was covered with loose sand of 0.10 mm mean size and in addition ripples formed in the sand bed near the walls as shown in fig. 17b. This apparent anomaly is explained by the effect of suspended sediment in run 10d in reducing the friction.

Runs 12-12d did not show such an effect because the bitumastic paint covering all the grains was fairly thick and the roughness of the bed was much less than representative of the .16 mm sand grain used (see Table 10). Thus the sediment-laden flow showed a net increase in friction factor when sand was added in steps due to the grain roughness and the dunes which formed next to the side walls.

The equivalent roughness κ_s for the bed in Table 10 was computed from the bed friction factor f_b and Reynolds number Re_b using the graph of f vs. Re for various roughnesses for pipes, given in standard textbooks on fluid mechanics.

B. Analytical Results

1. Velocity Profile

The analytical computations in the Appendix for the velocity profile when von Karman's constant k changes with sediment load indicate the following:

When k decreases, the value of B in the logarithmic velocity profile (equation 2.21) must change if the friction factor is to stay fixed. Even though the friction factor f changes with sediment load, the constant B, as well as Rannie's constant κ_1 and y_1^* can be approximated with the values computed assuming f constant. These values are derived in the Appendix and given in Table 11.

For rough walls the constant A_s of the logarithmic velocity profile changes with both the sediment load and the bed configuration. Since the change of A_s from the bed configuration

is much smaller than that due to the decrease in k from the sediment load, for practical purposes we can approximate κ_1 and y_1^* with the values obtained for smooth walls.

For relatively high concentrations with von Karman's constant k less than .280, the observed decrease of the friction factor f and the indicated tendency of increasing von Karman's k at the intermediate region close to the bed justify taking the approximate value of y_1^* the same as that for k $\simeq$ .280.

Table 11

Evaluation of Rannie's constant κ_1 and y_1^* assuming constant friction factor. (See Appendix).

von Karman's constant k	Rannie's constant κ_1	Dimensionless depth of the point for the matching of the velocity profiles y_1^*
.40	1/14.5	27.5
.35	1/13	22.5
.30	1/9.5	13.0
.275	1/7	8.5
.250	1/4.2	8.0
.225	1/2	8.0

2. Sediment Concentration Profile

Equations 2.29 and 2.35 derived in Chapter II, article E, were used to compute the sediment concentration for runs 1, 3, 5 and 7.

Substituting c_{md} for the mid-depth concentration in equation 2.35 one obtains:

$$\frac{c_{md}}{c_o} \simeq \left(\frac{y_1}{h-y_1}\right)^{z_o} \frac{e^{2n z_o \{E_i(2\kappa_1 y_1^*) - n E_i(4\kappa_1 y_1^*)\}}}{e^{\frac{z_1}{n-1} \tanh^{n-1} \kappa_1 y_1^*}} \qquad (5.01)$$

Substituting in equation 5.01 the arithmetical values for:

$z_o = \frac{w_o}{\beta \kappa u_*}$, $z_1 = \frac{w_o}{\beta_1 \kappa_1 u_*}$: exponents in sediment load equation,

κ_1, y_1 : Rannie's constant and distance from the depth of the matching point of the velocity profile depending on measured von Karman's k,

h : Depth of the flow,

u_* : Shear velocity,

c_{md} : Mid-depth concentration read off curve of concentration profile in fig. 20,

c_o : Bed concentration assumed equal to the bed density,

w_o : Settling velocity reduced by hindered settling for the average concentration,

taken from Tables 4, 7, 8 and 11, and solving for n, the exponent of the assumed formula for the settling velocity of sediment is defined for each run.

Table 12

Computation of exponent

of the equation $w = w_o \tanh^{n} k_1 y^*$

Run No.	n
1	1.77
3	2.10
5	9.00
7	3.30

The formulae computed for the sediment concentration profile are tabulated in Table 13 and plotted in fig. 21 for runs 1, 3, 5 and 7.

3. Turbulent Energy Production

The following equations derived in Chapter II, article G, were used to compute the rate of turbulent energy production and its average over the vertical depth for runs 1, 3, 5 and 7:

Region I : $$(P_\varepsilon)_\tau = \tanh^2 k_1 y^* \operatorname{sech}^2 k_1 y^* \qquad (2.45)$$

Region II : $$(P_\varepsilon)_\tau \simeq -\frac{1}{\kappa R^*} + \frac{1}{\kappa y^*} - \frac{1.5}{(\kappa y^*)^2} + \frac{1.125}{(\kappa y^*)^3} \qquad (2.47)$$

And for the average rate of turbulent energy production:

$$\overline{(P_\varepsilon)}_\tau = \frac{1}{R^*}\left\{\frac{1}{3k_1}\tanh^3 k_1 y_1^* + \frac{1}{\kappa}\left(\ln\frac{R^*}{y_1^*} - 1 - \frac{3}{2\kappa y_1^*} + \frac{9}{(4\kappa y_1^*)^2}\right)\right\} \qquad (2.53)$$

Substituting in the above equations the arithmetical values for k_1, y_1^*, κ, R^* computed from Tables 7 and 11 for each

Table 13. Calculated sediment concentration profile

Assumption: $w = w_o \tanh^{n} \kappa_1 y^*$

Run #	n	c/c_o in Region I	c/c_o in Region II
1	1.77	$e^{-3.56 \tanh^{.77} \kappa_1 y^*}$	$.0337 \left\{ \left(\frac{R-y}{y} \cdot \frac{1}{176.2} \right)^{.53} \frac{e^{-1.9 E_i(2\kappa_1 y^*)}}{e^{-3.3 E_i(4\kappa_1 y^*)}} \right\}$
3	2.1	$e^{-1.99 \tanh^{1.1} \kappa_1 y^*}$	$.2333 \left\{ \left(\frac{R-y}{y} \cdot \frac{1}{306.3} \right)^{.96} \frac{e^{-4.0 E_i(2\kappa_1 y^*)}}{e^{-8.4 E_i(4\kappa_1 y^*)}} \right\}$
5	9.0	$e^{-.68 \tanh^{8.0} \kappa_1 y^*}$	$.509 \left\{ \left(\frac{R-y}{y} \cdot \frac{1}{365.3} \right)^{1.13} \frac{e^{-20.3 E_i(2\kappa_1 y^*)}}{e^{-182.3 E_i(4\kappa_1 y^*)}} \right\}$
7	3.3	$e^{-1.83 \tanh^{2.3} \kappa_1 y^*}$	$.300 \left\{ \left(\frac{R-y}{y} \cdot \frac{1}{273.3} \right)^{1.50} \frac{e^{-9.9 E_i(2\kappa_1 y^*)}}{e^{-32.7 E_i(4\kappa_1 y^*)}} \right\}$

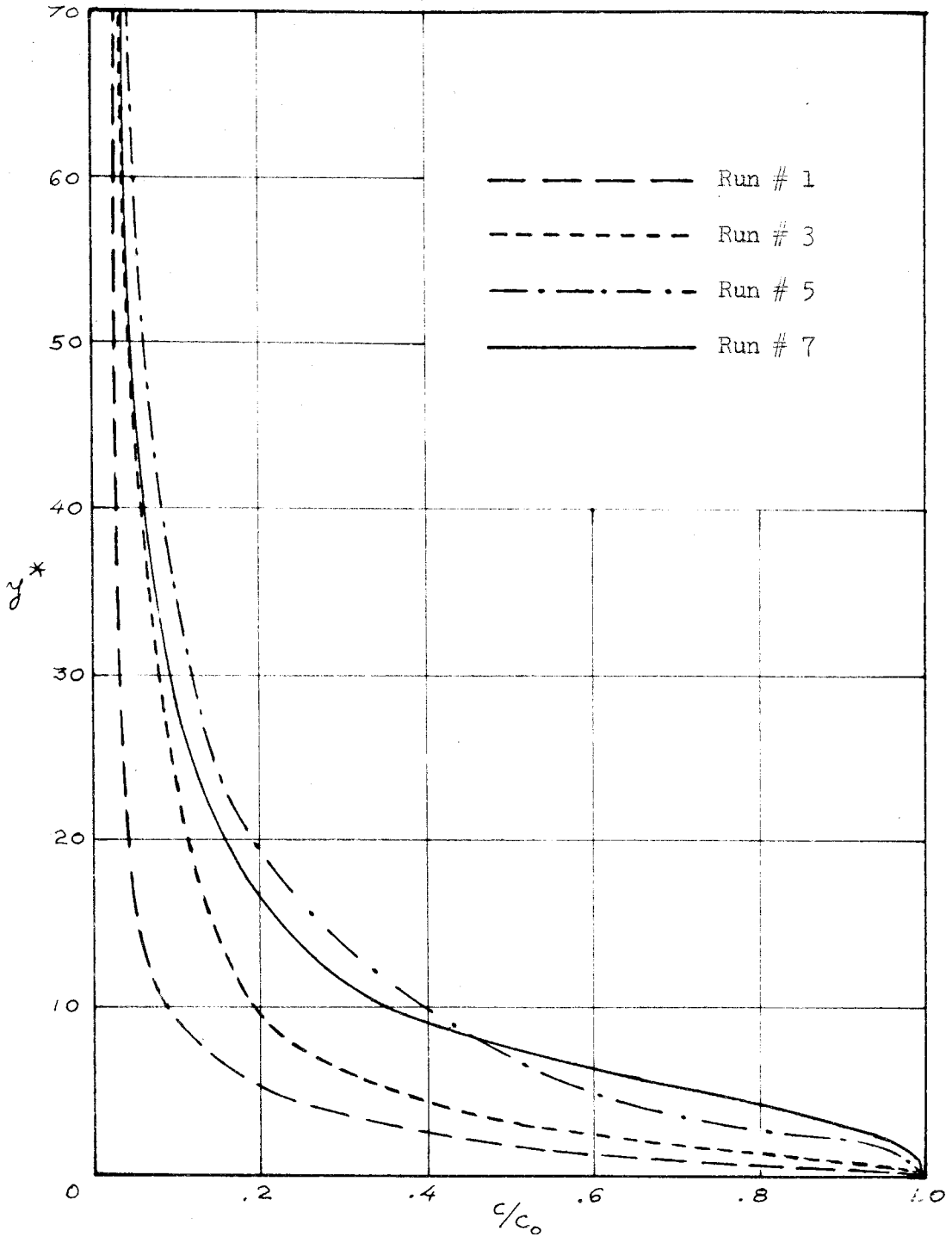

Fig. 21. Calculated sediment concentration profile

Assumption: $w = w_o \tanh^n k_1 y^*$

of runs 1, 3, 5 and 7 the dimensionless rate of turbulent energy production was computed from equations 2.45 and 2.47 and plotted in figs. 22 and 23.

Table 14

Average rate of turbulent energy production

$$\left(\overline{P_\varepsilon}\right)_\tau = \overline{P_\varepsilon}\,\frac{\nu}{\rho u_*^4}$$

Run No.	$\left(\overline{P_\varepsilon}\right)_\tau$ Average Dimensionless
1	$\frac{1}{4430}\left\{3.91 + 10.85\right\} = 33.34 \times 10^{-4}$
3	$\frac{1}{2765}\left\{1.42 + 15.56\right\} = 61.4 \times 10^{-4}$
5	$\frac{1}{2930}\left\{1.37 + 18.83\right\} = 69.0 \times 10^{-4}$
7	$\frac{1}{3570}\left\{2.15 + 14.21\right\} = 45.8 \times 10^{-4}$

4. Sediment Energy Dissipation

The following formulae derived in Chapter II, article H, were used to compute the rate of energy dissipation by suspended sediment and its average over the vertical depth, for runs 1, 3, 5 and 7.

$$W_s = c w \left(1 - \frac{\gamma_w}{\gamma_s}\right)$$

$$\left(W_s\right)_\tau = W_s\,\frac{\nu}{\rho u_*^4} \qquad (2.54)$$

And for the average rate of energy dissipation by the sediment in suspension,

$$\left(\overline{W_s}\right)_\tau = \frac{\nu}{\rho u_*^4}\, w_o \left(1 - \frac{\gamma_w}{\gamma_s}\right)\left\{c_o\, \Omega(\omega_1) + c_{md}\, H(\eta_1)\right\} \qquad (2.65)$$

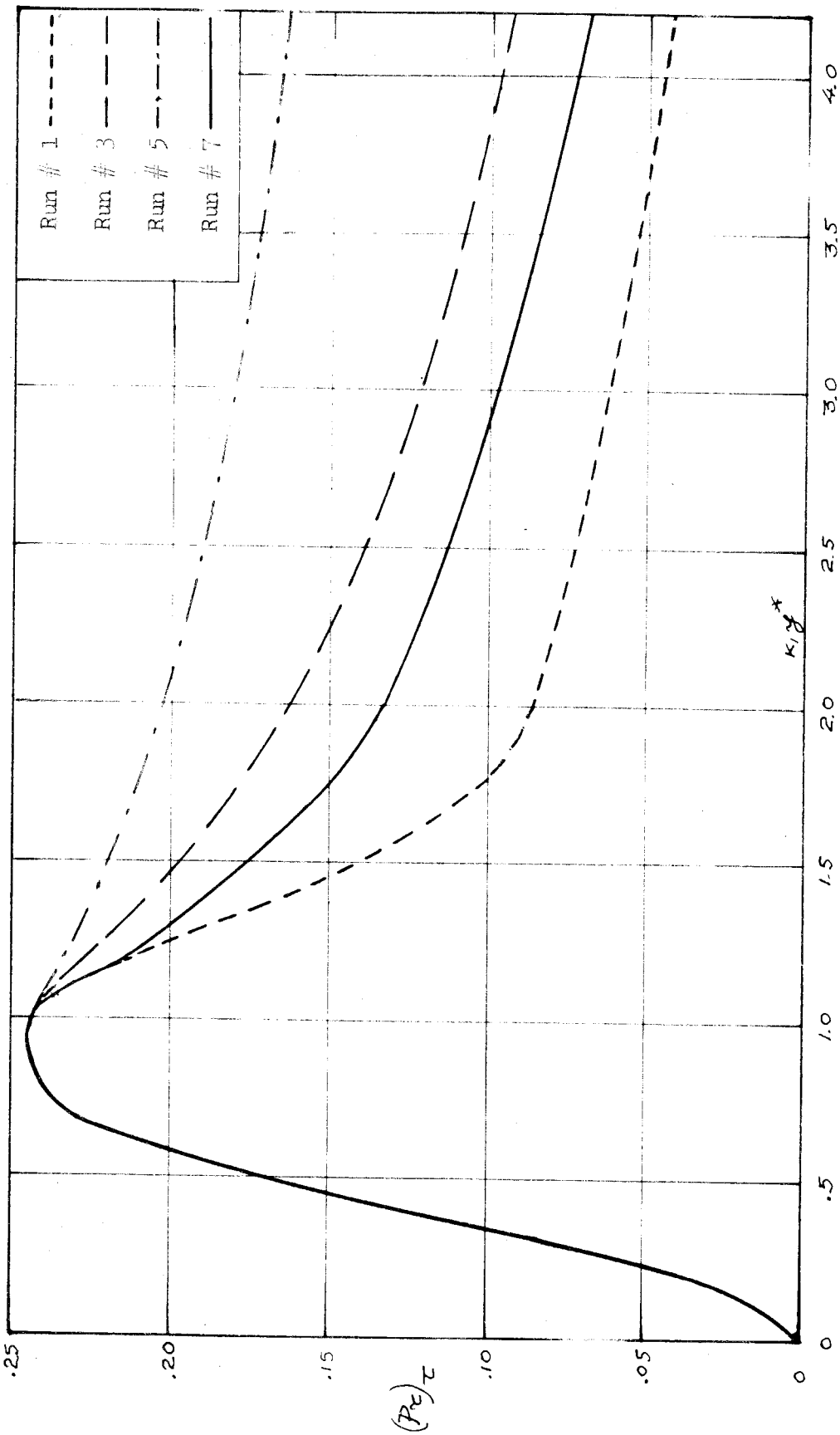

Fig. 22. Calculated dimensionless rate of turbulent energy production close to the wall

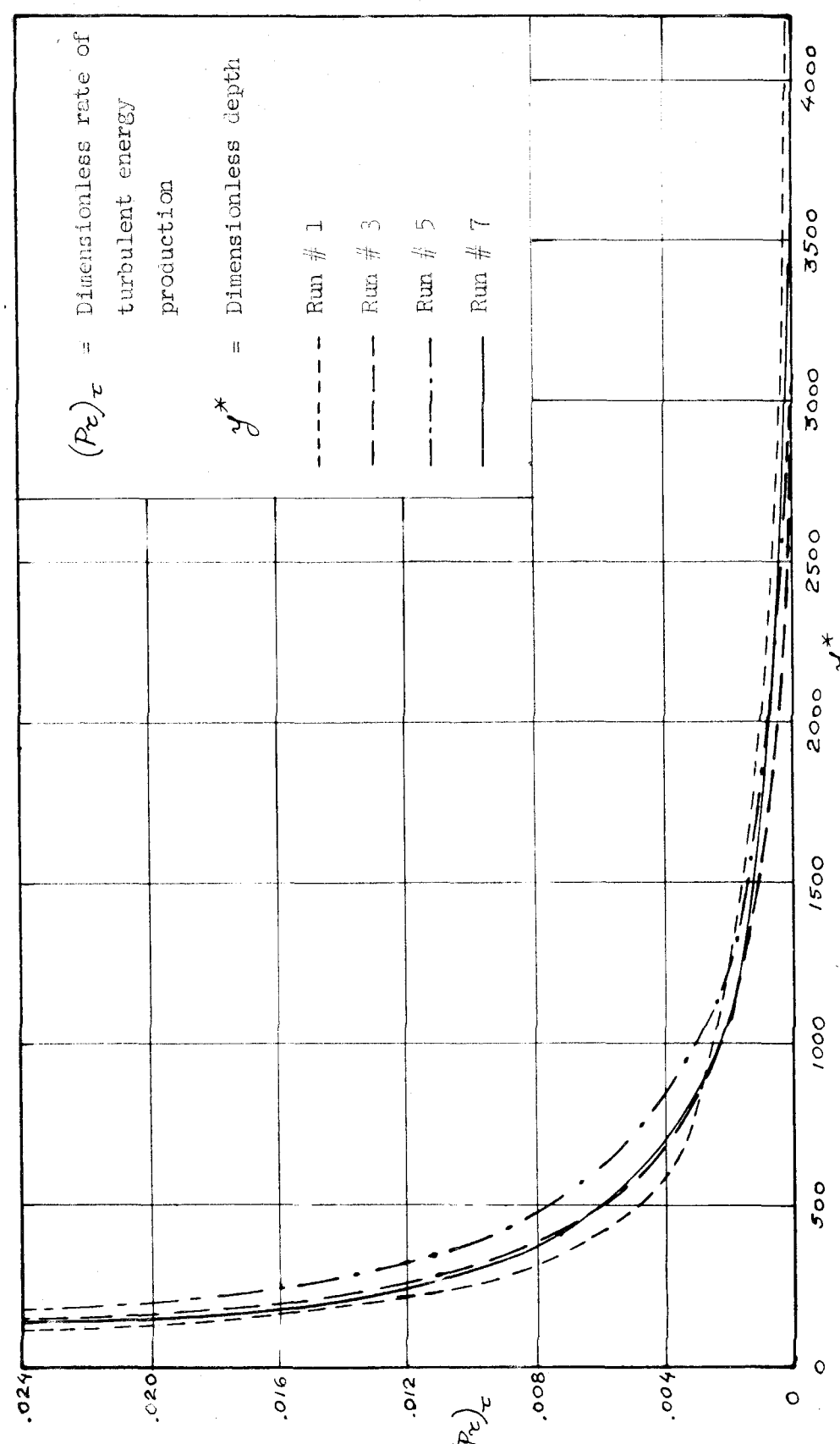

Fig. 23. Calculated rate of turbulent energy production

Substituting in the above equations the arithmetical values for C, C_o, w_o, C_{md}, ρ, γ_w, γ_s, ν, u_*, and $w = w_o \tanh^m k_1 y^*$ from Tables 7, 11 and 12 for each of the runs 1, 3, 5 and 7 the computed rate of energy dissipation by the suspended sediment is tabulated in Table 15 and plotted in figs. 24 and 25.

Table 15

Rate of energy dissipation by suspended sediment

Assumption $w = w_o \tanh^m k_1 y^*$

Run No.	$(W_s)_\tau$ Dimensionless rate of sed. en. dissip.	$(\overline{W_s})_\tau$ Av. Dimensionless rate of sed. en. dissip.
1	.000373 cw	$(.03 + .53) = .56 \times 10^{-4}$
3	.00138 cw	$(.16 + 2.05) = 2.21 \times 10^{-4}$
5	.00123 cw	$(.47 + 2.60) = 3.07 \times 10^{-4}$
7	.000578 cw	$(.18 + 1.00) = 1.18 \times 10^{-4}$

where: C = grms/liter

$w = f\rho s$

$\gamma_s = 2.65 \times 62.4$

$\gamma_w = 1.00 \times 62.4$

$T = 25.0^\circ$ C

Note: The first term in the parenthesis for $(\overline{W_s})_\tau$ shows the contribution of $\Omega(\omega_1)$ to the average rate of energy dissipation by the suspended sediment. For the above runs it varied from about 5°/o to 15°/o.

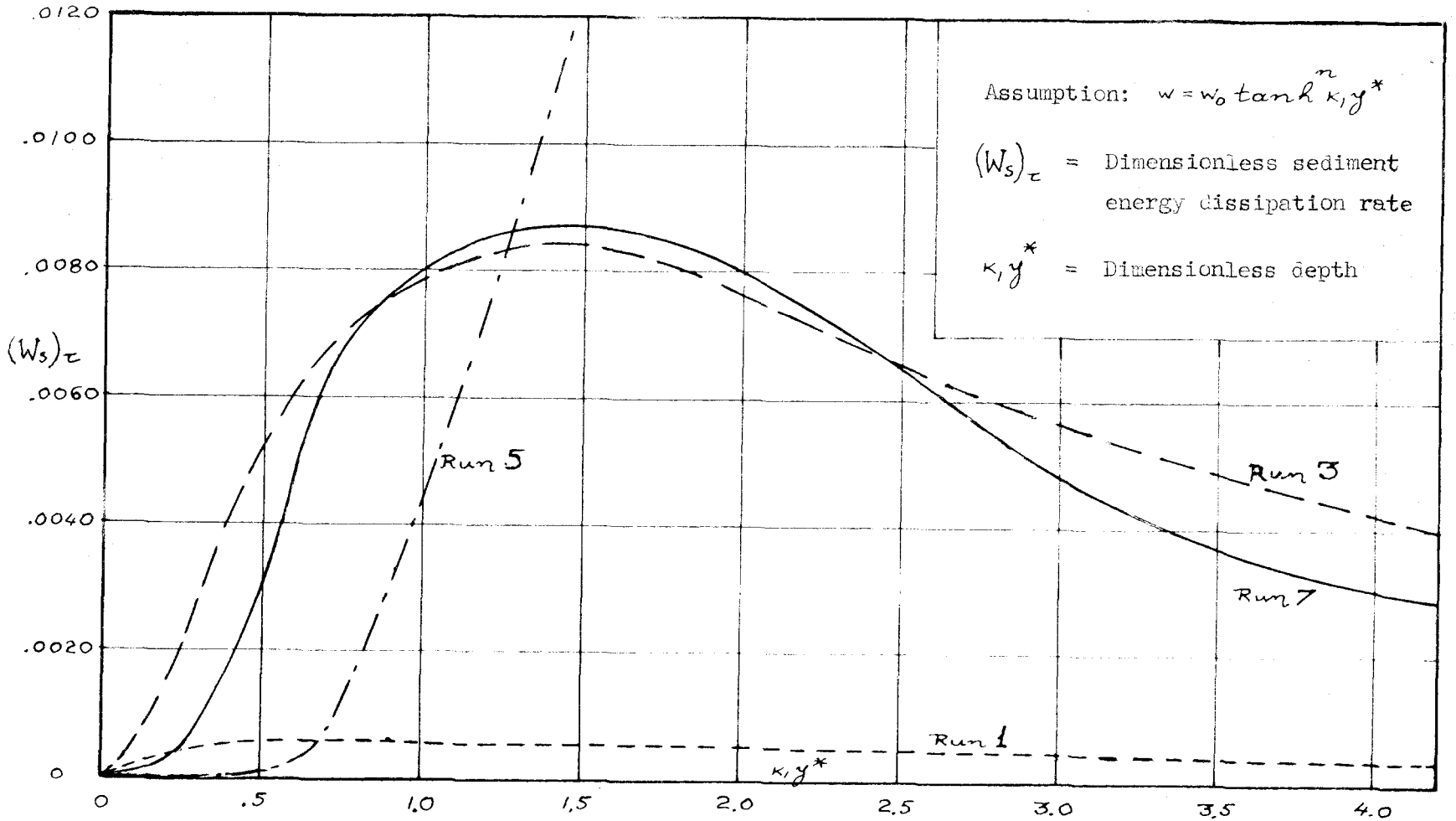

Fig. 24. Calculated dimensionless rate of energy dissipation by suspended sediment close to bed

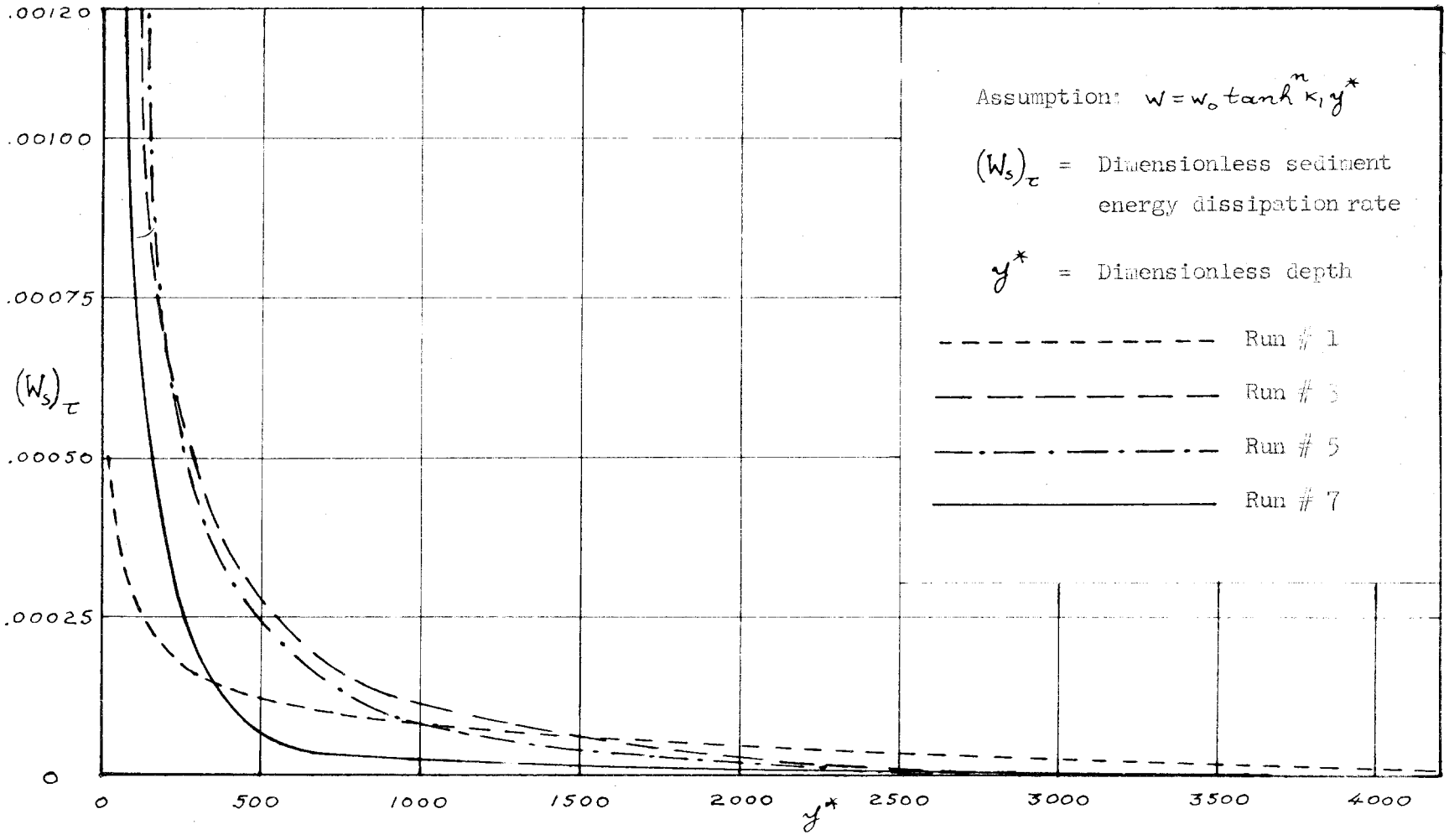

Fig. 25. Calculated dimensionless rate of energy dissipation by suspended sediment

5. von Karman's k and Friction Factor f vs. the Ratio $\frac{\overline{W_s}}{\overline{P_\varepsilon}}$

(a) von Karman's k vs. $\overline{W_s}/\overline{P_\varepsilon}$, or $\overline{W_s}/\overline{|D|}$

In the graphs of the rate of turbulent energy production and sediment energy dissipation in figs. 22 and 24 it is shown that the maxima occur at points very close to the bed, in region I.

For the comparison of the average rate of sediment-energy dissipation with the average rate of the absolute value of turbulent-energy diffusion, it would be necessary to calculate the diffusion from experimental measurements, because the analysis for the balance of turbulent energy did not give any relationships for the above calculation.

If it would be assumed that the ratio of the average rate of the absolute value of turbulent energy diffusion $\overline{|D|}$, to the average rate of turbulent energy production $\overline{P_\varepsilon}$, is independent of the amount of suspended sediment, then the ratio $\overline{|D|}/\overline{P_\varepsilon}$ would be obtained from Laufer's data shown in figs. 19, 20 and 21 of reference 1.

1. $(\overline{P_\varepsilon})_\tau \simeq .0111$ Dimensionless average rate of turbulent energy production

2. $\overline{|D|}_\tau \simeq .0024$ Dimensionless average rate of turbulent energy diffusion

Their ratio becomes: $\overline{|D|}_\tau/(\overline{P_\varepsilon})_\tau \simeq \frac{1}{4.6}$

When von Karman's k is plotted against the ratio of sediment energy dissipation to the turbulent energy production (or

diffusion) it is observed that k decreases as this ratio increases. As it is tabulated in Table 16 for a range of change of the ratio $\overline{W_s}/\overline{|D|}$ from 7.7% to 20.5%, von Karman's k changed from 0.37 to 0.23.

Table 16

von Karman's k vs. the ratio of the average rate of sediment-energy dissipation to that of turbulent-energy production.

Run No.	$(\overline{P_\varepsilon})_\tau$	Laufer $(\overline{P_\varepsilon})_\tau$	$(\overline{W_s})_\tau$	$\overline{P_\varepsilon}$	$\overline{W_s}$	κ	$\frac{\overline{W_s}}{\overline{P_\varepsilon}}$	$\frac{W_s}{\overline{\lvert D\rvert}}$*
	$\times 10^4$	$\times 10^4$	$\times 10^4$	$\frac{\text{lb}\cdot\text{ft}}{\text{ft}^3\cdot\text{sec}}$	$\frac{\text{lb}\cdot\text{ft}}{\text{ft}^3\cdot\text{sec}}$		%	%
1	33.3	30.0	0.56	.3500	.00588	.37	1.68	7.7
3	61.4	59.5	2.21	.1775	.00638	.27	3.60	16.6
5	69.0	68.3	3.07	.2063	.00918	.23	4.45	20.5
7	45.8	43.8	1.18	.3040	.00784	.30	2.58	11.9

Laufer's $(\overline{P_\varepsilon})_\tau$ for clear flows is approximately equal to:

$$(\overline{P_\varepsilon})_\tau \simeq \frac{\nu}{\rho u_*^4} \cdot \frac{\rho u_*^3}{\kappa R} \ln \frac{R^*}{12e} \simeq \frac{1}{\kappa R^*} \ln \frac{R^*}{12e}$$

*Footnote: Assumption $\overline{|D|} = \frac{\overline{P_\varepsilon}}{4.6}$

From the experiments of other investigators (refs. 8, 13, 16) the average rate of turbulent-energy production and sediment-energy dissipation were computed approximately from their data. The contribution of the sediment-energy dissipation of region I (i.e. $y^* < y_1^*$) was neglected and there was not any correction made for the reduction of the average settling velocity w_o of the particles. In Vanoni's data[8] the flow was considered two-

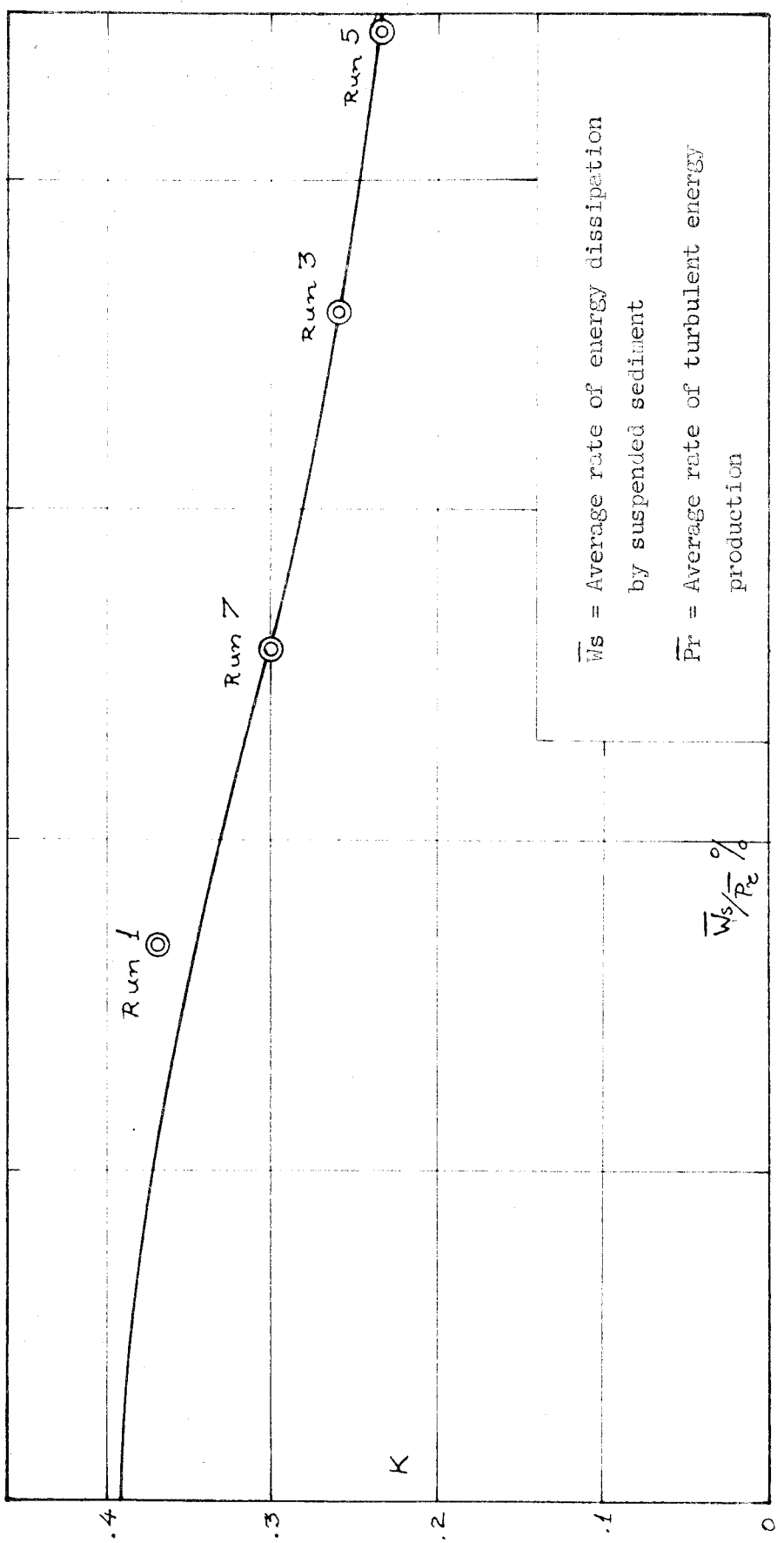

Fig. 26. von Karman's k vs. $\overline{Ws}/\overline{Pr}$ %

dimensional. In Ismail's data[16] there was not any sidewall correction made for the shear at the centerline of the flume and consequently for its k values.

Figure 27 shows the decrease of von Karman's k with the increase of the ratio of the average rate of energy dissipation by suspended sediment to the average rate of turbulent energy production for the approximate computations made for Vanoni's, Brooks' and Ismail's data.

(b) Friction Factor f vs. $\overline{W_s}/\overline{P_e}$

From the friction factors f, and f_b, (for the whole flow and the bed section of the flow, respectively) for the first four sets of experiments the percentage of change of the friction factor was computed. This change gave the decrease of the friction for a flow with sediment in suspension compared with the friction of clear water flow on the stabilized sand bed of the first flow, when the discharge and the depth were kept the same.

Comparing the percentage decrease in f and f_b with the ratio $\frac{\overline{W_s}}{\overline{P_e}}$ of the average sediment energy dissipation to the turbulent energy production (as tabulated in Table 17, and plotted in fig. 28) it was observed that the friction factors decreased with the increase of $\overline{W_s}/\overline{P_e}$. For a range of the ratio $\overline{W_s}/\overline{P_e}$ from 1.68% to 4.45% the friction factors f and f_b decreased by a percentage varying from 4.7 to 20.7, and 5.0 to 27.9, respectively.

The above percentages for sets II and III of experiments were rather high because of the difficulty in stabilizing very fine

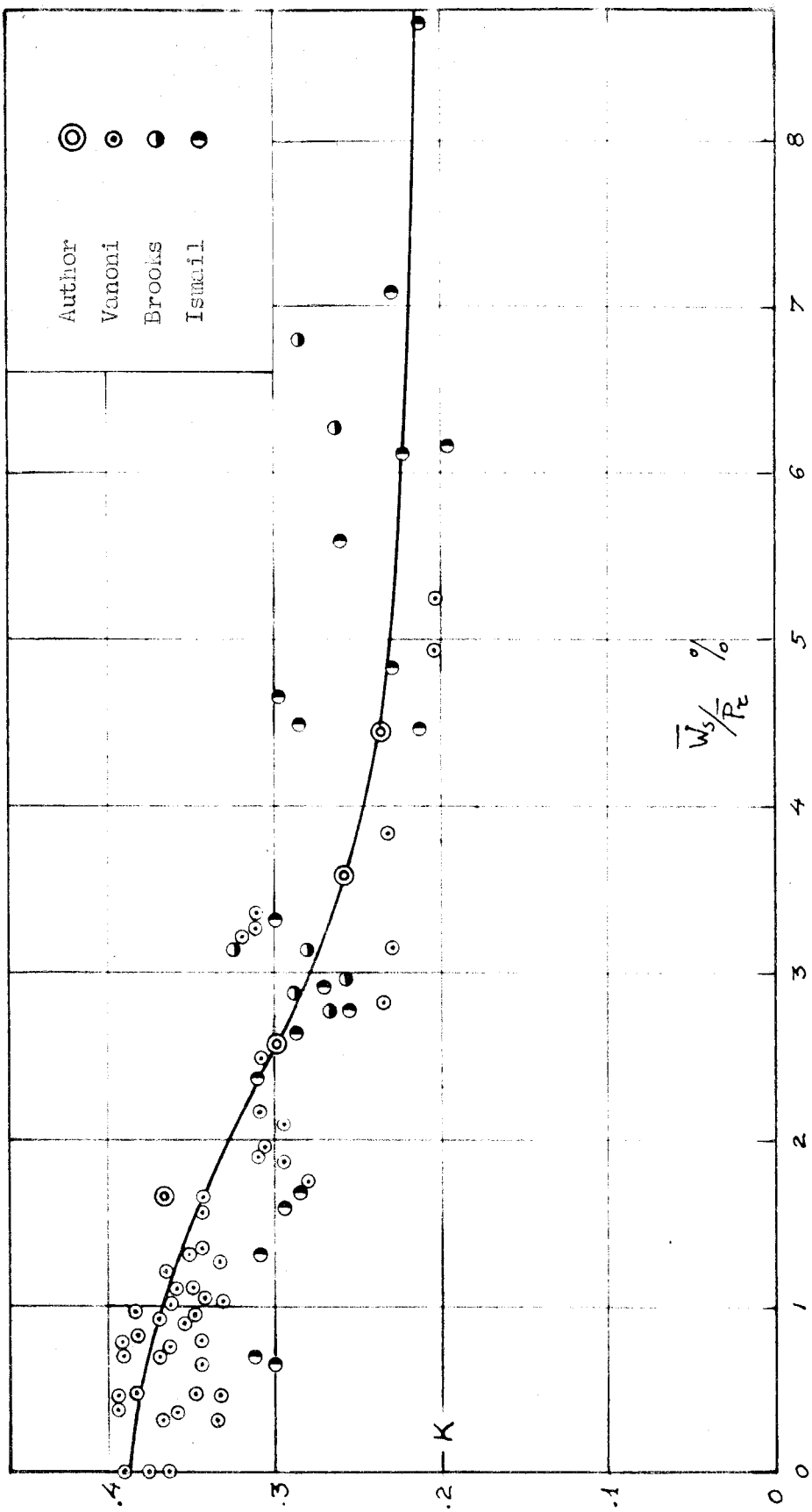

Fig. 27. von Karman's k vs. $\overline{W_s}/\overline{P_e}$ %

sand beds without disturbing the grain roughness, (which in these cases was practically the main part of the total equivalent roughness of the flow.) and the "stopping effect".

Table 17

Percentage decrease of friction factors f and f_b for sediment-laden flows in terms of clear water flows vs. the ratio of the average rate of sediment-energy dissipation to that of turbulent-energy production.

Set No.	Run No.	Ave. $\overline{C}_T$ grms/liter	Sand Size mm	Decrease % Δf	Decrease % Δf_b	$\overline{W_s}/P_z$ %
I	1	3.64	.10	4.7	5.0	1.68
	2	0				
II	3	4.60	.10	19.5	25.4	3.60
	4	0				
III	5A	8.08	.10	20.7	27.9	4.45
	6	0				
IV	7	3.61	.16	10.0	13.4	2.58*
	8	0				

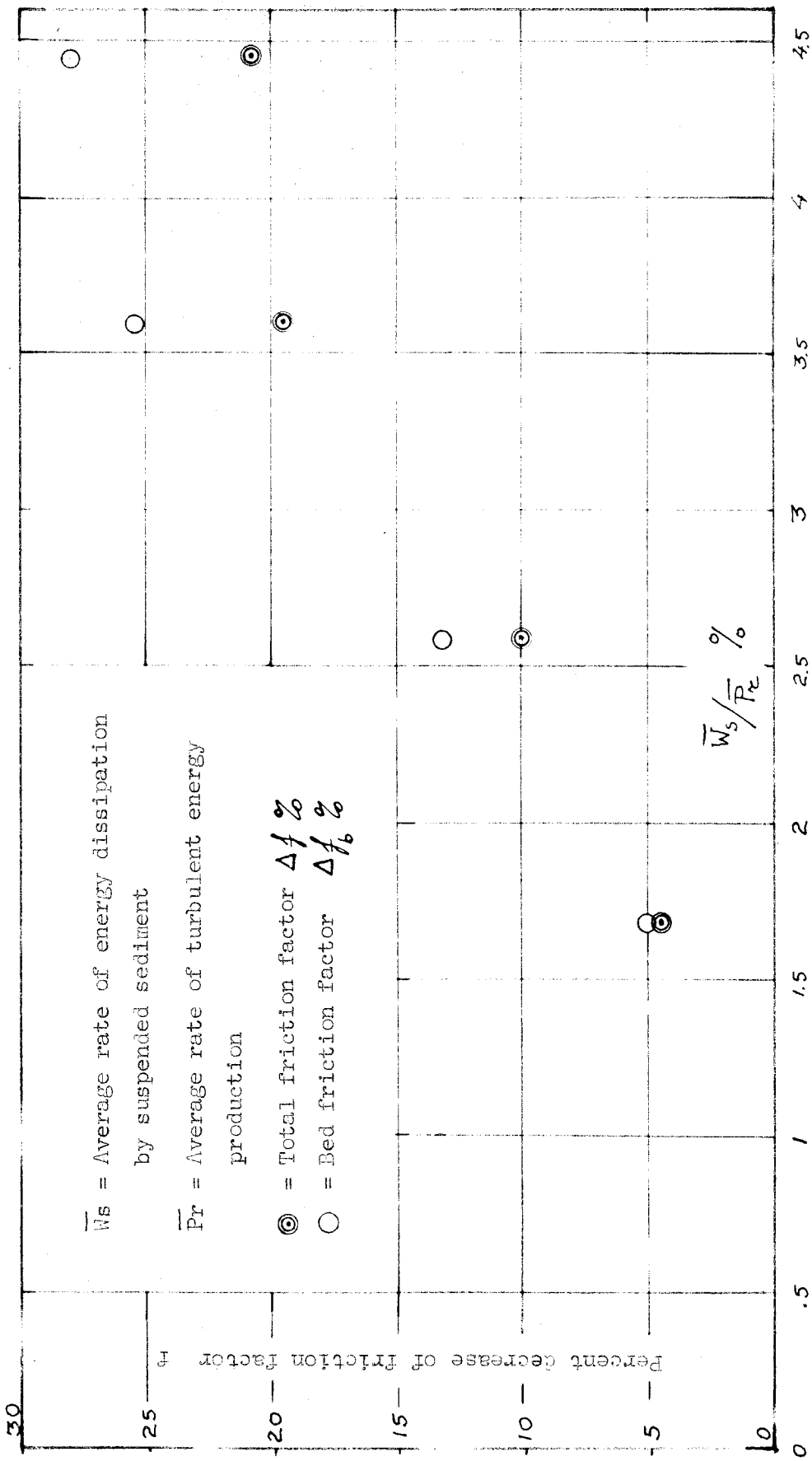

Fig. 23. Percent decrease of friction f vs. $\frac{\overline{W_s}}{\overline{P_r}}$

CHAPTER VI

DISCUSSION

The main objective of the present work was to obtain some information about the effect of sediment load on the friction factor of water flow in open channels. An attempt was made to understand the detailed mechanism responsible for this effect.

Since there is never sediment load in a laminar flow, regardless of how high the energy of the flow and its molecular diffusion are, only the turbulent diffusion has a direct effect on particle suspension. It was considered very helpful to express in detail the total energy and mechanical energy equations for turbulent flows. From these equations it was possible to find a relation between the different forms of turbulent energy, such as convection, production, dissipation and diffusion.

Although it was not possible to express explicitly the nature of transfer processes which take place in any turbulent field, a good comparison was obtained between the rates of turbulent energy production and energy dissipation by suspended sediment in different regions of the field. In the small region very close to the bed this comparison was made possible only by making some assumptions about the flow and settling velocity; these are discussed in the following paragraphs.

A. Velocity Profile

The experimental law of "Universal boundary layer flow" fitted very well the experimental data for velocity distribution in a region away from the bed. For the small region near the bed which includes the so-called laminar sublayer, Rannie's assumption[3] was used for the correlation of the fluctuating velocities $\overline{u'v'}$. This assumption, stating that:

$$-\overline{u'v'} = \kappa_1^2 u^2$$

has been checked experimentally by Rannie[3] from heat transfer in a clear flow with hydrodynamically smooth walls.

For rough walls the above assumption does not seem to work as well, but it is good enough for an average velocity profile corresponding to a theoretical $y=0$ at the wall, averaged over a small region. For beds covered with dunes there is no theory describing either the vortex characteristics of the flow in the troughs or over the crests of the dunes, or the velocity profile very close to them. For these cases a stochastic average of the zero distance from the bed has been considered. Then the theory of smooth walls has been applied for the above average bed elevation. The results obtained seem to be consistent with those of streams with plane bed, although physical interpretations of the results in terms of velocity and sediment profiles are not possible.

B. Effect of Sediment Load on von Karman's k

For the main flow $(y^* > 70)$ the "Universal boundary layer flow" $\frac{du}{dy} = \frac{u_*}{\kappa y}$ holds very well if the sediment load is not high.

The definition of the momentum transfer coefficient in two-dimensional flow gives,

$$\varepsilon_m = \frac{-\overline{u'v'}}{du/dy} \tag{6.01}$$

Since for $y^* > 70$ the effect of viscosity is quite negligible:

$$-\rho\overline{u'v'} = \tau_0\left(1 - y/d\right)$$

Dividing by ρ and substituting u_*^2 for $\frac{\tau_0}{\rho}$ we get:

$$-\overline{u'v'} = u_*^2\left(1 - y/d\right)$$

Substituting this equation and the equation $\frac{du}{dy} = \frac{u_*}{\kappa y}$ for "Universal boundary layer flow" in equation 6.01 for ε_m we get:

$$\varepsilon_m = \frac{-\overline{u'v'}}{du/dy} = \kappa u_* y\left(1 - y/d\right) \tag{6.02}$$

From Reynolds Analogy the sediment diffusion coefficient ε_s is given by $\varepsilon_s \simeq \beta\varepsilon_m$ where the coefficient β is approximately equal to 1. Consequently:

$$\varepsilon_s = \frac{-\overline{c'v'}}{dc/dy} = \beta\,\frac{-\overline{u'v'}}{du/dy} \tag{6.03}$$

and: $$\varepsilon_s = \beta \kappa u_* y \left(1 - y/d\right) \qquad (6.03)$$

This equation has been verified experimentally for the main region of the flow (neither close to the surface nor very close to the bed) where the universal boundary layer flow equation (2.20) holds very well (ref. 11). From the above it is obvious that the transfer process for sediment is interrelated with that of momentum and consequently with the transfer of turbulent energy. Thus, if the transfer process of turbulent energy is known, then it might be possible to express a law and relationships for the diffusion of sediment and in turn the sediment distribution and transportation.

From the experiments of the writer and other investigators (refs. 11, 13, 16, 17) it is clear that von Karman's constant k decreases when the sediment load increases (see Table 16). The decrease of k depends on the sediment load as well as on the balance of the turbulent energy of the flow.

From the mechanical energy equation (2.14) derived in Chapter II, article B, the following relation was found for the balance of the various rates of turbulent energy at every point of a uniform two-dimensional flow:

Rate of production = Rate of direct viscous dissipation + rate of diffusion

The rate of energy dissipation due to the settling of sediment is expected to decrease an equal amount of the rate of diffusion of turbulent energy. Therefore the above equation for the rates of

change of turbulent energy might be modified as follows:

Production = Direct viscous dissipation + Dissipation by sediment + Diffusion

From the above it is clear that the suspended sediment disturbs the balance of turbulent energy of clear flows, and it is deduced that there might be a direct relationship between von Karman's k and the ratio of the average rate of sediment energy dissipation to the average rate of diffusion of turbulent energy. However, no attempt was made to measure the rate of diffusion of turbulent energy, but it was assumed to be proportional to the rate of production in the fully developed turbulent flows of the experiments.

Consequently a graph of the measured k values versus the ratio of the average rate of sediment energy dissipation to that of turbulent energy production was made. It showed a decrease of k with an increase of this ratio.

From the above discussion it is clear that attempts to relate the k value to the total power of the flow are meaningless, since the rate of the molecular diffusion of energy, being always present and in very high amounts, (ref. 18), makes no effect whatsoever on von Karman's k, or the diffusion of sediment.

Einstein and Chien, in the appendix of ref. 17, correlated the reduction of von Karman's k with the ratio of the rate of energy dissipation in supporting the sediment in suspension to the rate of dissipation of the frictional energy of the fluid,

$$i.e. \qquad \kappa \quad vs. \quad \Sigma \frac{c_s w_s}{U S_e}\left(1 - \frac{\gamma_w}{\gamma_s}\right)$$

where c_s is the average concentration of a given grain size with settling velocity w_s, S_e is the slope of the energy grade line of the flow and Σ is the summation over all the grain sizes.

This is given by them as a preliminary approach in studying the reduction of k. It should be pointed out that the rate of dissipation of total energy of the fluid is not the main factor for direct comparison with the turbulent energy spent due to settling of sediment in the fluid. However, their plotted experimental points give a reasonable correlation of von Karman's k, with the a/m ratio.

Vanoni (ref. 11), taking as an average concentration the mean over the upper 95 percent of the profile at the center of the flume, calculated the ratio of the rate of energy dissipation due to suspended sediment to the rate of dissipation of the frictional energy of the fluid. Although his experimental points do not define a functional relationship, they correlate in a qualitative way the reduction of von Karman's k with the increase of the above-mentioned ratio.

From the graphs of Einstein and Chien (ref. 17), and Vanoni (ref. 11), and from fig. 27 it is apparent that the scatter in all three of these analyses is of about the same order of magnitude. There are several possible causes for this scatter. First of all there are varying ways to calculate the shear velocity, which is needed for the evaluation of k. Several investigations have used different methods of calculating the shear at

the center of the flume, where velocity profiles are measured. The plotted k values have not been corrected to take out this effect. Other difficulties are the varying ways in which the mean concentration and mean fall velocity are determined.

However, the basis on which fig. 27 is made seems to be more logical. There is some difficulty in predicting the k value from any of these graphs because it is necessary to know the sediment concentration distribution for the evaluation of the sediment energy dissipation. This in turn cannot be found without knowing k first. Furthermore, k is used to find the turbulent energy production term for the graph of the writer.

C. Effect of Sediment Load on Rannie's K_1

For the small region in the proximity of the wall the velocity profile depends on the viscosity and the wall characteristics. From Rannie's assumption for smooth walls the constant K_1 is calculated from the condition that the mean velocity profiles of both the regions should be continuous and have at least continuous first derivatives at their matching point $y^* = y_1^*$.

Since the effect of sediment load on von Karman's k in a fully developed turbulent flow is much bigger than

the effect on the friction factor, the values of y_1^* and κ_1 can be computed easily for various values of von Karman's k considering the friction factor as constant. This is done by solving numerically the system of equations:

$$\frac{1}{\kappa_1}\tanh \kappa_1 y_1^* = \frac{1}{\kappa}\ln y_1^* + \mathcal{B} + \frac{1}{2\kappa^2 y_1^*} - \frac{1}{4\kappa^3 y_1^{*2}} \qquad (6.04)$$

$$\operatorname{sech}^2 \kappa_1 y_1^* = \frac{1}{\kappa y_1^*} - \frac{1}{2(\kappa y_1^*)^2} + \frac{1}{8(\kappa y_1^*)^3} \qquad (6.05)$$

which give the continuity of the velocity profiles and their first derivatives at the matching point y_1^*, and where $\mathcal{B}$ is a function of k.

For the region very close to the matching point y_1^* the effect of viscosity has been taken into consideration for the extension of the "Universal boundary layer flow" down to this point.

For k values greater than 0.28 it is easy to compute the corresponding κ_1 and y_1^* values, but for k less than 0.28 there are no real solutions of equations 6.04 and 6.05. The extension of the theory to k values less than 0.28 was made by assuming that the matching point y_1^* remains the same as that for k = .28. For these values only the velocity profiles match at that point without continuity in its derivatives.

The velocity profiles measured for k less than 0.28 in the experiments of this work showed a tendency for k to increase in an intermediate region extending from $\frac{y}{d} \simeq .1$ down to the

region of the bed proximity. Neglecting the above change in k it was considered satisfactory for the computations of the results to make the assumption that k is constant all over the profile.

Since the range of von Karman's k values from .40 to .28 is very common in natural streams, and Rannie's assumption is satisfactory for the average velocity profile in slightly rough walls, the above theory for the flow conditions at the very proximity of the bed may be used to attack the problem of transportation of sediment.

The Reynolds Analogy is used for the transfer coefficients, so that $\varepsilon_s \simeq \beta \varepsilon_m$

From: $$\varepsilon_m = \frac{-\overline{u'v'}}{du/dy}$$

considering the shear stress constant in this region, and without neglecting the viscosity we get:

$$-\rho\overline{u'v'} = \tau_o - \mu \frac{du}{dy}$$

Dividing by ρ and substituting $\frac{\tau_o}{\rho} = u_*^2$ one gets:

$$-\overline{u'v'} = u_*^2 - \nu \frac{du}{dy}$$

Substituting this equation and equation 2.19 for $\frac{du}{dy^*}$ in region I into the equation for ε_m, and making some algebraic manipulations one obtains:

$$\varepsilon_m = \kappa \sinh^2 \kappa_1 y^* \qquad (6.06)$$

Consequently:

$$\varepsilon_s = \beta \kappa \sinh^2 \kappa_1 y^* \qquad (6.07)$$

From the above equations it is obvious that for constant kinematic viscosity the diffusion coefficients increase when κ_1 increases. Since an increase in sediment load decreases von Karman's k, it will increase Rannie's κ_1 for the bed proximity, provided that both k and κ_1 are constants for a given flow in regions II and I respectively. Therefore, ε_m and ε_s are increased by the suspended sediment according to equations 6.06 and 6.07.

Although the sediment load reduces the transfer coefficients of momentum, sediment and turbulent energy in the region away from the bed, it increases them in the very small region at the bed proximity.

D. Concentration Profile

Using the "Reynolds Analogy" for the diffusion coefficients, the differential equation for sediment concentration in regions I and II was given in a simple mathematical form.

The integration of the above equation was carried out, based on the assumption that the concentration at the bed elevation, i.e. at $y = 0$, is equal to the density of the bed.

From the experiments of McNown and Lin (ref. 15) it is known that the fall velocity of the particles is a continuous function of the concentration and it decreases when the latter increases. Since the concentration is a continuous

function of the distance from the bed, y , the fall velocity, w , will be a continuous function of y also.

From the above and the assumption that the concentration is equal to the bed density at $y=0$, it will be expected that the fall velocity of the particles reduces to zero at the bed elevation. Therefore it would be meaningless to assume that the settling velocity w is constant in the differential equation for sediment concentration, particularly in the region close to the bed, where the rate of change of the concentration with y is very large.

The exact evaluation of the function $w=w(c)$ is not yet known, although it would be universal for each grain size for all sediment-laden flows. To avoid the difficulties from both the evaluation of $w=w(c)$ and the integration of the differential equation for sediment concentration the following simple assumption for the fall velocity was made:

$$w = w_o \tanh^n k_1 y^*$$

where: w_o is the reduced settling velocity corresponding to the fall velocity at the average concentration, and n is a constant determined experimentally.

This formula gives $w=w_o$ for large y^* and $w=0$ for $y^*=0$.

The hindered settling in the main region of the flow has been included in the evaluation of w_o, since the factor $\tanh^n k_1 y^*$ is practically equal to one in this region of the flow. In the region close to the bed where the effect of hindered settling is

very large due to the high concentrations, further reduction in the fall velocity comes from the factor $\tanh^{n} k_1 y^*$, which reduces to zero at $y=0$.

As the exponent n increases, the fall velocity w decreases. From the differential equation for the concentration,

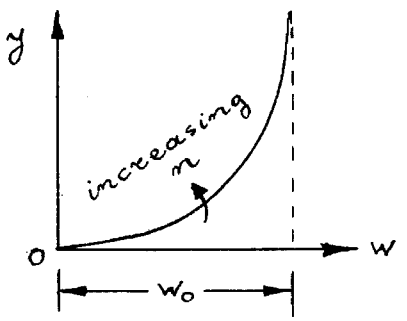

$\frac{dc}{-dy}$ is proportional to w. Consequently when w decreases, $\frac{dc}{-dy}$ decreases too, and the concentration curve becomes

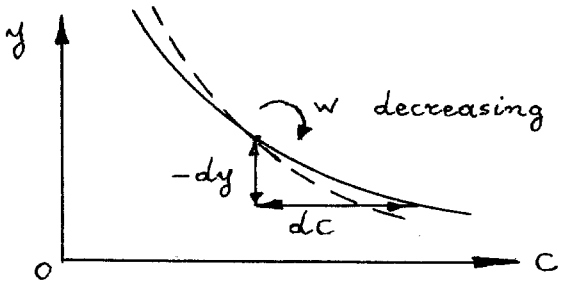

steeper. So when we start from a given boundary condition the concentration and consequently the sediment transport will be larger for larger values of the exponent n, other things being equal. For the experiments of this work, the range of n was from 1.75 to about 9.0, while the range of von Karman's k was from .37 to .23.

Throughout region II except for a very small section

between y_1^* and $5y_1^*$ the ratio $\frac{c(w)}{c(w_o)}$ was approximately equal

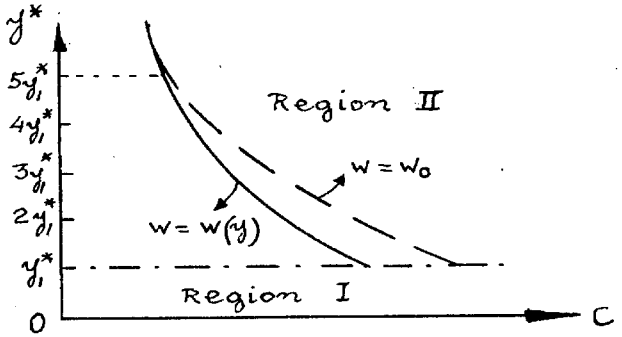

to one, where $c(w_o)$ corresponds to the concentration equation 2.36 derived by using $w = w_o$ = constant.

Thus for $y^* \geq 5y_1^*$ $\qquad c(w) \simeq c(w_o)$

and for $y^* \simeq y_1^*$ $\qquad c(w) \geq 0.8\, c(w_o)$

Consequently for the purposes of calculating the average concentration one could accept the approximation $w = w_o$ = constant in region II. However it would not be correct to take w as a constant for the evaluation of $c(w)$ from the boundary condition at the bed, even though the variation of w in region I would be taken into consideration. This is because then the exponent n would be computed larger and the concentration profile in region I would

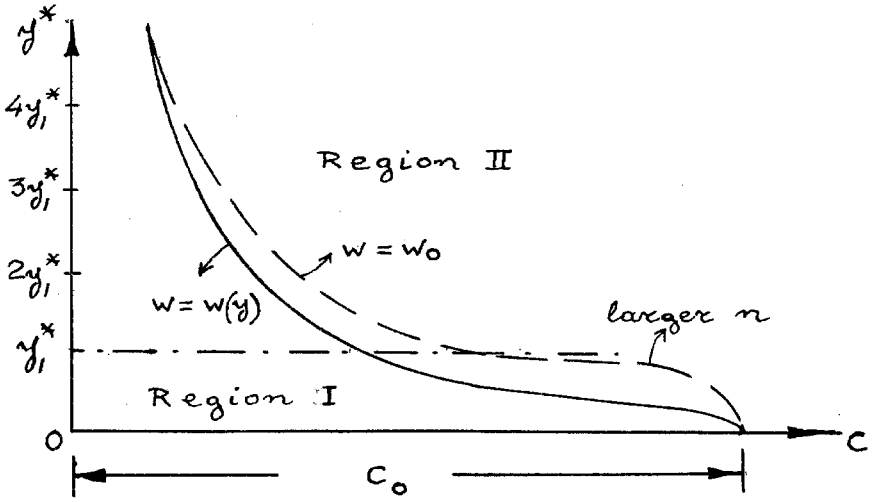

be larger than that given for the proper value of the exponent n.

The evaluation of the exponent n should be done experimentally, since the assumption for the fall velocity is empirical. Many experiments should be carried out and experimental curves be given for the above exponent. Such an investigation was not possible within the framework of the present experiments.

It should be noted that the assumption made for the fall velocity, (equation 2.25), does not correspond to that due to hindered settling in an intermediate region around $y^* = 50$. For that region w becomes approximately equal to w_0, constant. In most physical cases with fine sediment the actual settling velocity is much smaller than w_0 in that region where the concentrations are usually much higher than the average. Thus starting from a given mid-depth concentration, the actual values of $c(w)$ in this intermediate region are lower than those calculated by the assumption made in equation 2.25.

In the physical cases with coarse sediment the reduction of the fall velocity due to hindered settling is not very much and the above assumption seems to give better approximations in that intermediate region.

However, this region is so small that the final average results for sediment concentration and rate of sediment energy dissipation are probably not affected considerably from the above discussed deviations.

E. Sediment Load Relationship

From the foregoing discussion it is evident that the assumption made for the settling velocity of the particles gives a possible approximation for the solution of the problem of sediment discharge for a stream with uniform sediment and plane bed. Thus it might be possible to find the absolute concentration $c(y)$ at any y, instead of only the ratio of $c(y)$ to the concentration $c(a)$ at a reference point $y=a$, as in the simple suspended load equation.

The difficulty with the ordinary suspended load equation is that the concentration distribution based on the logarithmic velocity law and constant fall velocity gives infinite concentration at y equal to zero. The integration of sediment concentration to obtain an average concentration over the profile gives infinity for any value of the exponent z greater than, or equal to one.

Einstein (ref. 10) suggested a lower limit for the integration of the sediment concentration to avoid the above singularity. This lower limit was taken equal to twice the diameter of the grains. Brooks (ref. 13) suggested a lower limit which is largest out of four choices. Both suggestions give reasonably good results for average transport sediment concentration, due to the fact that the velocity is very small close to the wall and consequently the contribution of this region to the average is very small. However, for average sediment concentration in the profile, $\overline{C}$, the above suggestions sometimes do not give

reasonable values, because any small variation in the lower limit of the integration gives a large variation in the value of the integral.

F. Turbulence Characteristics of Sediment Laden Streams

For an overall view of the turbulence characteristics of any stream carrying sediment in suspension and a comparison of them with those of clear water flows, the effect of sediment on von Karman's constant k and the friction factor was measured.

From the discussion of the effect of sediment on the velocity profile in a previous article, and from investigation of turbulence (refs. 20-26), it is deduced that the rate of energy dissipation for the suspension of sediment has an overall effect on the turbulent energy balance. This actually appears by affecting directly the rate of diffusion of turbulent energy, which is of great importance in a very small region close to the bed. There the sediment concentration and consequently the rate of dissipation of energy from the suspension of sediment is also, relatively speaking, very large.

In Table 16 of Chapter V, article B, 5, it is implied that the sediment load has a small effect on the average production of turbulent energy, since the sediment energy dissipation is only a small percentage of the total turbulent energy production.

Assuming that the diffusion of turbulent energy for sediment laden streams is of about the same percentage of turbulent

energy production, as that for the clear flows, it may be found, (from Laufer's data (ref. 1) on fully established turbulent pipe flows) that the average rate of absolute value of diffusion is about 22% of the average rate of production.

In this way, the ratio of the average of the rate of sediment energy dissipation to the estimated rate of turbulent energy diffusion was found to be considerable, varying from 7.7% to about 20.5%, for runs 1, 3, 5 and 7.

This discussion explains the great importance of sediment load by its reduction of the rate of turbulent energy diffusion, changing thus the balance of the total turbulent energy and consequently the mechanism of the turbulent motions.

G. Effect of Sediment Load on Friction Factor

From the calculated friction factors tabulated in Table 7 (Chapter V, article B, 6) it is concluded that the friction factor decreases when the sediment load of a given grain size increases.

From the diagram of the friction factor versus Reynolds number for pipes, given in any textbook on fluid mechanics, it is known that for high Reynolds numbers and rough walls the friction factor f is independent of Re and depends only on the roughness of the boundary walls. The turbulence level of a uniform flow for high Reynolds numbers is independent of the velocity of the flow and depends on the geometric characteristics of the wall roughness. For a given Reynolds number, an increase in the roughness of the walls increases both the turbulence level and the friction factor of the flow, although k stays constant.

Consequently the friction factor might be expressed as a function of the turbulence level. Thus, when the turbulence level is increased with grids or other means (ref. 27), the friction factor of the flow will increase, provided that there is no change in the characteristics of the boundary walls.

In flows with sediment load the turbulence level is reduced due to the damping of the turbulent energy by the suspended sediment. Thus it seems reasonable to deduce that the reduction of turbulence level is the reason for the decrease of the friction factor in flows with sediment in suspension.

Since the reduction of the turbulence level of the flow by the sediment load is small, and the shear stress at the bed depends on this level of the flow, it would be expected that the decrease of the friction factor would be small also.

The experimental investigation of this reduction is not simple, because of the difficulty in keeping the same bed roughness characteristics for clear water flow on a fixed bed, and sediment laden flow on movable sand bed.

Ludwieg and Tillmann (ref. 27) studied experimentally the behavior of the friction factor in boundary layers with or without a turbulence grid or a square strip at the wall crosswise to the direction of the flow. Their measurements were made with a heat-transfer instrument developed by Ludwieg.

Using as a parametric characteristic the ratio of the displacement thickness δ_1, over the momentum thickness δ_2, of the flow, they determined the experimental relationship for

the friction coefficient at boundary layers:

$$f = 4 \cdot 0.246 \cdot 10^{-0.678\, H_{12}} \cdot Re^{-0.268} \qquad (6.09)$$

where: $H_{12} = \frac{\delta_1}{\delta_2}$ and $Re = \frac{U_{max}\, \delta_2}{\nu}$ (6.10)

and U_{max} was the velocity outside the boundary layer. Using a grid they increased the turbulence of the outer flow considerably, and their measurements showed an average increase in the friction factor of 10 percent. Also by disturbing the flow inside the boundary layer with a strip at the wall crosswise to the direction of the flow, they measured practically the same increase in the friction factor.

Consequently it is obvious that the increase in turbulence level of the flow increased the friction. It is also expected that when the turbulence is damped by sediment load the friction would decrease.

This tendency of the decrease of the friction factor for sediment-laden flows is shown from the consideration of the experimental formula:

$$f = 4 \cdot 0.246 \cdot 10^{-0.678\, H_{12}} \cdot Re^{-0.268} \qquad (6.09)$$

For uniform channel flow:

$\delta_1 = d = R$ (depth of flow)

$U_m = u_{max}$ at the surface by extending the logarithmic profile.

From the definition of δ_1 and δ_2 we get:

$$\delta_1 = \int_0^h \left(1 - \frac{u}{U_m}\right) dy \qquad \text{and} \qquad \delta_2 = \int_0^h \frac{u}{U_m}\left(1 - \frac{u}{U_m}\right) dy$$

Substituting the values for u in regions I and II we get:

$$\delta_1 = \int_0^{y_1} \left(1 - \frac{u_*}{U_m \kappa_1} \tanh \kappa_1 y^*\right) dy + \int_{y_1}^h \left\{1 - \frac{u_*}{U_m}\left(\frac{1}{\kappa} \ln y^* + B\right)\right\} dy$$

$$\delta_2 = \int_0^{y_1} \left(\frac{u_*}{U_m \kappa_1} \tanh \kappa_1 y^*\right)\left(1 - \frac{u_*}{U_m \kappa_1} \tanh \kappa_1 y^*\right) dy + \int_{y_1}^h \frac{u_*}{U_m}\left(\frac{1}{\kappa} \ln y^* + B\right)\left\{1 - \frac{u_*}{U_m}\left(\frac{1}{\kappa} \ln y^* + B\right)\right\} dy$$

Integrating, making some arithmetical manipulations and neglecting terms of higher order we get:

$$\delta_1 \simeq \frac{u_*}{U_m \kappa} h \qquad (6.11)$$

$$\delta_2 \simeq \frac{u_*}{U_m \kappa} h \left(1 - \frac{2u_*}{\kappa U_m}\right) \qquad (6.12)$$

And their ratio becomes:

$$H_{12} = \frac{\delta_1}{\delta_2} = \frac{1}{1 - \frac{2u_*}{\kappa U_m}} \qquad (6.13)$$

Considering that the experimental formula for f is theoretically correct, we could have the following for the qualitative behavior of f. When there is sediment load, Karman's k decreases faster than the U_{max} increases, as it is shown from the velocity profiles of the experiments of this work. From equation 6.13 for H_{12} it is obvious that $\frac{2u_*}{\kappa U_m}$ will increase regardless of the small changes in u_* and U_m, and the parameter H_{12} will increase.

From equation 6.10 for Re we get:

$$R_e = \frac{U_{max}\,\delta_2}{\nu} = \frac{U_m}{\nu}\,\frac{u_*}{U_m \kappa}\left(1 - \frac{2u_*}{\kappa U_m}\right)$$

or

$$R_e = \frac{R^*}{\kappa}\left(1 - \frac{2u_*}{\kappa U_m}\right) \qquad (6.14)$$

Since for the cases of natural streams and usual laboratory experiments the factor $\frac{2u_*}{\kappa U_m}$ is much smaller than one, any decrease in k would increase the Reynolds number. So the friction factor given by the experimental equation, 6.09, will decrease.

From the above discussion it is deduced that the friction factor is reduced in flows with suspended sediment due to the damping of the turbulent fluctuations.

CHAPTER VII

CONCLUSIONS

The principal conclusions and deductions drawn from this investigation may be summarized as follows:

1. It is hypothesized that the suspended sediment appreciably reduces the rate of diffusion of turbulent energy but only slightly (reduces) the turbulent energy level. Thus, the balance of the rate of turbulent energy production, dissipation and diffusion is disturbed considerably while the turbulence level of the flow decreases slightly.

2. The friction factor of the flow is reduced by the damping effect of the suspended sediment on the turbulence. Thus, sediment laden flows have a smaller friction factor than clear water flows, provided that the Reynolds number and the roughness characteristics of the boundaries are the same.

3. It is deduced that von Karman's k depends on the balance of the turbulent energy which for a uniform two-dimensional flow is given by:

Rate of production = rate of direct viscous dissipation + rate of diffusion.

Hence k is affected more by the suspended sediment than the friction factor f, which depends on the turbulence level of the flow.

4. von Karman's k might be expressed as a function of the ratio of the average rate of dissipation of energy by the

suspended sediment to the average rate of the absolute value of the rate of diffusion of turbulent energy. However, k is independent of the molecular rate of diffusion of energy, which always exists in very high amounts in any boundary layer flow.

5. The friction factor f might be expressed as a function of the ratio of the average rate of energy dissipation by suspended sediment to the average rate of turbulent energy production, in addition to the Reynolds number and the geometric roughness characteristics of the stream.

6. The computed rates of turbulent energy production and energy dissipation by suspended sediment have very large values in a very small region near the bed.

7. The so-called "Reynolds Analogy" for the turbulent diffusion coefficients of momentum and sediment was found to hold very well, and it was verified experimentally in the region where sediment samples were taken. In other words, the diffusion coefficient of sediment ε_s is proportional to the diffusion coefficient of momentum ε_m, with the constant of proportionality approximately equal to one.

8. As found by others the experimental law of "Universal Boundary Layer Flow" was found very good in fitting the measured velocity distributions in a region away from the bed.

The suspended sediment load decreased von Karman's constant k. However there was some evidence that suspended sediment at the higher concentrations reduced k more in the main region of the flow far away from the bed than in an inter-

mediate region extending from $y^* = 100$ to about $\frac{y}{d} \simeq 0.1$.

9. The integration of the sediment load differential equation was carried out by assuming an expression for the settling velocity of the particles as a function of the distance from the bed. This function makes the settling velocity approximately constant in a region away from the bed, but makes it decrease rapidly in a very small region close to the bed, becoming zero at the bed elevation.

CHAPTER VIII

REFERENCES

1. Laufer, J.: "The Structure of Turbulence in Fully Developed Pipe Flow." NACA Tech. Note 2954, 1953.

2. Laufer, J.: "Investigation of Turbulent Flow in a Two-Dimensional Channel." NACA Rep. 1053, 1951.

3. Rannie, W. D.: "Heat Transfer in Turbulent Shear Flow." Ph.D. Thesis, Calif. Inst. of Techn., 1951.

4. Schlichting, H.: "Grenzchicht Theorie." Verlag und Druck G. Braun, Karlsruhe, 1951.

5. von Karman, Th.: "The Fundamentals of the Statistical Theory of Turbulence." Jour. Aero. Sci., Vol. No. 4, 1937.

6. Prandtl, L.: "Ueber ein neues Formelsystem für die ausgebildete Turbulenz." Nachr. d. Akad. d. Wissensch. in Göttingen. Mathematischphysikalische Klasse aus den Jahre, 1945.

7. Rotta, J.: "On the Theory of the Turbulent Boundary Layer." NACA Tech. Mem. 1344, 1953.

8. Vanoni, V. A.: "Experiments on the Transportation of Suspended Sediment by Water." Ph.D. Thesis, Calif. Inst. of Techn., 1940.

9. Vanoni, V. A.: "Transportation of Suspended Sediment by Water." Transaction A.S.C.E., Vol. 111, 1946.

10. Einstein, H. A.: The Bed Load Function for Sediment Transportation in Open Channels". U. S. Dept. of Agr., Soil Conservation Service. Tech. Bull. No. 1026, 1950.

11. Vanoni, V. A.: "Some Effects of Suspended Sediment on Flow Characteristics." Proc. Fifth Hydraulics Conf. State Univ. of Iowa. Bulletin 34, No. 420, 1952.

12. Rouse, H.: "Engineering Hydraulics." Proc. Fourth Hydro. Conf., Wiley and Sons, 1949.

13. Brooks, N. H.: "Laboratory Studies of the Mechanics of Streams Flowing over a Movable Bed of Fine Sand." Ph.D. Thesis, Calif. Inst. of Techn., 1954.

14. Otto, G. and Rouse, H.: "Wind Tunnel Classifier for Sand and Silt". Civil Engineering Vol. 9, No. 7, July 1939.

15. McNown, J. and Lin, P. N.: "Sediment Concentration and Fall Velocity". Proc. 2nd Midwest Conf. on Fluid Mech., Ohio State Univ., 1952.

16. Ismail, M.: "Study of Suspended Sediment in Closed Channels"; Ph.D. Thesis, California Inst. of Technology, 1948.

17. Einstein, H. A. and Chien, Ning: "Second Approximation to the Solution of the Suspended Load Theory." Instit. of Engin. Research, Univ. of Calif., 1954.

18. Bakhmeteff, B. A. and Allan, W.: "The Mechanism of Energy Loss in Fluid Friction." Transactions ASCE, Vol. 111, 1946.

19. Johnson, J. W.: "The Importance of Side-Wall Friction in Bed-Load Investigations." Civil Engineering, Vol. 12, No. 6, 1942, pp. 329-331.

20. Batchelor, G. K.: "Diffusion in a Field of Homogeneous Turbulence." I. Eulerian Analysis. Australian J. Sc. Res. 2, 437, 1949.

21. Dryden, H. L. and Schubauer, G. B.: "Use of Damping Screens for the Reduction of Wind Tunnel Turbulence." Jour. Aero. Sc. Vol. 14, April 1947.

22. Taylor, G. I.: "Statistical Theory of Turbulence. III. Distribution of Dissipation of Energy in a Pipe over its Cross-section." Proc. Roy. Soc. London, Ser. A, vol. 151, No. 183, 1935.

23. Heisenberg, W.: "Zur Statistischen Theorie der Turbulenz." Z. Phys. 124, 628, 1948.

24. Kampe de Feriet, J.: "Sur l'ecoulement d'un fluide visqueux incompressible entre deux plaques paralleles indefinies." La Houille Blanche, vol. 3, No. 6, Nov.-Dec. 1948.

25. von Karman, Th.: "Some Aspects of the Turbulence Problem." Proc. Fourth Intern. Congr. for Appl. Mech., Cambridge, England, 1934.

26. Kolmogoroff, A.: Dissipation of Energy in Locally Isotropic Turbulence." Comp. rend. acad. sci. U.R.S.S., vol. 31, 538 and vol. 32, 16, 1941.

27. Ludwieg, H. and Tillmann, W.: "Investigations of the Wall-Shearing Stress in Turbulent Boundary Layers." NACA Tech. Mem. 1285, 1950.

28. Ludwieg, H.: Ein Gerät zur Messung der Wandschubspannung turbulenter Reibungsschichten. Ing-Arch. (Available as NACA T.M. 1284).

CHAPTER IX

SYMBOLS

a	Reference level of sediment concentration function
b	Width of a rectangular channel
c, c_a, c_1, c_0	Time mean concentration of sediment (grms/liter dry weight) at points $y=y$, $y=a$, $y=y_1$ & $y=0$ respectively
C	Venturi meter discharge coefficient
c'	Fluctuation component of the concentration at a point
C	Time mean-plus-fluctuation concentration:
d	Depth of flow $\{d \equiv h$ is used in differentiations, i.e. $\frac{dh}{dx}\}$ $\{$i.e. $\frac{dh}{dx} = \frac{\partial h}{\partial x} = \frac{\partial d}{\partial x} = \frac{dd}{dx}\}$
d_g	Geometric mean grain size of sand
d_s, d_{s_i}	Mean sedimentation diameter, total and for a sieve fraction
e	Instantaneous value of internal energy of fluid: $e = \bar{e} + e'$
$\bar{e}$	Time mean internal energy of fluid
e'	Instantaneous fluctuation of internal energy
e_h	Specific energy of the flow
f, f_b, f_w	Darcy-Weisbach friction factor. (Total, bed sectional, and wall sectional, respectively)
g	Gravitational acceleration
h	Depth of flow: $h \equiv d$
h^*	$h^* = h \frac{u_*}{\nu}$
K	Thermal conductivity
κ	von Karman's universal constant

K_1	Rannie's constant for the velocity profile close to the wall
K_s	Equivalent roughness
K_s^*	$K_s^* = K_s \frac{u_*}{\nu}$
m	Slope of the velocity profile: $m = du/d(\log_{10} y)$
n	Dimensionless exponent variable of the fall velocity
P, P_b, P_w	Wetted perimeter of the stream (Total, bed sectional, and wall sectional, respectively)
p	Total mean-plus-fluctuation pressure: $p = P + p'$
p'	Instantaneous value of pressure fluctuations
q	Discharge per unit width
q_s	Sediment transportation rate per unit width
r, r_b, r_w	Hydraulic radius (Total, bed sectional, and wall sectional, respectively)
t	Time
u_1, u_2, u_3	Instantaneous values of velocity in x, y, z, direction, respectively
u, v, w	Time mean velocity in x, y, z direction respectively
u', v', w'	Instantaneous values of velocity fluctuations in x, y, z direction, respectively.
u_{max}	Maximum velocity
u_*	Shear or friction velocity: $u_* = \sqrt{\tau_0/\rho}$
$u_{*\mathbb{C}}$	Shear velocity at the center of the bed
u_{*m}	Maximum shear velocity
u_{*2-D}	Shear velocity in two-dimensional flow $u_{*2-D} = \sqrt{gdS}$

w, w_o Time mean settling velocity, reduced due to average concentration

w Instantaneous value of settling velocity:

w_i Settling velocity for a sieve fraction

y Distance from the bed of stream

y^* $y^* = y \frac{u_*}{\nu}$

y_1 Distance from bed of the matching point of the two velocity profiles in region I (close to the wall), and in region II (away from the wall)

y_1^* $y_1^* = y_1 \frac{u_*}{\nu}$

z, z_o, z_1 Exponents in sediment load equation, equal to:

$$\frac{w}{\beta \kappa u_*} \;,\; \frac{w_o}{\beta \kappa u_*} \;,\; \frac{w_o}{\beta \kappa_1 u_*} \quad \text{, respectively}$$

A, A_b, A_w Cross-sectional area of the stream (Total, bed sectional, wall sectional, respectively)

A_s Constant in logarithmic velocity profile for rough walls

A_1, A_2 Venturi meter cross-sectional area

B Constant in logarithmic velocity profile for smooth walls

C Time mean concentration at a point

$\bar{C}$ Average concentration over a profile: $\bar{C} = \frac{1}{R}\int_0^R c\,dy$

$\bar{C}_T$ Average sediment transport concentration: $\bar{C}_T = \frac{1}{UA}\int_0^R cu\,dy$

D Turbulent energy diffusion rate: $D = \rho \frac{\partial}{\partial x_k}\left[\overline{u_k'\left(E + \frac{p'}{\rho}\right)}\right] - \mu \nabla^2 E$

D_τ Dimensionless turbulent energy diffusion rate: $D_\tau = \frac{\nu}{\rho u_*^4} D$

$|\bar{D}|$ Average rate of absolute value of turbulent energy diffusion

$|\overline{D}|_\tau$ Dimensionless average rate of absolute value of turbulent energy diffusion

$$|\overline{D}|_\tau = |\overline{D}| \frac{\nu}{\rho u_*^4}$$

E Instantaneous turbulent energy: $E = \frac{u'^2+v'^2+w'^2}{2}$

$E_i(x)$ Integral defined by: $E_i(x) = \int_x^\infty \frac{e^{-\varsigma}}{\varsigma} d\varsigma$

F_r Froude number: $F_r = \frac{U}{\sqrt{dg}}$

G Total sediment transportation rate

$H(\eta_1)$ Integral defined by: $H(\eta_1) = \int_{\eta_1}^{1} \left(\frac{1-\eta}{\eta}\right)^{\beta_0} d\eta$

$H(\omega_1, \omega_R)$ Integral defined by: $H(\omega_1, \omega_R) = \frac{1}{\omega_R} \int_{\omega_1}^{\omega_R} \left(\frac{\omega_R-\omega}{\omega}\right)^{\beta_0} \frac{e^{-2n\beta_0 E_i(2\omega)}}{e^{-2n^2\beta_0 E_i(4\omega)}}$

H_{12} Ratio $\frac{\delta_1}{\delta_2}$

$I_i(x)$ Integral defined by: $I_i(x) = \int_x^{-\infty} \frac{e^{\varsigma}}{\varsigma} d\varsigma$

$L(\eta_1)$ Integral defined by: $L(\eta_1) = \int_1^{\eta_1} \left(\frac{1-\eta}{\eta}\right)^{\beta_0} \ln\eta \, d\eta$

P Time mean pressure at any point

P_r Turbulent energy production rate: $P_r = -\rho\overline{u'v'}\frac{dU}{dy}$

$(P_r)_\tau$ $(P_r)_\tau = \frac{\nu}{\rho u_*^4} P_r$

$\overline{P_r}$ Average turbulent energy production rate:

$$\overline{P_r} = \frac{1}{R}\int_0^R -\rho\overline{u'v'}\frac{dU}{dy}dy$$

$\overline{(P_r)_\tau}$ Dimensionless average turbulent energy production rate:

$$\overline{(P_r)_\tau} = \frac{\nu}{R u_*^4}\int_0^R \left(-\overline{u'v'}\right)\frac{dU}{dy}dy$$

Q Total discharge

Re, Re_b, Re_w Reynolds number $\frac{4Ur}{\nu}$ (Total, bed sectional, and wall sectional, respectively)

S Slope of the flume

S_e Slope of the energy grade line for the stream

T Time mean of water temperature

T' Instantaneous value of temperature fluctuation

U, V, W Time mean velocities in x, y, z direction, respectively

U Average flow velocity

U_{max} Maximum velocity of the flow

U_*, U_{*b}, U_{*w} Average shear velocity for the total section $\sqrt{grS_e}$, bed section $\sqrt{gr_bS_e}$, and wall section $\sqrt{gr_wS_e}$, respectively.

W_s Rate of energy dissipation by suspended sediment:

$$W_s = cw\left(1 - \frac{\gamma_w}{\gamma_s}\right)$$

$(W_s)_\tau$ Dimensionless rate of energy dissipation by suspended sediment:

$$(W_s)_\tau = \frac{\nu}{\rho u_*^4} cw\left(1 - \frac{\gamma_w}{\gamma_s}\right)$$

$\overline{W_s}$ Average rate of energy dissipation by suspended sediment:

$$\overline{W_s} = \frac{1}{R}\int_0^R cw\left(1 - \frac{\gamma_w}{\gamma_s}\right)dy$$

$(\overline{W_s})_\tau$ Dimensionless average rate of energy dissipation by suspended sediment:

$$(\overline{W_s})_\tau = \frac{\nu}{R\rho u_*^4}\int_0^R cw\left(1 - \frac{\gamma_w}{\gamma_s}\right)dy$$

X_i Body force per unit mass on x_1, x_2, x_3 direction

β Ratio of diffusion coefficients: $\beta = \varepsilon_{comp} / \varepsilon_{meas.}$

γ Ratio of thicknesses: $\gamma = \delta_1 / \delta_2$

γ_w, γ Unit weight of water

γ_s Unit weight of sediment

δ_1 Displacement thickness: $\delta_1 = \int_0^h \left(1 - \frac{u}{U_m}\right) dy$

δ_2 Momentum thickness: $\delta_2 = \int_0^h \frac{u}{U_m}\left(1 - \frac{u}{U_m}\right) dy$

ε_m Turbulent diffusion coefficient for momentum:

$$\varepsilon_m = - \overline{u'v'} / du/dy$$

ε_s Turbulent diffusion coefficient for sediment:

$$\varepsilon_s = - \overline{c'v'} / dc/dy$$

η $y/d = y/h$

η_1 $y_1/d = y_1/h$

μ Dynamic viscosity of water

ν Kinematic viscosity of water

ρ Mass density of water

ρ_s Mass density of sediment

σ_g Geometric standard deviation of grain size

σ_{ik} Total time mean-plus-fluctuation shear stress:

$$\sigma_{ik} = \tau_{ik} + \tau'_{ik}$$

τ Shear stress in the fluid: $\tau = \tau_{xy}$

τ_o Shear stress at the boundary

$\bar{\tau}_o$, $\bar{\tau}_b$, $\bar{\tau}_w$ Average shear stress on the entire boundary, the bed section, and the wall section, respectively

τ_{ij} Time mean shear stress

τ^R_{ij} Total shear stress including Reynolds stresses:

$$\tau^R_{ij} = \tau_{ij} + \tau^*_{ij}$$

τ^*_{ij} Turbulent shear stress (Reynolds): $\tau^*_{ij} = -\rho\overline{u'_i u'_j}$

τ'_{ij} Instantaneous fluctuation of the shear stress

ω, ω_1, ω_R $\omega = \kappa_1 y^*$, $\omega_1 = \kappa_1 y_1^*$, $\omega_R = \kappa_1 R^*$

ϕ_L Dissipation defined by $\phi_L = \tau_{ik}\dfrac{\partial U_i}{\partial x_k}$

ϕ_T Dissipation defined by $\phi_\tau = \overline{\tau'_{ik}\dfrac{\partial u'_i}{\partial x_k}}$

ϕ Dissipation function: $\phi = \tau_{ik}\dfrac{\partial U_i}{\partial x_k} + \overline{\tau'_{ik}\dfrac{\partial u'_i}{\partial x_k}}$

$\Omega(\omega_1)$ Integral defined by: $\Omega(\omega_1) = \dfrac{1}{\omega_R}\displaystyle\int_0^{\omega_1} e^{-\frac{\beta_1}{n-1}\tanh^{n-1}\omega} \cdot \tanh^n\omega\, d\omega$

$\Omega'(\omega_1)$ Integral defined by: $\Omega'(\omega_1) = \dfrac{1}{\omega_R}\displaystyle\int_0^{\omega_1} e^{-\frac{\beta_1}{n-1}\tanh^{n-1}\omega} \cdot d\omega$

$\Omega_T(\omega_1)$ Integral defined by: $\Omega_T(\omega_1) = \dfrac{1}{\omega_R}\displaystyle\int_0^{\omega_1} e^{-\frac{\beta_1}{n-1}\tanh^{n-1}\omega} \cdot \tanh\omega\, d\omega$

CHAPTER X

APPENDIX

A. Velocity Profile for Various Values of k

1. Smooth Walls

In region I the velocity profile is given by equation 2.18 (Chapter II, article D)

$$\frac{u}{u_*} = \frac{1}{k_1} \tanh k_1 y^* \tag{2.18}$$

In region II and very close to region I the velocity profile is given by equation 2.24

$$\frac{u}{u_*} = \frac{1}{k} \ln y^* + B + \frac{1}{2k^2 y^*} - \frac{1}{4^2 k^3 y^{*2}} \cdots \tag{2.24}$$

where B is the same as that of equation 2.21

$$\frac{u}{u_*} = \frac{1}{k} \ln y^* + B \tag{2.21}$$

holding for large values of y^*, because the terms $\frac{1}{2k^2 y^*}, \frac{1}{4^2 k^3 y^{*2}}) \cdots$ become negligible.

The slope of the velocity profile in region I is given by equation 2.19

$$\frac{du}{dy^*} = u_* \operatorname{sech}^2 k_1 y^* \tag{2.19}$$

And in region II by equation 2.24

$$\frac{du}{dy^*} = u_* \left(\frac{1}{ky^*} - \frac{1}{2(ky^*)^2} + \frac{1}{8(ky^*)^3} \cdots \right) \tag{2.23}$$

The mean velocity of the flow occurs at $\frac{y}{d} \simeq \frac{1}{e}$ i.e. $y \simeq .37d$.

And from equation 2.24 we get:

$$\frac{\overline{U}}{u_*} = \frac{1}{K}\ln(.37R^*) + B + \frac{1}{2K^2(.37R^*)} - \frac{1}{4^2K^3(.37R^*)^2} \cdots$$

For $K = .40$ $\quad B = 5.5$

Then for any other value of k and for no change in the friction factor we get B.

$$B = 5.5 + (\ln 0.37R^*)\left\{\frac{1}{.4} - \frac{1}{K}\right\} + \frac{1}{2(.37R^*)}\left\{\frac{1}{.4^2} - \frac{1}{K^2}\right\} - \frac{1}{4^2(.37R^*)^2}\left\{\frac{1}{.4^3} - \frac{1}{K^3}\right\} \cdots \tag{10.01}$$

Substituting for various values of k and assuming $R^* \simeq 3500$ we find the following values for B.

$K = .40$	$B = 5.5$
$= .35$	$= 2.91$
$= .30$	$= -0.5$
$= .275$	$= -2.71$
$= .250$	$= -5.30$
$= .225$	$= -8.53$

For continuous velocity u and slope du/dy^* at the matching point $y^* = y_1^*$ of the velocity profile we get:

$$\frac{1}{K_1}\tanh K_1 y_1^* = \frac{1}{K}\ln y_1^* + B + \frac{1}{2K^2 y_1^*} - \frac{1}{4^2K^3 y_1^{*2}} \tag{10.02}$$

$$\operatorname{sech}^2 K_1 y_1^* = \frac{1}{Ky_1^*} - \frac{1}{2(Ky_1^*)^2} + \frac{1}{8(Ky_1^*)^3} \tag{10.03}$$

The numerical solution of this system for various values of k and its corresponding values of $\mathcal{B}$ gives:

$K = .40$	$\mathcal{B} = 5.5$	$K_1 = 1/14.5$	$y_1^* = 27.5$
.35	2.91	1/13	22.5
.30	-0.5	1/9.5	13.0
.275	-2.71	1/7	8.5
.250	-5.30	1/4.2	8.0
.225	-8.53	1/2.0	8.0

The last two lines are obtained from the graph of the velocity profiles (fig. 29), because the system of equations 10.02 and 10.03 has not any real solution for $K < .275$. It should be pointed out that the above values have been derived assuming no change in the friction factor. This was done to simplify the calculations and its justification is indicated as follows:

From equation 2.21 the average velocity for the profile is given at $y = .37d = .37R$,

$$\frac{\bar{U}}{u_*} = \frac{1}{K}\ln(.37R^*) + \mathcal{B}$$

Substituting $\frac{\bar{U}}{u_*}$ by $\sqrt{\frac{8}{f}}$ and rearranging terms we find,

$$\mathcal{B} = \sqrt{\frac{8}{f}} - \frac{\ln(.37R^*)}{K}$$

Since $\ln .37R^*$ is usually equal to ~ 6 for $f \simeq .02$, we can approximate $\mathcal{B}$ by,

$$\mathcal{B} \sim \sqrt{\frac{8}{f}} - \frac{6}{K}$$

For $K = .40$

$$\mathcal{B} \sim \sqrt{\frac{8}{.02}} - \frac{6}{.4} = 20 - 15 = 5$$

For $\kappa = .20$ and no change in f we find,

$$\mathcal{B} \sim \sqrt{\frac{8}{.02}} - \frac{6}{.2} = 20 - 30 = -10$$

For $\kappa = .20$ and 25 percent change in f we find

$$\mathcal{B} \sim \sqrt{\frac{8}{.016}} - \frac{6}{.2} \simeq 22 - 30 = -8$$

This example indicates the justification in considering f fixed in the calculations for the values of $\mathcal{B}$.

The measured velocity profiles for runs 3 and 5 with high sediment transportations (fig. 18 and Table 7) showed that there was a tendency for von Karman's k to increase at the intermediate region between the main region of the flow and the small region very close to the wall. However there is some doubt about it as it has already been mentioned in Chapter V, article A, 4.

Taking the above tendency of increasing von Karman's k into consideration, as well as the observed decrease of the friction factor for high sediment concentrations it is deduced that the values of both κ_1 and y_1^* for very high concentrations with $\kappa < .280$ will not differ much from those for $\kappa \simeq .280$.

2. Rough Walls

In region II and very close to region I the velocity profile is given by:

$$\frac{u}{u_*} = \frac{1}{\kappa} \ln \frac{y^*}{k_s^*} + A_s + \frac{1}{2\kappa^2 y^*} - \frac{1}{4^2 \kappa^3 y^{*2}} \cdots \qquad (10.04)$$

where A_s is the same as that of the equation:

$$\frac{u}{u_*} = \frac{1}{\kappa} \ln \frac{y^*}{k_s^*} + A_s \qquad (10.05)$$

holding for large values of y^*, because the terms $\frac{1}{2k^2y^*}$, $\frac{1}{4^2k^3y^{*2}}$, ... become negligible.

The coefficient $\mathcal{B}$ of smooth walls corresponds to

$$\mathcal{B} \sim A_s - \frac{1}{\kappa} \ln \kappa_s^*$$

The slope of the velocity profile is given by equation 2.24, which is the same for both smooth and rough walls.

The mean velocity of the flow for open channels is given by:

$$\frac{\overline{U}}{u_*} \simeq -\frac{1}{\kappa} + \frac{1}{\kappa} \ln \frac{R^*}{\kappa_s^*} + A_s \qquad (10.06)$$

If we assume $A_s = 8.5$ for $\kappa = .40$ and no change in the friction factor, we find A_s for various values of k.

$$A_s \simeq 8.5 + \left(\ln \frac{R^*}{\kappa_s^*}\right)\left\{\frac{1}{.4} - \frac{1}{\kappa}\right\} - \left(\frac{1}{.4} - \frac{1}{\kappa}\right) \qquad (10.07)$$

Assuming again that the equations 2.18 and 2.19 hold for the velocity profile in region I, and continuity of u and du/dy^* at $y^* = y_1^*$ we get:

$$\frac{1}{\kappa_1} \tanh \kappa_1 y_1^* = \frac{1}{\kappa} \ln \frac{y_1^*}{\kappa_s^*} + A_s + \frac{1}{2\kappa^2 y_1^*} - \frac{1}{4^2 \kappa^3 y_1^{*2}} \cdots \qquad (10.08)$$

$$\operatorname{sech}^2 \kappa_1 y^* = \frac{1}{\kappa y_1^*} - \frac{1}{2(\kappa y_1^*)^2} + \frac{1}{8(\kappa y_1^*)^3} \qquad (10.03)$$

The numerical solution of this system for various values of k and its corresponding values of A_s gives the values of κ_1 and y_1^*.

The numerical values of A_s change also with the Re number of the flow (particularly in the transition zone) and with the

equivalent roughness of the stream κ_s. So it would be rather interesting to see how well the values of κ_1 and y_1^*, found in the preceding article for smooth walls, satisfy the system of equations 10.08 and 10.03, for both sizes of sand used in the experiments.

From the application of the above values it was found that it would be reasonably satisfactory for our purposes to get the same κ_1 and y_1^* for both rough and smooth walls.

Table 11

Evaluation of Rannie's constant κ_1 and y_1^* assuming constant friction factor

von Karman's constant k	Rannie's constant κ_1	Dimensionless depth of the matching point for the vel. profiles
$K = .40$	$\kappa_1 = 1/14.5$	$y_1^* = 27.5$
.35	1/13	22.5
.30	1/9.5	13.0
.275	1/7	8.5
.250	1/4.2	8.0
.225	1/2	8.0

For very rough walls see discussion in Chapter VI, article A.

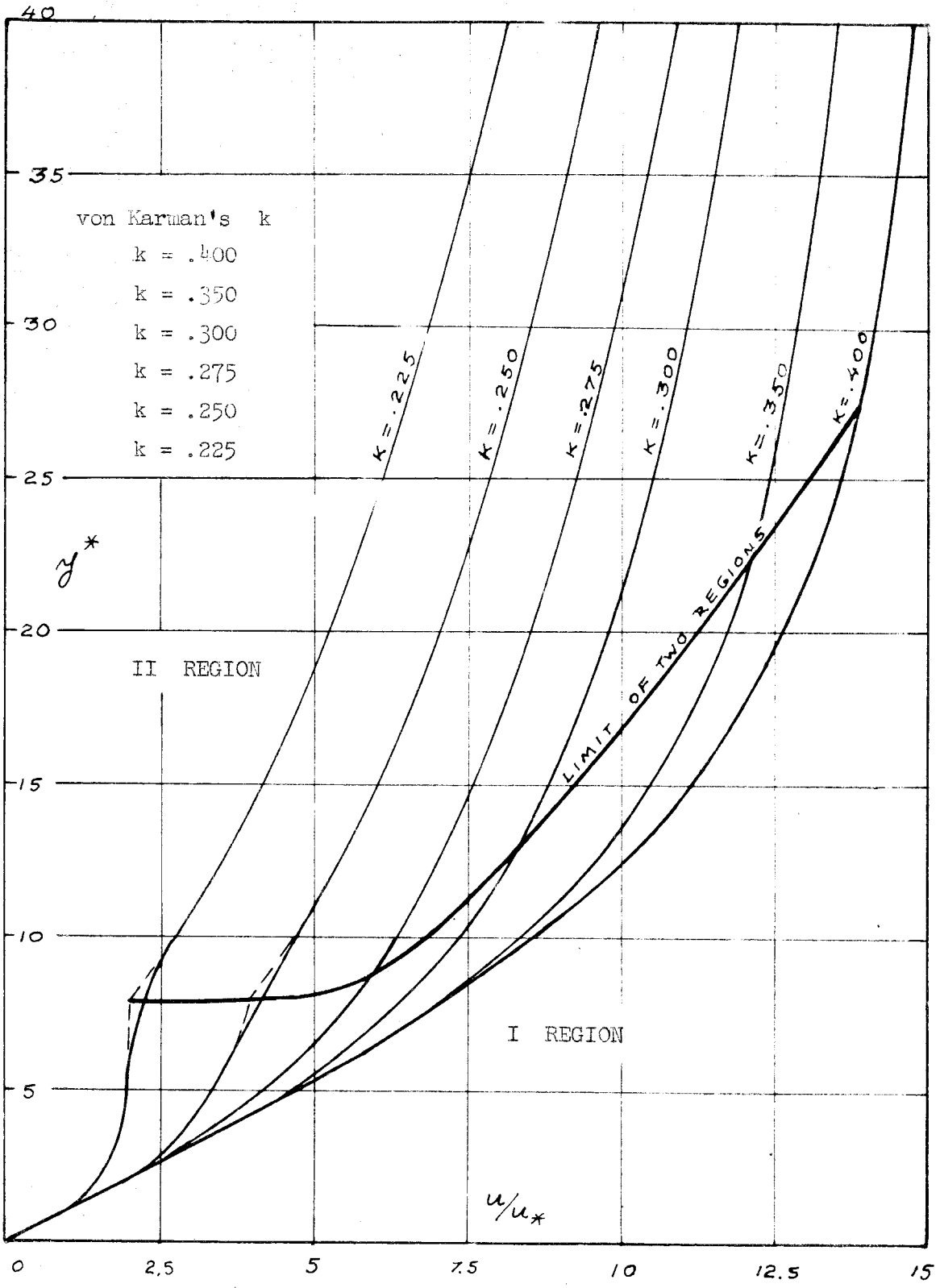

Fig. 29. Analytical velocity profiles